

USE OF NANOPARTICULATE DRUG-CARRIERS, DOSING ALTERATION,
PHARMACOKINETIC AND PHARMACODYNAMIC MODELING
TO OPTIMIZE THERAPY

by

IBRAHIM A. ALJUFFALI

(Under the Direction of ROBERT D. ARNOLD)

ABSTRACT

The overall goals of this dissertation were to exploit differences in tumor microenvironment, develop dosing schedules to facilitate optimization of nanoparticulate drug-carriers, and use pharmacokinetic/pharmacodynamic modeling to improve therapy.

Cancer represents the second leading cause of death in the US. Developing therapeutic strategies for metastatic disease can improve clinical outcomes and survival. Low-dose chemotherapeutic exposure can increase anticancer activity, but the mechanisms underlying this effect are not understood fully. Metronomic dosing is hypothesized to suppress tumor angiogenesis, however, we hypothesized that metronomic schedules could also mediate direct effects on the tumor parenchyma, further improving antitumor activity. Using *in vitro* and *in vivo* studies we demonstrated that topotecan dosed metronomically increased its antitumor activity. Molecular studies suggest mechanisms distinct from the established mechanism for conventional therapy.

Spatial differences in tumor microenvironment can impact treatment efficacy. We found that tumor oxygenation and pH had significant effects on the anticancer activity of topotecan. Exploiting the acidic tumor microenvironment, a novel topotecan nanoparticulate drug targeting strategy was developed to improve its anticancer activity and reduce toxicity.

A goal of drug therapy is to achieve optimal target-site exposure *in vivo* and reduce non-target tissue toxicity. Controlling the rate and extent of drug release from drug-carriers is one approach that can be used, but is difficult to quantify *in vivo*. We prepared and characterized prototype liposomes encapsulating *gadolinium-DTPA*, a magnetic resonance imaging probe, to determine carrier release kinetics *in vivo* and optimize target-site drug exposure.

These studies suggest that tumor microenvironment and metronomic schedules can be exploited to improve cancer chemotherapy. Furthermore, we have developed a novel approach to quantify drug-carrier release kinetics non-invasively.

Pharmacokinetic/pharmacodynamic modeling offers a computational method to describe data and develop testable hypothesis that can lead to novel treatment strategies. We determined the pharmacokinetics of ketanserin, a 5HT₂-antagonist, and developed a pharmacokinetic/pharmacodynamic model to optimize its dosing in horses. The model accurately captured the plasma concentration time data and was used to predict alternate dosing schedules that could be used to treat equine laminitis. Similar approaches can be used to facilitate development of drug-carriers and optimization of dosing schedules for cancer chemotherapies.

INDEX WORDS: Prostate cancer, metronomic dosing, topotecan, tumor microenvironment, nanoparticulate drug-carriers, liposomes, equine laminitis, pharmacokinetics and pharmacodynamic modeling.

USE OF NANOPARTICULATE DRUG-CARRIERS, DOSING ALTERATION,
PHARMACOKINETIC AND PHARMACODYNAMIC MODELING
TO OPTIMIZE THERAPY

by

IBRAHIM A. ALJUFFALI

B. Pharm., King Saud University, Saudi Arabia, 2004

A Dissertation Submitted to the Graduate Faculty of The University of Georgia in Partial
Fulfillment of the Requirements for the Degree

DOCTOR OF PHILOSOPHY

ATHENS, GEORGIA

2010

© 2010

Ibrahim A. Aljuffali

All Rights Reserved

USE OF NANOPARTICULATE DRUG-CARRIERS, DOSING ALTERATION,
PHARMACOKINETIC AND PHARMACODYNAMIC MODELING
TO OPTIMIZE THERAPY

by

IBRAHIM A. ALJUFFALI

Major Professor: Robert D. Arnold

Committee: Michael G. Bartlett
Shelley B. Hooks
Catherine A. White
James N. Moore

Electronic Version Approved:

Maureen Grasso
Dean of the Graduate School
The University of Georgia
December 2010

DEDICATION

To my mother Monirah, my father Abdulrahman, my lovely wife Manal and my beautiful kids, Rund and Abdulrahman.

ACKNOWLEDGEMENTS

I would like to thank God All Mighty, the One and Only, for His countless blessings and guidance throughout my life.

I would like to thank my parents for believing in me and supporting me throughout this long journey. None of my success would have been possible without their love, support, and encouragement.

I would like to thank my wife for her patience and unconditional sacrifices through my graduate life. I have no words to describe her sacrifice, and I just want her to know that I am very thankful. I would like to thank my two beautiful kids, Rund and Abdulrahman, for keeping me busy when I am not spending my time in the lab.

I would like to thank my advisor, Dr. Robert D. Arnold, for his direction, patience and mentorship. Also, my sincere appreciation to my thesis advisory committee members: Drs. Bartlett, Hook, Moore and White for taking their time and providing comments that helped shape my dissertation in its final form. I would like to express my gratitude to Dr. Lyndon West and Bruce LeRoy who previously served on my advisory committee.

Next, I would like to convey my appreciation to past and present Arnold's lab members. Guodong, Ha, Jeong-yeon, Leah, Wided, Yahya and other undergraduate students; research is never a one person effort. Also, I would like to acknowledge our collaborators at the University of Georgia and the State University of New York at Buffalo.

Finally, I would like to thank my sponsor, The Saudi Arabian Cultural Mission, The Ministry of Higher Education at Saudi Arabia, King Saud University and the University of Georgia Graduate School for financial support through my graduate tenure.

TABLE OF CONTENTS

	Page
ACKNOWLEDGEMENTS	v
LIST OF TABLES	ix
LIST OF FIGURES	xi
CHAPTER	
1 INTRODUCTION AND LITERATURE REVIEW	1
2 THE EFFECTS OF METRONOMIC DOSING OF TOPOTECAN ON PROSTATE CANCER	25
3 EFFECT OF TUMOR MICROENVIRONMENT ON ANTI-CANCER ACTIVITY OF TOPOTECAN	75
4 NON-INVASIVE RELEASE MEASUREMENT OF MAGNETIC RESONANCE IMAGING PROBE FROM NANOPARTICULATE DRUG- CARRIERS	111
5 PHARMACOKINETIC AND PHARMACODYNAMIC ASSESSMENT OF KETANSERIN IN HORSES, PART I: PHARMACOKINETIC AND PHARMACODYNAMIC MODELING	132
6 SUMMARY	158

APPENDICES

A PHARMACOKINETIC AND PHARMACODYNAMIC ASSESSMENT OF
KETANSERIN IN HORSES, PART II: *IN VIVO* AND *EX VIVO* EFFECTS
ON EQUINE PLATELET FUNCTION.....161

B *IN VIVO* TECHNIQUES AND METHODS185

LIST OF TABLES

	Page
Table 2-1: Effect of treatment and time of exposure on topotecan potency (IC ₅₀).....	49
Table 2-2: Alteration in mRNA expression (fold regulation) in comparison to control for key regulatory genes	50
Table 3-1: Effect of tumor microenvironment on topotecan potency (IC ₅₀) against androgen-independent human prostate cancer (PC-3).....	93
Table 3-2: Extracellular concentrations of topotecan forms after topotecan addition to PC-3 cells in conventional media (pH of 7.4).....	94
Table 3-3: Extracellular concentrations of topotecan forms after topotecan addition to PC-3 cells in acidic media (pH of 6.8).....	95
Table 5-1: Pooled non-compartmental pharmacokinetic parameter estimates of six healthy adult horses after a single ketanserin I.V. dose of 0.1 mg/kg to 6 horses	146
Table 5-2: Pharmacokinetics parameters obtained by compartmental analysis after single I.V. dose (0.1 mg/kg, n=6) or multiple doses (0.3 mg/kg, n=3)	147
Table 5-3: Pharmacodynamic parameters for platelet aggregation after single I.V dose of ketanserin (0.1 mg/kg) in healthy adult horses	148
Table A-1: Percent aggregation measured by optical aggregometry for all experimental groups (n=4 horses each) after <i>in vitro</i> addition of ketanserin or DMSO to equine platelet rich plasma (PRP).....	177

Table A-2: Percent aggregation measured by optical aggregometry in platelet rich plasma obtained from horses treated with a single dose of 0.1 mg/kg IV ketanserin at time 0178

Table A-3: Percent aggregation measured by optical aggregometry in platelet rich plasma obtained from three horses treated with 3 doses of 0.1 mg/kg IV ketanserin at time 0, 8, and 16 h.....179

Table A-4: Plasma and serum 5HT concentrations (ng/mL) in three horses treated with ketanserin 0.3 mg/kg IV q. 8h, starting at t = 0180

LIST OF FIGURES

	Page
Figure 1-1: Camptothecins chemical structure	14
Figure 2-1: Effect of topotecan on the growth of prostate (PC-3) cells <i>in vitro</i>	51
Figure 2-2: Effect of different dosing regimens of topotecan on cellular morphology	52
Figure 2-3: Effect of topotecan on PC-3 and LNCaP cell cycle.....	54
Figure 2-4: Gene expression profiling by RT-PCR array of PC-3 and LNCaP cells exposed to metronomic or conventional treatment of topotecan	56
Figure 2-5: Gene expression profiling by RT-PCR array of PC-3 cells exposed to metronomic or conventional treatment of topotecan.....	57
Figure 2-6: Gene expression profiling by RT-PCR array of LNCaP cells exposed to metronomic or conventional treatment of topotecan.....	58
Figure 2-7: Effect of topotecan on p21 expression in LNCaP and PC-3 cells	59
Figure 2-8: Effect of topotecan <i>in vivo</i> using xenograft model of human prostate cancer.....	60
Figure 2-9: Representative histological images of mouse PC-3 tumor xenografts treated with different dosing regimens of topotecan and stained with hematoxylin and eosin (H&E).....	62
Figure 2-10: Representative histological images of mouse PC-3 tumor xenografts treated with different dosing regimens of topotecan and stained for CD31	64

Figure 2-11: Effects of continuous topotecan exposure on topotecan plasma concentration.....	65
Figure 2-12: Effect of continuous topotecan systemic exposure <i>in vivo</i> using xenograft model of human prostate cancer	66
Figure 3-1: Topotecan structure.....	96
Figure 3-2: Schematic representation of remote loading, entrapment and release of topotecan	97
Figure 3-3: Effect of topotecan on growth of prostate cancer cells (PC-3) <i>in vitro</i> at pH 7.4	98
Figure 3-4: Effect of topotecan on growth of prostate cancer cells (PC-3) <i>in vitro</i> at pH 6.8.....	99
Figure 3-5: Effect of topotecan on growth of prostate cancer cells (PC-3) <i>in vitro</i> under acute hypoxia (2 % O ₂)	100
Figure 3-6: Extracellular concentration of topotecan (lactone form) after topotecan addition to PC-3 cells	101
Figure 3-7: Extracellular concentration of topotecan (carboxylate form) after topotecan addition to PC-3 cells	102
Figure 3-8: Ratio of carboxylate to lactone concentrations of topotecan in extracellular media	103
Figure 3-9: Alteration in extracellular pH following treatment with different concentration of topotecan	104
Figure 3-10: Intracellular concentration of the lactone form of topotecan.....	105
Figure 3-11: <i>In vitro</i> release profile of topotecan liposome	106

Figure 4-1: Research hypothesis.....	121
Figure 4-2: Determination of different liposome formulations relaxivity using MRI.....	122
Figure 4-3: R_1 relaxation rate of different liposome-dilution ratio.....	123
Figure 4-4: Measurement of T_1 relaxation times using NMR	124
Figure 4-5: Plots of T_1 relaxation time versus Gd-DTPA encapsulated liposome (Gd-lip) of different liposome concentrations	125
Figure 4-6: Release profile of Gd-DTPA from Gd-liposome.....	126
Figure 4-7: Plots of T_1 relaxation rate versus free Gd-DTPA concentrations in normal saline.....	127
Figure 4-8: Plots of T_1 relaxation rate versus free Gd-DTPA concentrations in rat plasma.....	128
Figure 5-1: Ketanserin structure	149
Figure 5-2: Diagram of pharmacokinetic/pharmacodynamic model used to describe ketanserin deposition and <i>ex vivo</i> platelets aggregation activity after single and multiple dose administration	150
Figure 5-3: Pharmacokinetic profiles of ketanserin in healthy horses after a single dose (0.1 mg/kg I.V.).....	151
Figure 5-4: Model simulation with different dose and dosing schedules.....	152
Figure 5-5: Time course of <i>ex vivo</i> platelets aggregation induced using two methods to stimulate platelet aggregation.....	153
Figure 5-6: <i>Ex vivo</i> platelets aggregation data fitted using indirect response pharmacodynamic model	154

CHAPTER 1

INTRODUCTION AND LITERATURE REVIEW

Cancer

Cancer is the second leading cause of death and accounts for approximately 1 out of 4 deaths in the United States. The lifetime probability of developing cancer is 1 in 2 for both genders. Prostate cancer is the most common non-cutaneous malignancy in men; and is estimated to account for 11 % of cancer-related deaths. The lifetime probability of developing prostate cancer is 1 in 6 [1]. Initially, prostate cancer cells are confined within the prostate gland and require androgen for growth and survival. However, tumor cells can start invading surrounding tissues and metastasize to distant organs and become androgen-refractory [2]. For a cancer to grow beyond its microscopic size (1-2 mm in diameter), the vasculature supporting the tumor mass needs to expand to meet the increased demand for nutrients and oxygen [3, 4].

Angiogenesis

Angiogenesis, formation of new blood vessels, is a process required for normal and malignant tissue growth. Without angiogenesis, local cancer growth is limited due to decreases in oxygen and nutrient supply [5]. Therefore, the growth of new blood vessels is a critical step in developing clinically relevant tumors. In the absence of blood supply, tumor growth is restricted to a microscopic size and the tumor is less likely to metastasize

[6]. Cellular stress factors such as hypoxia, nutrient deprivation, and reactive oxygen species can trigger the angiogenic process [7]. The fact that removal of angiogenic stimuli resulted in vessel regression suggested that angiogenesis inhibition can be exploited as a therapeutic approach [8]. Once tumors changed from a non-angiogenic to an angiogenic status, cells do not remain quiescent but start growing and can metastasize to distant organs [9].

There is evidence that tumor angiogenesis is different from normal physiological angiogenesis. In physiological angiogenesis, newly developed vessels rapidly mature and become stable. In contrast, tumor vessels fail to become quiescent, which results in constant and uncontrolled formation of new blood vessels [10]. Due to this abnormal growth, solid tumors have leaky vessels that are structurally and functionally abnormal [11]. Furthermore, tumor vessels have incomplete endothelial cell junctions that increase vessel permeability [12, 13]. The resulting leaky vessels combined with poor or nonfunctional lymphatics increase the interstitial pressure [14].

When compared to normal capillaries, tumor capillaries are tortuous, leaky and disorganized [15]. Most capillaries in normal tissues are continuous, with small paracellular spaces between 6.7-8.0 nm. In contrast, pores within tumor vessels are 200-780 nm in solid tumors except those in the brain which are 100-380 nm [16-18]. While the continuous nature of endothelial cells in normal vascular system prevents accumulation of macromolecules in most tissues, architectural defects in tumor vessels provide an opportunity for macromolecules to accumulate in solid tumors. This phenomenon is called the enhanced permeation and retention effect [19]. However, liver, lung and spleen are all known to have discontinuous vasculature and will be additional

sites for the leakage of macromolecules.

Tumor Microenvironment

Tumor microenvironment has been reported to be different from other that of non-cancerous tissues [20]. Microenvironment of cancer tissues is a complex environment composed of over expression of different enzymes, such as vascular endothelial growth factor (VEGF), a slightly acidic environment, low oxygen tension, elevated interstitial pressure and impaired function of the lymphatics supporting the tumor area [16]. Also, cancerous tissues in advanced stages are characterized by regions that have different levels of oxygenation [21-23]. The direct cause of hypoxia is restricted blood supply which is due to the irregular vascular architecture [24]. Restricted blood supply will result in formation of regions with different degrees of oxygenation. Adaptation of tumor cells to the hypoxic microenvironment results in an aggressive tumor phenotypes that are associated with increased malignancy, resistance to treatment modalities and unfavorable treatment outcomes [25, 26]. Further, restricted blood supply limits distribution of systemically administered anticancer agents [27], and the hypoxic microenvironment mediates increases in the expression of genes that are related to drug resistance (e.g.: MDR1, MRP and HIF-1) [28-30].

While the tumor microenvironment is reportedly acidic, especially in solid tumors, the pH values have been reported to vary in different malignances [31, 32]. The hypoxic microenvironment forces malignant cells to shift to anaerobic energy production. This mode of energy production results in an increase in lactic acid production within the tumor supporting tissue and drop in pH [33-35].

Treatment Modalities

Conventional cancer therapy consists of surgery, chemotherapy and sterilizing radiation. Recommended treatment for early stage and organ-confined cancer is surgical dissection with or without regional lymph node removal [36, 37]. For local and primary prostate cancer, the initial clinical assessments are made (*e.g.* PSA level) to identify the patient's stage of disease and prognosis. Initial therapy can involve active surveillance and regular monitoring of PSA levels and other symptoms [36]. For advanced and recurrent disease or if surgical resection is not preferred, treatment options include androgen ablation by orchiectomy, luteinizing hormone releasing hormone agonists or androgen receptor antagonists [36]. Androgen ablation offers initial success in controlling metastatic disease, but some patients become refractory to androgen ablation and cancers grow in an androgen-independent manner [2]. Another hindrance for successful treatment of cancer by classical chemotherapy or radiation is the development of resistance towards treatment regimens and low tissue oxygen level that negatively impact the efficacy of radiation therapy [38, 39]. Other strategies to control this type of malignancy, include, antiangiogenic drugs, endothelin receptor antagonists, immunotherapy and cytotoxic agents [40-43].

Most current anticancer agents do not differentiate between cancerous and normal cells. Systemic application of chemotherapeutic agents often causes severe adverse effects in non-targeted tissues, which limits maximal drug exposure. Also, rapid distribution and elimination of chemotherapeutic agents require high doses be administered to achieve sufficient target drug concentrations. Therefore, it is important to develop new strategies for tumor therapy, especially for progressed and advanced disease

that is unresponsive to classical treatment options.

Antiangiogenic therapy

The complex process of tumor angiogenesis offers multiple options in terms of interfering with the angiogenic process. Current approaches are based on the inhibition of one or more angiogenic factors [44]. The US FDA had approved several therapeutic products with recognized antiangiogenic characteristics. These agents can be categorized into different groups: 1- monoclonal antibodies against specific angiogenic growth factors and/or their receptors (e.g.: Bevacizumab “Avastin[®]” and Cetuximab “Erbix[®]”), 2- small molecule tyrosine kinase inhibitors of angiogenic growth factor receptors (e.g.: Erlotinib “Tarveca[®]” and Sunitinib “Sutent[®]”), and 3- inhibitor of the mammalian target of rapamycin (Temsirrolimus “Torisel[®]”). Another strategy for angiogenesis inhibition is based on altered dosing schedules of existing chemotherapeutic agents [45].

Metronomic Dosing of Chemotherapeutic Agents

Conventional chemotherapeutics are cytotoxic agents that affect proliferating tumor cells, healthy cells and interfere with endothelial cells in growing tumor vessels [46]. Whereas bolus high dose chemotherapy is directed mainly against rapidly dividing tumor cells, another possible approach is to utilize anticancer drugs administered at continuous low dose schedules (metronomic dosing) in order to target active blood vessels [38]. Bolus high dose chemotherapy requires treatment free-intervals to allow patients to recover from severe side effects associated with high-dose drug exposure. However, these treatment-free intervals can increase the growth of chemotherapy-resistant tumor

cells and allow the tumor vasculature recovery [38]. Sustained inhibition of endothelial cells can be achieved more effectively by continuous or frequent administration of cytotoxic agents at lower dose with the omission of treatment-free intervals [47-49]. Hence the first cells exposed to the drug are endothelial cells at sites of angiogenesis. In contrast tumor cells that are either distant from blood vessels or in a non-proliferating or dormant state will remain unaffected and can start growing during treatment free periods. Changing the dosing schedule from administration of the maximum tolerable dose (MTD) to a metronomic low-dose scheme is hypothesized to target both tumor and endothelial cells [50, 51].

The differential activity of some of chemotherapeutic agents, in which the growth of endothelial cells are inhibited at doses lower than those needed to inhibit tumor cell growth, may help to explain the *in vivo* anti-tumor responses with fewer side effects [46]. The observed anti-tumor effect is likely a secondary effect of the drug on the tumor vasculature. As vascular structures collapse, tumor cells undergo cell death. Evidence for this effect is further supported by the observed of anti-tumor activity of metronomic schedules against tumors exhibiting resistance to the same agents administered using MTD regimens [50].

Frequent low-dose drug exposure increases chemotherapeutic efficacy of some chemotherapeutic agents in various animal cancer models [52]. Clinical evidence of beneficial effects of metronomic dosing also exist [53]. In contrast, not all of anticancer activities of metronomic dosing can be correlated to anti-angiogenic activity. For example, a recent report showed that concurrent metronomic administration of cyclophosphamide and tirapazamine for the treatment of gliosarcoma reduced tumor size

without impacting the tumor vasculature [54]. Other suggested mechanisms for the beneficial effects of metronomic dosing schedules include activation of immunity and induction of tumor dormancy [55]. These reports support the hypothesis that the beneficial effects of metronomic dosing cannot be solely explained by the observed anti-angiogenic effect. Chemotherapeutic agents used in metronomic dosing regimens *in vivo* and *in vitro* include: trofosfamide, cyclophosphamide, methotrexate, capecitabine, docetaxel, paclitaxel and topotecan [56-60].

Camptothecins

Camptothecin analogues are a group of chemotherapeutic agents that share similar structural and functional activity with camptothecin [61]. Camptothecin (**Figure 1-1**) is a cytotoxic agent isolated from the stem wood of the Chinese tree (*Camptotheca acuminata*) [62, 63]. Camptothecin is an S-phase specific antineoplastic agent that eradicates cellular growth by inhibiting Topoisomerase-I. Topoisomerase-I is one of two enzymes in this family that change the topological state of DNA; these enzymes are important in every step of DNA replication and repair [64, 65]. Camptothecin was discontinued from clinical trials (phase II) due to its severe side effects including myelosuppression, vomiting, diarrhea and severe hemorrhagic cystitis [66]. To overcome camptothecin's poor aqueous solubility, a Na⁺ salt was developed but resulted in a less efficacious derivative; which suggested that a closed lactone ring is required for activity [64, 67]. To overcome these limitations, camptothecin derivatives were synthesized including topotecan and irinotecan [64].

Topotecan ($C_{23}H_{23}N_3O_5.HCL$, molecular weight=457.9 Da, **Figure 1-1**) is a semi-synthetic derivative of camptothecin and one of the most potent antineoplastic agents developed [68]. Topotecan is a water soluble compound that undergoes reversible non-enzymatic hydrolysis (from a closed lactone ring to an open carboxylate-ion form) at physiological pH (7.4), and the lactone ring is intact at acidic pH [64, 69, 70]. The intact lactone ring is required for activity and must be protected to maintain topotecan's cytotoxicity. Topotecan plasma concentration exhibit a multi-exponential decline with a terminal phase's half-life of 2-3 hr [71]. Topotecan affects cell proliferation by inhibiting Topoisomerase-I [69]. The U.S. FDA has approved topotecan for the treatment of relapsed small cell lung cancer, metastatic carcinoma of the ovary and carcinoma of the cervix. In addition, topotecan exert an antiangiogenic activity when administered continuously at low doses to normal human endothelial cells *in vitro* and *in vivo* using a disc angiogenesis system [73, 74].

Drug Delivery Systems and Nanoparticles

Drug-carriers (e.g. nanoparticles) could offer a new treatment modality that may enhance patient survival and quality of life [75]. Nanoparticles have a large surface area and functional groups that can be coupled to targeting moieties, imaging probes or therapeutic agents [76]. Liposomes are one of the most common types of drug-carriers used [75]. Liposomes are spherical nanostructures composed of phospholipids and other amphipathic lipids that mimic human cell membranes [77]. Phospholipids are composed of a hydrophilic head and a hydrophobic tail. In an aqueous environment, phospholipids spontaneously rearrange to form a closed, bi-layer spherical shape with an aqueous core

[78, 79]. The liposome's core can be used to entrap hydrophilic molecules, and hydrophobic molecules can be carried within the lipid bilayer or at the interfacial region [16]. Depending on their physicochemical properties, drugs can be associated with the lipid bilayer or the aqueous core of liposomes.

Liposomes are biocompatible and biodegradable drug carriers; they are used to alter the distribution, pharmacokinetics and/or metabolism of encapsulated compounds [80]. Several types of liposomes can be synthesized from natural or synthetic lipids. These types differ in their lipid components and acyl chain length, size of liposomes (small unilamellar vesicles or large unilamellar vesicles), number of lipid bilayers (multilamellar or unilamellar vesicles) and the surface charge (anionic, cationic or neutral) [77, 81]. Liposomes can differ in size from less than 50 nm to several micrometers, depending on the conditions carried out in the preparation and the type of lipids used [77]. Nanoparticulate drug-carrier can accumulate passively in solid tumors due the enhanced permeability and retention phenomena. For this passive targeting strategy to work, the size and surface properties of drug-carriers must be controlled to avoid their uptake by the reticular endothelial system. To increase circulation times and targeting, the optimal size of drug-carriers should be less than 200 nm in diameter and the surface should be coated with hydrophilic polymer to limit their interaction with opsonins that facilitate their uptake.

Limitations of using liposomes include macrophage uptake and reticular endothelial system destabilization. Modifications have been made to overcome these limitations through the addition of cholesterol molecules to the lipid membrane which decreases membrane fluidity and reduces liposome interactions with plasma proteins [82, 83].

These alterations result in a longer circulation half-life with an increased retention of encapsulated compounds. Other modifications include surface hydration by incorporating polyethylene glycol (PEG) and other hydrophilic polymers (e.g.: ganglioside) [75, 79]. Incorporation of PEG will result in sterically-stabilized liposomes (SSL) with higher surface hydration [84]. Surface hydration will reduce the penetration of opsonins and other plasma proteins which in turn decrease recognition of liposomes by the reticular endothelial system [79, 81, 85].

Sterically-stabilized liposomes containing PEG can circulate in the blood longer than conventional liposomes lacking PEG. Using sterically-stabilized liposomes with diameters of 50-200 nm will facilitate their accumulation in cancerous tissues due to leaky vasculatures and minimize their extravasation in healthy tissues that have smaller pores (2-6 nm) and tight intercellular junctions [86, 87]. Prolonged blood circulation of these liposomes results in greater accumulation in solid tumors.

The liver and kidney are the major elimination sites for drug carriers [88]. Controlling clearance from these organs can increase systemic drug exposure. Glomerular capillaries in the kidney are fenestrated, with pores estimated to be 40-60 nm in diameter. The basement membrane in the kidney acts as a size and charge barrier, which can hinder the transport of molecules greater than 6 nm [88]. In the liver, the basement membrane is absent and the capillaries are fenestrated with pores 200 nm in diameter and endothelial gaps ranging from 100 nm to 1000 nm. As the result, the passages of drug-carriers is not restricted. However, cellular uptake of drug carriers can be lowered by decreasing the interaction between cells and drug carriers [88].

Dissertation Objectives

The overall goals of this dissertation were to examine tumor microenvironment and dosing schedules to optimize the therapeutic potential of drugs for the treatment of cancer and equine laminitis.

Chapter II

Continuous low-dose drug exposure (metronomic dosing) increases chemotherapeutic efficacy of some agents in various models of human cancer. The underlying mechanisms of these beneficial effects are not understood fully, but metronomic dosing is hypothesized to alter tumor endothelial cell function and suppress tumor angiogenesis. However, these effects do not explain all the observed activities. We hypothesized that metronomic schedules can be developed to improve antitumor activity *in vivo* by exploiting known antiangiogenic activity with **direct effects on tumor cells**. This chapter focuses on two specific aims, *i*) to determine the *in vitro* effect of topotecan treatment schedules using human prostate cancer cell lines (PC-3 and LNCaP), and *ii*) to determine the *in vivo* tumor regression activity of metronomic dosing of topotecan in a murine model of human prostate cancer. A secondary objective was to identify mechanisms that may mediate the observed schedule-dependent effects of topotecan so that they could be used to optimize drug therapy and/or provide novel targets.

Chapter III

Solid tumors exhibit spatial differences in oxygenation status and various degrees of acidity within the extracellular fluid. These differences in oxygenation can greatly

impact treatment outcome. In this chapter, we studied the impact of tumor oxygenation and alterations in pH on activity of topotecan *in vitro* using a prostate cancer cell line.

We hypothesized that encapsulation of the inactive (carboxylate-ion) form of topotecan will enhance the retention of topotecan in the core of liposomes and the slightly acidic microenvironment in prostate cancer tissues would facilitate conversion of the inactive carboxylate-ion form of topotecan to the active lactone form. Another goal of the studies described in this chapter was to develop a prototype liposome formulation that encapsulates the inactive form of topotecan. We hypothesize that the acidic microenvironment could be exploited to reform the active lactone moiety selectively within a tumor enhancing its antitumor activity, but minimizing non-target tissue toxicity.

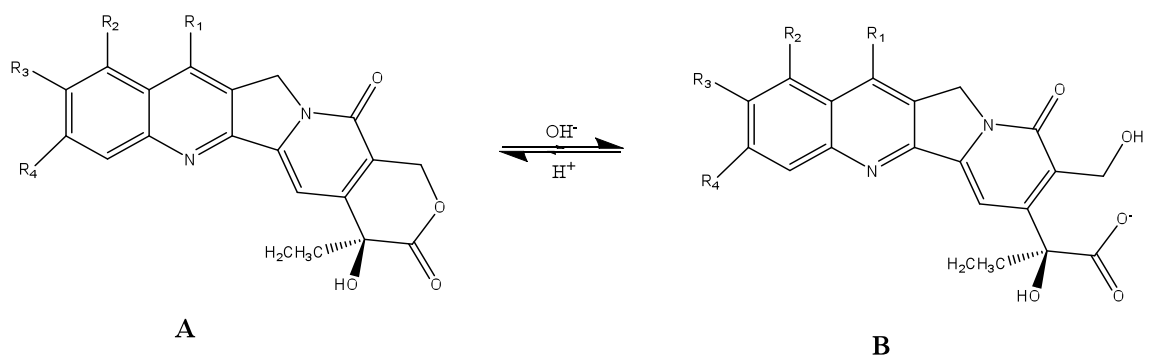
Chapter IV

Optimizing therapeutic capability of nanoparticulate drug-carriers requires a functional understanding and measurement of the release of encapsulated compounds *in vivo*. Controlling the rate and extent of drug release from nanoparticulate drug-carriers is an important step in formulation development. The goal is to achieve high drug exposure *in vivo* at the target site to improve antitumor activity, while reducing non-target tissue toxicity. Determining the release rate *in vivo* (within the tissue) remains a challenge within the scientific community. Our primary objectives were to develop the techniques necessary to prepare and characterize prototype liposomes that would be used to encapsulate Gd-DTPA, a Magnetic Resonance Imaging (MRI) contrast agent. The first part of this study was to encapsulate Gd-DTPA into lipid-based drug-carriers. The second

goal was to measure the rate and extent of Gd release via nuclear magnetic resonance (NMR) and MRI and to correlate its release to that of therapeutic compounds.

Chapter V

The overall goal of this chapter was to develop and optimize a novel treatment strategy for equine laminitis. Using drug concentration in plasma-time profiles, we determined the pharmacokinetics of ketanserin and then developed a pharmacokinetic and pharmacodynamic model. The model was used to make predictions of alternate dosing schedules to be tested clinically. The goal of this study was to determine the PK and develop a pharmacokinetic model that describes the plasma concentrations of ketanserin and its effect on platelet aggregation in healthy adult horses.



Compound	R ₁	R ₂	R ₃	R ₄
Camptothecin	H	H	H	H
Topotecan	H	$\begin{array}{c} \text{CH}_3 \\ \diagup \\ \text{CH}_2\text{N} \\ \diagdown \\ \text{CH}_3 \end{array}$	OH	H

Figure 1-1. Camptothecins chemical structure. A- Active α -hydroxy- δ -lactone form, **B-** Inactive carboxylate-ion form.

REFERENCES

1. Jemal, A., et al., *Cancer statistics, 2010*. CA: A Cancer Journal for Clinicians, 2010.
2. Feldman, B. and D. Feldman, *The development of androgen-independent prostate cancer*. Nature Reviews Cancer, 2001. **1**(1): p. 34-45.
3. Brem, H. and J. Folkman, *Inhibition of tumor angiogenesis mediated by cartilage*. The Journal of experimental medicine, 1975. **141**(2): p. 427.
4. Gimbrone, M., et al., *Tumor dormancy in vivo by prevention of neovascularization*. The Journal of experimental medicine, 1972. **136**(2): p. 261.
5. Torres Filho, I., et al., *Noninvasive measurement of microvascular and interstitial oxygen profiles in a human tumor in SCID mice*. Proceedings of the National Academy of Sciences, 1994. **91**(6): p. 2081.
6. Folkman, J. *Role of angiogenesis in tumor growth and metastasis*. 2002: Elsevier.
7. North, S., M. Moenner, and A. Bikfalvi, *Recent developments in the regulation of the angiogenic switch by cellular stress factors in tumors*. Cancer letters, 2005. **218**(1): p. 1-14.
8. Ausprunk, D., K. Falterman, and J. Folkman, *The sequence of events in the regression of corneal capillaries*. Laboratory investigation; a journal of technical methods and pathology, 1978. **38**(3): p. 284.
9. Folkman, J. and R. Kalluri, *Cancer without disease*. Nature, 2004. **427**(6977): p. 787-787.
10. Bergers, G. and L. Benjamin, *Tumorigenesis and the angiogenic switch*. Nature Reviews Cancer, 2003. **3**(6): p. 401-410.

11. Carmeliet, P. and R.K. Jain, *Angiogenesis in cancer and other diseases*. Nature, 2000. **407**(6801): p. 249-257.
12. Eberhard, A., et al., *Heterogeneity of angiogenesis and blood vessel maturation in human tumors: implications for antiangiogenic tumor therapies*. Cancer research, 2000. **60**(5): p. 1388.
13. Carmeliet, P. and R. Jain, *Angiogenesis in cancer and other diseases*. Nature, 2000. **407**(6801): p. 249-257.
14. Roberts, W. and G. Palade, *Increased microvascular permeability and endothelial fenestration induced by vascular endothelial growth factor*. Journal of cell science, 1995. **108**(6): p. 2369.
15. Yuan, F., et al., *Microvascular permeability and interstitial penetration of sterically stabilized (Stealth) liposomes in a human tumor xenograft*. Cancer research, 1994. **54**(13): p. 3352.
16. Drummond, D.C., et al., *Optimizing liposomes for delivery of chemotherapeutic agents to solid tumors*. Pharmacological Reviews, 1999. **51**(4): p. 691-743.
17. Siegal, T., A. Horowitz, and A. Gabizon, *Doxorubicin encapsulated in sterically stabilized liposomes for the treatment of a brain tumor model: biodistribution and therapeutic efficacy*. Journal Of Neurosurgery, 1995. **83**(6): p. 1029-1037.
18. Hobbs, S.K., et al., *Regulation of transport pathways in tumor vessels: role of tumor type and microenvironment*. Proceedings Of The National Academy Of Sciences Of The United States Of America, 1998. **95**(8): p. 4607-4612.

19. Matsumura, Y. and H. Maeda, *A new concept for macromolecular therapeutics in cancer chemotherapy: mechanism of tumorotropic accumulation of proteins and the antitumor agent smancs*. Cancer research, 1986. **46**(12 Part 1): p. 6387.
20. Whiteside, T., *The tumor microenvironment and its role in promoting tumor growth*. Oncogene, 2008. **27**(45): p. 5904-5912.
21. Movsas, B., et al., *Hypoxia in human prostate carcinoma: an Eppendorf PO2 study*. Am J Clin Oncol, 2001. **24**(5): p. 458-61.
22. Rasey, J.S., et al., *Quantifying regional hypoxia in human tumors with positron emission tomography of [18F]fluoromisonidazole: a pretherapy study of 37 patients*. Int J Radiat Oncol Biol Phys, 1996. **36**(2): p. 417-28.
23. Movsas, B., et al., *Hypoxic regions exist in human prostate carcinoma*. Urology, 1999. **53**(1): p. 11-8.
24. Pouyssegur, J., F. Dayan, and N.M. Mazure, *Hypoxia signalling in cancer and approaches to enforce tumour regression*. Nature, 2006. **441**(7092): p. 437-43.
25. Harris, A., *Hypoxia-a key regulatory factor in tumour growth*. Nature Reviews Cancer, 2002. **2**(1): p. 38-47.
26. Harris, A., *Hypoxia a key regulatory factor in tumour growth*. Nature Reviews Cancer, 2002. **2**(1): p. 38-47.
27. Brown, J. and W. Wilson, *Exploiting tumour hypoxia in cancer treatment*. Nature Reviews Cancer, 2004. **4**(6): p. 437-447.
28. Comerford, K., et al., *Hypoxia-inducible factor-1-dependent regulation of the multidrug resistance (MDR1) gene*. Cancer research, 2002. **62**(12): p. 3387.

29. Maxwell, P., et al., *Hypoxia-inducible factor-1 modulates gene expression in solid tumors and influences both angiogenesis and tumor growth*. Proceedings of the National Academy of Sciences of the United States of America, 1997. **94**(15): p. 8104.
30. Liang, B., *Effects of hypoxia on drug resistance phenotype and genotype in human glioma cell lines*. Journal of neuro-oncology, 1996. **29**(2): p. 149-155.
31. Tannock, I.F. and D. Rotin, *Acid pH in tumors and its potential for therapeutic exploitation*. Cancer Res, 1989. **49**(16): p. 4373-4384.
32. Gerweck, L.E. and K. Seetharaman, *Cellular pH gradient in tumor versus normal tissue: potential exploitation for the treatment of cancer*. Cancer Res, 1996. **56**(6): p. 1194-1198.
33. Raghunand, N., et al., *Enhancement of chemotherapy by manipulation of tumour pH*. British Journal Of Cancer, 1999. **80**(7): p. 1005-1011.
34. Warburg, O., *On the origin of cancer cells*. Science, 1956. **123**(3191): p. 309-314.
35. Prescott, D., et al., *The relationship between intracellular and extracellular pH in spontaneous canine tumors*. Clinical Cancer Research, 2000. **6**(6): p. 2501.
36. Mohler, J., *NCCN Clinical Practice Guidelines in Oncology: Prostate Cancer*. National Comprehensive Cancer Network, 2010. **V.2**.
37. Carlson, R., *NCCN Clinical Practice Guidelines in Oncology: Breast Cancer*. National Comprehensive Cancer Network, 2010. **V.2**.
38. Kerbel, R. and B. Kamen, *The anti-angiogenic basis of metronomic chemotherapy*. Nature Reviews Cancer, 2004. **4**(6): p. 423-436.

39. Semenza, G., *Intratumoral hypoxia, radiation resistance, and HIF-1*. *Cancer Cell*, 2004. **5**(5): p. 405-406.
40. Horwich, A., *Prostate cancer management*. *Annals Of Oncology: Official Journal Of The European Society For Medical Oncology / ESMO*, 2004. **15 Suppl 4**: p. iv307-12.
41. Carducci, M.A., et al., *Effect of endothelin-A receptor blockade with atrasentan on tumor progression in men with hormone-refractory prostate cancer: a randomized, phase II, placebo-controlled trial*. *Journal Of Clinical Oncology: Official Journal Of The American Society Of Clinical Oncology*, 2003. **21**(4): p. 679-689.
42. Figg, W.D., et al., *Inhibition of angiogenesis: treatment options for patients with metastatic prostate cancer*. *Investigational New Drugs*, 2002. **20**(2): p. 183-194.
43. Gulley, J. and W. Dahut, *Novel clinical trials in androgen-independent prostate cancer*. *Clinical Prostate Cancer*, 2002. **1**(1): p. 51-57.
44. Dutour, A. and M. Rigaud, *Tumor endothelial cells are targets for selective therapies: in vitro and in vivo models to evaluate antiangiogenic strategies*. *Anticancer research*, 2005. **25**(6B): p. 3799.
45. Kerbel, R.S., *Antiangiogenic therapy: a universal chemosensitization strategy for cancer?* *Science*, 2006. **312**(5777): p. 1171-5.
46. Bocci, G., K. Nicolaou, and R. Kerbel, *Protracted low-dose effects on human endothelial cell proliferation and survival in vitro reveal a selective antiangiogenic window for various chemotherapeutic drugs*. *Cancer research*, 2002. **62**(23): p. 6938.

47. Miller, K., C. Sweeney, and G. Sledge Jr, *Redefining the target: chemotherapeutics as antiangiogenics*. Journal of Clinical Oncology, 2001. **19**(4): p. 1195.
48. Hanahan, D., G. Bergers, and E. Bergsland, *Less is more, regularly: metronomic dosing of cytotoxic drugs can target tumor angiogenesis in mice*. Journal of Clinical Investigation, 2000. **105**(8): p. 1045-1056.
49. Klement, G., et al., *Continuous low-dose therapy with vinblastine and VEGF receptor-2 antibody induces sustained tumor regression without overt toxicity*. Journal of Clinical Investigation, 2000. **105**(8): p. 15-24.
50. Browder, T., et al., *Antiangiogenic scheduling of chemotherapy improves efficacy against experimental drug-resistant cancer*. Cancer research, 2000. **60**(7): p. 1878.
51. Bertolini, F., et al., *Maximum tolerable dose and low-dose metronomic chemotherapy have opposite effects on the mobilization and viability of circulating endothelial progenitor cells*. Cancer Res, 2003. **63**(15): p. 4342-6.
52. Munoz, R., et al., *Anti-angiogenic treatment of breast cancer using metronomic low-dose chemotherapy*. The Breast, 2005. **14**(6): p. 466-479.
53. Orlando, L., et al., *Prolonged clinical benefit with metronomic chemotherapy in patients with metastatic breast cancer*. Anticancer Drugs, 2006. **17**(8): p. 961-967.
54. Doloff, J., et al., *Increased Tumor Oxygenation and Drug Uptake During Anti-Angiogenic Weekly Low Dose Cyclophosphamide Enhances the Anti-Tumor Effect*

- of Weekly Tirapazamine (Supplementary Material)*. *Current Cancer Drug Targets*, 2009. **9**(6): p. 777-788.
55. Pasquier, E., M. Kavallaris, and N. André, *Metronomic chemotherapy: new rationale for new directions*. *Nature Reviews Clinical Oncology*, 2010. **7**(8): p. 455-465.
 56. Vogt, T., et al., *Antiangiogenic therapy with pioglitazone, rofecoxib, and metronomic trofosfamide in patients with advanced malignant vascular tumors*. *Cancer*, 2003. **98**(10): p. 2251-2256.
 57. Lennernäs, B., et al., *Antiangiogenic effect of metronomic paclitaxel treatment in prostate cancer and non-tumor tissue in the same animals: a quantitative study*. *Apmis*, 2004. **112**(3): p. 201-209.
 58. Colleoni, M., et al., *Metronomic low-dose oral cyclophosphamide and methotrexate plus or minus thalidomide in metastatic breast cancer: antitumor activity and biological effects*. *Annals of Oncology*, 2006. **17**(2): p. 232.
 59. Kamat, A., et al., *Metronomic chemotherapy enhances the efficacy of antivascular therapy in ovarian cancer*. *Cancer Research*, 2007. **67**(1): p. 281.
 60. Dellapasqua, S., et al., *Metronomic cyclophosphamide and capecitabine combined with bevacizumab in advanced breast cancer*. *Journal of Clinical Oncology*, 2008. **26**(30): p. 4899.
 61. Basili, S. and S. Moro, *Novel camptothecin derivatives as topoisomerase I inhibitors*. *Expert Opin Ther Pat*, 2009. **19**(5): p. 555-74.
 62. Monroe E. Wall, M.C.W., C. E. Cook, Keith H. Palmer, A. T. McPhail, G. A. Sim, *Plant Antitumor Agents. I. The Isolation and Structure of Camptothecin, a*

- Novel Alkaloidal Leukemia and Tumor Inhibitor from Camptotheca acuminata.*
Journal of the American Chemical Society, 1966. **88**(16): p. 3888-3890.
63. Wani, M. and M. Wall, *Plant antitumor agents. II. Structure of two new alkaloids from Camptotheca acuminata.* The Journal of Organic Chemistry, 1969. **34**(5): p. 1364-1367.
64. Ulukan, H. and P.W. Swaan, *Camptothecins: a review of their chemotherapeutic potential.* Drugs, 2002. **62**(14): p. 2039-2057.
65. Liu, L.F., et al., *Mechanism of action of camptothecin.* Annals Of The New York Academy Of Sciences, 2000. **922**: p. 1-10.
66. Moertel, C.G., et al., *Phase II study of camptothecin (NSC-100880) in the treatment of advanced gastrointestinal cancer.* Cancer Chemotherapy Reports. Part 1, 1972. **56**(1): p. 95-101.
67. Gottlieb, J.A., et al., *Preliminary pharmacologic and clinical evaluation of camptothecin sodium (NSC-100880).* Cancer Chemotherapy Reports. Part 1, 1970. **54**(6): p. 461-470.
68. Cersosimo, R.J., *Topotecan: a new topoisomerase I inhibiting antineoplastic agent.* Ann Pharmacother, 1998. **32**(12): p. 1334-43.
69. Kollmannsberger, C., et al., *Topotecan - A novel topoisomerase I inhibitor: pharmacology and clinical experience.* Oncology, 1999. **56**(1): p. 1-12.
70. Loos, W.J., et al., *Determination of camptothecin analogs in biological matrices by high-performance liquid chromatography.* Anti-Cancer Drugs, 2000. **11**(5): p. 315-324.

71. *HYCAMTIN® (topotecan hydrochloride) prescribing information, available at http://www.accessdata.fda.gov/drugsatfda_docs/label/2006/020671s014lbl.pdf.*
72. Herben, V.M., W.W. ten Bokkel Huinink, and J.H. Beijnen, *Clinical pharmacokinetics of topotecan*. Clin Pharmacokinet, 1996. **31**(2): p. 85-8102.
73. O'Leary, J.J., et al., *Antiangiogenic effects of camptothecin analogues 9-amino-20(S)-camptothecin, topotecan, and CPT-11 studied in the mouse cornea model*. Clin Cancer Res, 1999. **5**(1): p. 181-7.
74. Clements, M.K., et al., *Antiangiogenic potential of camptothecin and topotecan*. Cancer Chemother Pharmacol, 1999. **44**(5): p. 411-416.
75. Drummond, D., et al., *Optimizing liposomes for delivery of chemotherapeutic agents to solid tumors*. Pharmacological reviews, 1999. **51**(4): p. 691.
76. Nobs, L., et al., *Current methods for attaching targeting ligands to liposomes and nanoparticles*. Journal of pharmaceutical sciences, 2004. **93**(8): p. 1980-1992.
77. Fielding, R.M., *Liposomal drug delivery. Advantages and limitations from a clinical pharmacokinetic and therapeutic perspective*. Clinical Pharmacokinetics, 1991. **21**(3): p. 155-164.
78. Lasic, D.D., *The mechanism of vesicle formation*. The Biochemical Journal, 1988. **256**(1): p. 1-11.
79. Torchilin, V.P., *Recent advances with liposomes as pharmaceutical carriers*. Nature Reviews. Drug Discovery, 2005. **4**(2): p. 145-160.
80. Gabizon, A., *Emerging role of liposomal drug carrier systems in cancer chemotherapy*. Journal Of Liposome Research, 2003. **13**(1): p. 17-20.

81. Amarnath Sharma , U.S.S., *Liposomes in drug delivery: progress and limitations*. 1997.
82. Kirby, C., J. Clarke, and G. Gregoriadis, *Effect of the cholesterol content of small unilamellar liposomes on their stability in vivo and in vitro*. *Biochemical Journal*, 1980. **186**(2): p. 591.
83. Senior, J. and G. Gregoriadis, *Stability of small unilamellar liposomes in serum and clearance from the circulation: the effect of the phospholipid and cholesterol components*. *Life Sciences*, 1982. **30**(24): p. 2123-2136.
84. Papahadjopoulos, D., et al., *Sterically stabilized liposomes: improvements in pharmacokinetics and antitumor therapeutic efficacy*. *Proceedings of the National Academy of Sciences of the United States of America*, 1991. **88**(24): p. 11460.
85. Yan, X., G.L. Scherphof, and J.A.A.M. Kamps, *Liposome opsonization*. *Journal Of Liposome Research*, 2005. **15**(1-2): p. 109-139.
86. Brown, D.M., *Drug Delivery System in Cancer Therapy*. 2004: Humana Press.
87. Yuan, F., et al., *Vascular permeability in a human tumor xenograft: molecular size dependence and cutoff size*. *Cancer Research*, 1995. **55**(17): p. 3752-3756.
88. Hashida, M. and Y. Takakura, *Pharmacokinetics in design of polymeric drug delivery systems*. *Journal of Controlled Release*, 1994. **31**(2): p. 163-171.

CHAPTER 2
THE EFFECTS OF METRONOMIC DOSING OF TOPOTECAN ON PROSTATE
CANCER

Ibrahim A. Aljuffali¹, Jason N. Mock¹, Brian S. Cummings¹, Tamas Nagy² and Robert D. Arnold¹

To be submitted to the Journal of Clinical Cancer Research

¹ Department of Pharmaceutical and Biomedical Sciences, College of Pharmacy, University of Georgia.

² Department of Pathology, College of Veterinary Medicine, University of Georgia.

ABBREVIATIONS

DMSO	dimethyl sulfoxide
FBS	fetal bovine serum
IC ₅₀	the half maximal inhibitory concentration
LNCaP	androgen-dependent human prostate cancer epithelial cells
MTT	3-(4,5-Dimethylthiazol-2-yl)-2,5-diphenyltetrazolium bromide
PBS	phosphate buffered saline
PC-3	androgen-independent human prostate cancer epithelial cells
PI	propidium iodide
Rnase A	ribonuclease A
SRB	sulforhodamine B
TCA	trichloro acetic acid
TBS	tris buffered saline
TRIS	tris(hydroxymethyl)aminomethane buffer

ABSTRACT

Purpose: The objective of this study was to determine the effect of metronomic dosing on the activity of topotecan in prostate cancer cells *in vitro* and *in vivo*. **Methods:** The cytotoxicity of topotecan after conventional or metronomic dosing was determined by examining cellular morphology, mitochondrial enzymatic activity (MTT), total cellular protein (SRB), cell cycle, gene expression and Western blot analysis in human prostate cancer cell lines (PC-3 and LNCaP) and the effects on tumor growth in an *in vivo* tumor xenograft model. **Results:** A concentration-dependent increase in cytotoxicity was

observed in PC-3 and LNCaP cells after conventional and metronomic treatment with topotecan. A significant increase in potency (8-18 fold, after 72 hr) was observed following metronomic dosing compared to conventional administration in both cell lines. Metronomic dosing also increased the percentage of PC-3 cells in the G₂/M, compared to control, but did not alter cell cycle distribution in LNCaP cells. Differences in gene expression between cell lines and treatment schedules were observed. Metronomic dosing increased p21 protein expression in LNCaP and PC-3 cells compared to conventional dosing. The observed *in vitro* activity was confirmed using an *in vivo* model of human prostate cancer. Metronomic dosing decreased tumor volume significantly compared to control and conventional topotecan treatment. **Conclusions:** These data support the hypothesis that metronomic dosing of topotecan can increase potency compared to conventional dosing in prostate cancer. These data also suggest the novel finding that the enhanced antitumor activity of topotecan following fractionated dosing correlates to cell cycle arrest and increased expression of p21.

INTRODUCTION

Prostate cancer is the second leading cause of non-cutaneous cancer related deaths in men in the United States (www.cancer.org). Organ-confined prostate cancers are generally treated with surgery and/or radiation, and residual disease is managed with systemic therapies [1-3]. In cases of inoperable tumors, evidence of metastases, or unresponsive to radiation, chemotherapy may be the only treatment option. The location, grade, and type of tumor limit the effectiveness of therapy. Androgen ablation is the standard therapy for primary tumors and metastatic spread [4]. Unfortunately, most of the

latter patients will eventually develop castration-refractory prostate cancer, for which there are no effective treatments [5].

Advanced prostate cancers also do not respond well to current treatment protocols, which include anti-cancer drug therapy, typically cisplatin [6-8] and vincristine [9, 10], in combination with hormone ablation and/or surgery. Conventional administration schedules of traditional chemotherapeutic (*e.g.*, DNA-damaging or microtubule inhibitors) agents at or near their maximum tolerated dose (MTD) is based on their selectivity for rapidly dividing cells [11, 12]. The effectiveness of most chemotherapeutic agents is limited by the slow rate of tumor growth, non-target tissue toxicity and poor or heterogeneous intra-tumor distribution of drug [13, 14]. Thus, effective chemotherapeutic strategies for treating prostate cancer and other slow growing solid malignancies are needed.

Continuous or frequent low-dose administration (*i.e.*, metronomic or fractionated dosing) of some chemotherapeutic agents (*e.g.*, trofosfamide, cyclophosphamide, methotrexate, capecitabine, docetaxel and paclitaxel) decreases tumor growth [11, 15-18]. *In vitro* studies using human endothelial cells (ECs), human umbilical vein endothelial cells (HUVEC) and the human dermal microvascular endothelial cells (HMVEC-d) [19, 20], and *in vivo* studies show that metronomic dosing schedules inhibit tumor angiogenesis and decrease tumor vascular density and tumor growth [21-23]. However, not all of the benefits of metronomic dosing directly correlate to antiangiogenic activity. For example, a recent report showed that concurrent administration of metronomic dosing of cyclophosphamide and tirapazamine reduced gliosarcoma tumor size without impacting tumor vasculature density [24]. Although the mechanism(s) responsible for

this activity are not fully known, developing dosing schedules that exploit both direct antitumor and antiangiogenic effects may improve treatment outcomes.

The goal of this study was to determine if topotecan exhibited direct antitumor activity on human prostate cancer cell lines when dosed metronomically and to gain mechanistic insights into its cellular activity to support development of optimal dosing schedules for *in vivo* testing. Topotecan, and other camptothecin derivatives (*e.g.*, gimatecan and irinotecan) exert antiangiogenic activity when administered frequently at low doses [19, 25-27]. Camptothecins are potent cell-cycle dependent inhibitors of DNA synthesis that induce DNA double strands break through topoisomerase I inhibition [28]. Topotecan is a semi-synthetic water-soluble derivative of camptothecin. The U.S. FDA has approved topotecan for the treatment of relapsed small cell lung cancer, metastatic carcinoma of the ovary and carcinoma of the cervix. Topotecan use in prostate cancer has been limited, in part, due to its low efficacy and high non-target toxicity [29, 30]. Currently Phase I & II trials of oral topotecan administered metronomically for the treatment of gynecologic and other solid tumors are ongoing to evaluate its safety and efficacy [31, 32]; however, no studies exist assessing the effect of metronomic dosing of topotecan on prostate cancer.

MATERIALS AND METHODS

Chemicals and Reagents

FBS (fetal bovine serum) and trypsin (0.25 % w/v) were purchased from (Hyclone, Thermo Fisher Scientific Inc. Rockford, IL). F-12K Nutrient Mixture (Kaighn's Mod.) was obtained from (Mediatech, Manassas, VA). Topotecan was

purchased from 21st Century Global E-Commerce Network (East Sussex, UK). Dimethyl sulfoxide (DMSO), sulforhodamine B (SRB), TRIS buffer, acetic acid and Pierce ECL western blotting substrate for chemiluminescence were obtained from Thermo Fisher Scientific Inc. (Rockford, IL). 3-(4,5-dimethylthiazol-2-yl)-2,5-diphenyltetrazolium bromide (MTT), propidium iodide (PI), phosphate buffered saline (PBS), glucose and RNase A were purchased from Sigma-Aldrich Inc (St. Louis, MO). Absolute ethanol was purchased from Pharmco-AAPER. Mouse anti-human p53, p21 and GAPDH antibodies were purchased from Santa Cruz Biotechnology (Santa Cruz, CA). The anti-mouse secondary antibody was purchased from Promega (Madison, WI).

Cell Lines

Androgen-independent human prostate cancer epithelial cells (PC-3) and androgen-dependent human prostate cancer epithelial cells (LNCaP) were obtained from American Type Culture Collection (ATCC) (Rockville, MD). PC-3 cells were maintained in 10 % (v/v) fetal bovine serum supplemented F-12K and LNCaP cells were maintained in 10 % (v/v) fetal bovine serum supplemented RPMI-1640 media at 37 °C, 21 % O₂ and 5 % CO₂ in a humidified cell culture chamber (NuAire Inc. Plymouth, MN). Cells were sub-cultured when they reached approximately 80-90 % confluence.

Treatment Protocols

The effect of topotecan on prostate cell growth inhibition studies was conducted at 24, 48 and 72 hr. Three studies (n=3) were performed with 5 replicates for each

concentration of topotecan. Cell growth was assessed at each time point using SRB and MTT cellular staining and examination of cellular morphology.

Conventional Dosing of Topotecan

Prostate cancer cell lines (PC-3 and LNCaP) were seeded at 2×10^3 and 4×10^3 cells in 96 well plates with a 10 % (v/v) fetal bovine serum supplemented F-12K and RPMI-1640 media, respectively. Plates were incubated for 24 hr prior to media change and replacement with serum supplemented media containing topotecan (0.04 to 10,000 nM). Plates were then incubated at the same conditions for an additional 24, 48 or 72 hr.

Metronomic Dosing of Topotecan

Prostate cancer cell lines (PC-3 and LNCaP) were seeded as described in conventional dosing. To simulate metronomic dosing, cells were dosed at $t=0$, *i.e.* 24 hr after seeding as described for conventional exposures above; however, at 24 and 48 hr after initial dosing, media was removed and cells were exposed to freshly prepared serum supplemented media containing topotecan (0.04 to 10,000 nM). Media for control cells was changed daily and did not contain drug.

Assessment of Cell Growth and Viability

Cell growth and viability were assessed by measuring MTT and SRB staining at 24, 48 and 72 hr post initial topotecan exposure. SRB and MTT staining were performed as described previously [33, 34]. Briefly, MTT reagent was added to each well and plates were returned to the same conditions for 2 hr. The resultant formazan crystals were

dissolved in 200 μ L DMSO and absorbance measured at 550 nm using a Synergy HT Multi-Mode Microplate Reader (BioTek Instruments, Inc, Winooski, VT). SRB staining was performed by fixing live cells in cold 10 % (w/v) TCA for one hr at 4 °C. Fixed cells were washed with water and stained with SRB dye for 5 minutes. Excess SRB was removed by washing plates with 1 % (v/v) acetic acid, and SRB dye bound to cellular protein was dissolved in 200 μ L TRIS (10 mM). Absorbance was measured at 490 nm using a Synergy HT Multi-Mode Microplate Reader.

Assessment of Cell Morphology

Cell morphology was assessed using phase-contrast microscopy. PC-3 and LNCaP cells were seeded in 6-well plates (8×10^4 for PC-3 cells and 16×10^4 for LNCaP cells) and exposed to topotecan at the calculated IC_{50} for 72 hr (MTT) using each treatment protocol (conventional and metronomic), which was calculated from growth inhibition experiments. PC-3 cells were exposed to 80 and 10 nM, while LNCaP were exposed to 30 and 2 nM. At least three areas with approximately equal cell densities were identified in each well and images of these areas were captured with a Nikon AZ100 stereo-fluorescent microscope mounted with a Nikon Digital Sight DS-QiMc camera utilizing NIS-Elements image analysis software (Nikon, Melville, NY).

Assessment of Cell Cycle

Cell cycle was assessed at the calculated IC_{50} of topotecan after each treatment protocol (conventional and metronomic) of PC-3 and LNCaP. Cells were seeded in 6-well plates (8×10^4 for PC-3 cells and 16×10^4 for LNCaP cells) and exposed to topotecan

(conventional and metronomic dosing) at the corresponding IC₅₀ of each treatment protocol, which was calculated from growth inhibition experiments. After 24, 48 and 72 hr of exposure, cells were harvested and fixed in 70 % (v/v) ethanol and stored at 4 °C until staining. Cells were prepared for cell cycle analysis by staining with PI (50 mg/ml) in sample buffer, PBS + 1 % (w/v) glucose, containing RNase A (100 units/ml) for 30 min at room temperature. Cells (1×10⁴) were sorted and analyzed by flow cytometry using a Becton Dickinson FACSCalibur flow cytometer (BD Biosciences, San Jose, CA).

Assessment of Gene Expression

The effects of conventional and metronomic topotecan exposure on gene expression in PC-3 and LNCaP cells were assessed at the calculated IC₅₀ of topotecan after each treatment protocol 72 hr after initial topotecan exposure. RNA was isolated from cultured cells using the E.Z.N.A.[®] Total RNA Kit according to the manufacturer's protocol. Real time-PCR was performed to measure mRNA level in treated and control samples (2 µg total RNA) using the human cancer pathway finder RT² Profiler™ PCR Array System from SA Biosciences (Frederick, MD). RT-PCR analysis was done using a LightCycler[®] 480 II Real-Time PCR System from Roche Applied Science (Indianapolis, IN).

Assessment of p21 and p53 Expression

Treatment mediated effects on p21 and p53 expression were assessed at the calculated IC₅₀ of topotecan for each treatment protocol in PC-3 and LNCaP cell lines 72 hr after initial topotecan exposure. Cells were seeded in 6-well plates (8×10⁴ for PC-3

cells and 16×10^4 for LNCaP cells) and exposed to topotecan (conventional and metronomic) at the corresponding IC_{50} of each treatment protocol. At each time point, media was aspirated from the wells and cells were lysed in immunoblot buffer (0.25 M Tris-HCl, pH 6.8, 10 % glycerol, 1 mg/ml bromophenol blue, and 0.5 % (v/v) 2-mercaptoethanol). Samples were then sonicated and heated for 10 minutes at 80 °C before being loaded onto a 12 % SDS-polyacrylamide gel. Proteins were separated under reducing conditions and then transferred to a nitrocellulose membrane. Transfer efficiency was confirmed with Ponceau S staining. Nonspecific binding was limited by incubating the membrane in blocking buffer (2.5 % (w/v) casein, pH 7.6, 150 mM NaCl, 10 mM Tris-HCl, and 0.02 % sodium azide) for 3 hr. Following blocking, the membrane was incubated with the primary antibody overnight (p53 1:500, p21 1:250 and GAPDH 1:1000) and then with the appropriate secondary antibody (1:10,000) for 1.5 hr at room temperature. Bands were detected using Pierce ECL Western Blotting substrate (Thermo Scientific, Rockford, IL) for chemiluminescence.

Activity of Topotecan In Vivo

The effect of conventional and metronomic dosing of topotecan on prostate tumor growth was determined by implanting PC-3 cells subcutaneously in 8 week old male nude (NCr) mice obtained from Taconic (Taconic Farms, Inc., Germantown, NY). Animals were housed and maintained in accordance with an approved Institutional Animal Care and Use Committee (IACUC) protocol at the University of Georgia. Animals were housed in pathogen-free cages within a light and temperature-controlled isolated room and provided with autoclaved rodent chow and autoclaved water *ad libitum*.

For tumor implantation, sub confluent PC-3 cells grown in 10 % fetal bovine serum supplemented F-12K were harvested using 0.25 % trypsin (v/v). Cells were counted and re-suspended in serum free media to a final concentration of 1×10^7 cells/mL. Media was mixed with ice-cold Matrigel (1:1, v/v), and 200 μ L of the mixture was injected subcutaneously into the mouse flank. Tumors were allowed to grow and mice were monitored every other day. Tumor diameters were measured using digital calipers, recorded and tumor volumes were calculated according to the following formula, (larger dimension) \times (smaller dimension) $^2 \times 0.5$ as described previously [35, 36]. When tumors reached ~ 400 mm 3 mice were treated with intra-tumor injections of topotecan, 20 μ g/kg/day \times 30 days (metronomic dosing) or 160 μ g/kg/week \times 5 weeks (conventional dosing). Individual tumor volumes were normalized to their tumor volume on the day treatment was initiated. Treatment continued for 4 weeks, tumor dimension and animals weights were measured every other day. Animals were euthanized 3 and 7 days after the last treatment. Tumors were collected, fixed for 24 hr in 10 % (v/v) formalin, and embedded in paraffin. Tumors were sectioned and stained with hematoxylin and eosin (H&E) for histopathological examination. Micrographs were captured using a Nikon AZ100 stereo-fluorescent microscope mounted with a Nikon DS-Qi1Mc color camera and processed using NIS-Elements image analysis software.

The effect of topotecan administration on formation of blood vessels *in vivo* was assessed by immunohistochemical staining of CD31 for vascular endothelial cells. Tumor sections were treated with 3 % hydrogen peroxide for 5 min. Antigen retrieval was performed using EDTA/Tris buffer with pH 9.0, this step was heat induced using a pressure cooker for 10 min at 120 $^{\circ}$ C and protein was blocked with Powerblock[®]

(Biogenex) for 5 min. For primary antibody, sections were treated with monoclonal mouse anti-human CD31 (1:50) (DakoCytomation) for 60 min. After washing with TBS, sections were incubated with biotinylated mouse IgG for 10 min followed by streptavidin-biotin-labeled (LSAB) for 10 min (DakoCytomation). Sections were incubated with substrate-chromogen (DAB, 3,3'-diaminobenzidine) (DakoCytomation) for 12 min and counterstained with hematoxylin and 3,3'-diaminobenzidine (DakoCytomation) for 12 min. Sections micrographs were captured using a Nikon AZ100 stereo-fluorescent microscope.

Another *in vivo* study was initiated to determine the effect of continuous topotecan exposure on xenograft model of human prostate cancer. ALZET[®] micro-osmotic pumps were implanted according to the manufacturer method that is detailed in APPENDEX B. These pumps were designed to deliver topotecan at the specified doses over a period of 28 days. A group of nude mice (4 mice) were implanted subcutaneously with ALZET[®] pumps to determine topotecan plasma concentrations. Blood samples were collected using repetitive sampling from the mouse cheek and analyzed according to the method described below. Another group of mice (at least 4 animals in each cohort) were implanted with PC-3 cells in the mouse flank as described previously. When the tumor reached a volume of 200-300 mm³, mice were assigned to receive one of the following treatments: high dose (2.45 mg/kg/day) continuous exposure of topotecan, low dose (0.10 mg/kg/day) continuous exposure of topotecan, conventional high dose (4 mg/kg, q4day) I.V. or no treatment (I.V. with normal saline). Continuous exposure was achieved using a subcutaneously implanted ALZET[®] micro-osmotic pump.

Measurement of Topotecan Concentration

Total topotecan was extracted from plasma samples according to a modified published procedure [37]. Plasma samples (20 μ L) were extracted using protein precipitation with 60 μ L ice-cold methanol and by acidification with 20 μ L 100 mM phosphoric acid (H_3PO_4) to allow the detection of total topotecan. SN-38 was used as an internal standard. Samples were vortexed, kept on ice for 5 min then centrifuged at $10,000 \times g$ for 10 min at 4 $^{\circ}C$. The resultant supernatants were transferred to low volume glass vial inserts. The supernatant (20 μ L) was injected onto the HPLC column. Calibration standards of total topotecan were prepared in drug free mouse plasma and extracted as described above. A concentration range of 625-2.44 ng/mL of topotecan was used to construct standard curve and the ratios of topotecan area to the internal standard area were used to prepare the calibration curve.

Measurement of topotecan was performed on an Agilent 1100 HPLC system coupled to fluorescence detector (Santa Clara, CA) using a modified published method [38]. Topotecan was separated on a Agilent Eclipse plus C18 column (3.5 μ m, 100 \times 4.6 mm) from Agilent technologies (Santa Clara, CA) equipped with a Phenomenex Security C18 guard column (4.0 \times 3.0 mm). Analytes were eluted from the column using a gradient elution. Mobile phase A was composed of 75 mM ammonium acetate and 7.5 mM tetrabutylammonium bromide (TBAB) with pH adjusted to 6.4 using glacial acetic acid. Acetonitrile was used as mobile phase B. Gradient elution started from 12 % B and reached 30 % B at 13 min at a flow rate of 1 ml/min. Analytes signals were measured using a fluorescence detector (at excitation/emission wavelengths of 370/520 nm).

Statistical and Data Analysis

The potency (IC_{50}) of each dosing schedule was calculated by fitting data from the growth inhibition studies against topotecan concentration (C) to an inhibitory maximum effect (I_{max}) model with a baseline (E_0) effect parameter, *i.e.*, $I = E_0 - (I_{max} \times C)/(C + IC_{50})$, using WinNonlin professional software, version 5.2 (Pharsight corporation, Mountain View, CA), pharmacodynamic models were chosen to fit the data from three independent studies ($n=3$). Cell cycle data were analyzed using FlowJo software (Tree Star, Inc., Ashland, OR). PCR array data were analyzed using RT² profiler PCR array data analysis tool from SA Bioscience (Frederick, MD). A one-way ANOVA followed by Bonferroni t-tests was used to assess differences between the calculated IC_{50} 's and cell cycle distributions. Differences were considered statistically significant if a p -value was ≤ 0.05 . SigmaStat for Windows (v 3.11, Systat Software, Inc.) was used for statistical analysis.

RESULTS

Topotecan Exposure

The effect of conventional and metronomic administration of topotecan on prostate cancer cells were assessed by measurement of MTT and SRB staining. Metronomic dosing was simulated by aspirating and replacing with fresh media and drug after 24 and 48 hr. Metronomic exposure of PC-3 cells to topotecan resulted in significant ($p \leq 0.05$) time-dependent decreases in SRB and MTT staining as well as IC_{50} after 24, 48 and 72 hr, compared to conventional treatment (**Figure 2-1, Table 2-1**). A similar

decrease in MTT (**Table 2-1**) and SRB staining, *i.e.*, increased potency, was observed in LNCaP cells following metronomic dosing compared to conventional exposure.

Table 2-1 demonstrates that metronomic dosing with topotecan increased the potency (lowered the IC_{50} , by MTT) of topotecan significantly compared to conventional dosing in both LNCaP and PC-3 cells. In LNCaP cells, metronomic dosing decreased the IC_{50} by 18-fold (1.4 *vs.* 26 nM) after 72 hr. For PC-3 cells, metronomic dosing decreased the IC_{50} 8-fold (9.3 *vs.* 80 nM at 72 hr) in comparison to conventional dosing.

Morphology Assessment

PC-3 and LNCaP cells were exposed to metronomic and conventional dosing of topotecan at the calculated IC_{50} for each treatment regimen at 72 hr and cellular morphology was assessed using phase-contrast microscopy. Micrographs of PC-3 cells exposed to both conventional and metronomic dosing regimens showed decreases in cell density compared to control cells (**Figure 2-2 A-C**). In agreement with SRB and MTT assays, cell densities of PC-3 cells exposed to metronomic and conventional dosing regimens decreased compared to untreated controls (**Figure 2-2 B and C**). For LNCaP cells, similar decreases in cell density were observed following conventional (**Figure 2-2 E**) and metronomic treatment (**Figure 2-2 F**) in comparison to untreated controls (**Figure 2-2 D**).

Cell Cycle Analysis

PC-3 cells were exposed to topotecan at the calculated IC_{50} for both treatment protocols. Treatment of PC-3 cells with topotecan at the conventional calculated IC_{50}

resulted in cellular toxicity that inhibited assessment of cell cycle (data not shown). Treatment of PC-3 cells metronomically at IC₅₀ (10 nM) increased the percentage of cells in G₂/M phase significantly (**Figure 2-3 A-C**), with a concomitant decrease in G₁ population. An increase in the S phase was also observed, but this difference was not statistically significant. The only differences in cell cycle observed in LNCaP cells after conventional or metronomic dosing at any time point was a slight increase in sub G₁ cells compared to control (**Figure 2-3 D-F**).

Assessment of Gene Expression

In order to gain insight into the molecular events mediating decrease in IC₅₀ during metronomic treatment of PC-3 and LNCaP. Cells were treated with topotecan for 48 and 72 hr at the calculated IC₅₀ for each treatment protocol (conventional vs. metronomic) and mRNA expression was analyzed using RT-PCR. A global change in gene expression was noted between cell lines (PC-3 vs. LNCaP) (**Figure 2-4**) and between treatment protocols in both cell lines (**Figure 2-5 and 2-6**). In PC-3 cells 6 out of 84 genes were altered after 72 hr treatment with conventional high dose exposures in comparison to untreated control. These genes include CDKN1A (p21), FOS, IFNB1, MTSS1, TNF and VEGFA (**Table 2-2**). For LNCaP cells, 6 genes were altered after 72 hr treatment with conventional high-dose exposure in comparison to untreated control. These genes include ANGPT2, CDKN1A (p21), PLAU, SERPINB5 and TNF (**Table 2-2**).

Assessment of p21 and p53 Expression

Our previous studies in LNCaP and PC-3 cells using other lactone derivatives demonstrated that G₂/M arrest correlated to activation of p21, and that p21 could be activated in the absence of p53 [39, 40]. Thus, we assessed the hypothesis that changes in cell cycle induced by metronomic dosing regimens were mediated by p21 using immunoblot analysis. We also assessed p53 expression in LNCaP cells as these underwent a slight, but significant sub G₁ arrest after 72 hr, which can be mediated by p53. The expression of GAPDH was used as a loading control. An increase in p21 expression was detected following metronomic topotecan exposure in both cell lines (**Figure 2-7**) compared to untreated controls. Increases in p21 expression were detected 72 hr post initial metronomic topotecan exposure in LNCaP and PC-3 cells. Expression of p21 increased after 72 hr exposure in both cells lines. Slight increases in p21 expression were also observed in PC-3 cells after conventional dosing regimens, which were lower than that seen with metronomic dosing. No increases in p53 expression were detected in LNCaP cells under any condition tested (data not shown). The expression of p53 in PC-3 cells was not observed. This is not unexpected, as these cells are p53 null.

Topotecan In Vivo Tumor Xenograft Activity

The effect of metronomic dosing of topotecan on tumor growth was determined using an *in vivo*, xenograft tumor model of human prostate cancer in male (NCr) nude mice. The doses of topotecan were chosen based on a previous study examining the effect of intra-cerebral administration of topotecan for the treatment of brain tumors [41]. Conventional dosing of topotecan (160 µg/kg) was carried out by direct tumor injection

once a week, while metronomic dosing of topotecan (20 µg/kg) was carried out by direct tumor injection daily. After 17 days of treatment, animals subjected to metronomic dosing with topotecan had a significantly ($p \leq 0.05$) smaller tumor volume (65.4 % ± 11.2) compared to control animals (136 % ± 14) and those treated conventionally (138 % ± 10) (**Figure 2-8 A**). At the conclusion of the study animals subjected to the metronomic dosing regimens of topotecan had significantly ($p \leq 0.05$) smaller tumor volumes (54.8 % ± 16.5) than animals receiving conventional dosing (144 % ± 11) or the control group (207 % ± 26). No significant differences in animal weights were observed during treatment (**Figure 2-8 B**). Histopathological examination revealed treatment mediated differences between control and treatment groups. Control (**Figure 2-9 A and B**) and animals treated conventionally (**Figure 2-9 C and D**) had larger tumors and evidence of necrosis, regions of hypereosinophilia and loss of tissue architecture, compared to metronomically (**Figure 2-9 E and F**) dosed groups. Animals treated metronomically had tumors that were smaller in size with no evidence of necrosis.

The effect of topotecan exposure on formation of blood vessels *in vivo* was assessed by CD31 staining for vascular endothelial cells. Initial assessment of the tumor slide suggests decreased CD31 staining in tissue slices from tumor exposed to metronomic schedule (**Figure 2-10 C**). For control and conventionally treated cells, CD31 staining was high in comparison to metronomically treated mice (**Figure 2-10 A-B**). This finding suggests that topotecan can exert an angiogenic activity with metronomic dosing against prostate cancer *in vivo*. Also, non-specific staining of spindle cells (fibroblasts and myofibroblasts), tumor cells, tumor infiltrating lymphocytes, and

debris within and at the periphery of the tumor were observed in conventional and control group.

In order to achieve a continuous low dose exposure of topotecan, ALZET[®] micro-osmotic pumps were implanted subcutaneously into nude mice and plasma concentrations were determined by HPLC-FL. With a constant dose of 2.45 mg/kg/day, plasma topotecan achieved a plasma concentration of 3-4 ng/mL (**Figure 2-11**). This plasma concentration is similar to the calculated IC₅₀ of topotecan *in vitro* (4.57 ng/mL). Further studies were carried out to characterize the efficacy of topotecan when administered continuously *in vivo*.

For topotecan activity *in vivo* following continuous systemic exposure. After 21 days of treatment, animals subjected to metronomic dosing with high and low dose of topotecan had a significantly ($p \leq 0.05$) smaller tumor volume compared to control animals (**Figure 2-12 A**). No significant difference was detected between animals treated conventionally with topotecan and the control group. No significant differences in animal weights were observed during treatment (**Figure 2-12 B**).

DISCUSSION

Treatment options for prostate cancers are limited, and no effective chemotherapy for advanced prostatic cancer (androgen-independent) is available. The use of conventional high dose topotecan for the treatment of prostate cancer clinically is limited due to its low efficacy and high incidence of side effects [29]. Thus, we hypothesized that low-dose continuous administration of topotecan may be used to increase its potency in prostate cancer compared to conventional dosing regimens. This hypothesis is supported

by metronomic dosing studies in normal human endothelial cells *in vitro*, and *in vivo* studies using mouse corneal revascularization models [25, 26]. Further, topotecan significantly inhibited tumor growth following low-dose exposure in experimental Wilms' tumor [42]. Data reported in this study advances previous work by suggesting the novel finding that metronomic dosing increases the efficacy of topotecan in models of human prostate cancer. Furthermore this study suggests that the mechanisms of these events correlate to changes in cell cycle and the expression of p21.

Understanding the effect of metronomic low-dose exposure on the activity of topotecan against cancer cells can be used as a guide to optimize dosing regimens of topotecan and to enhance the activity of topotecan on angiogenesis and directly on tumor parenchyma. To understand differences in drug activity against different prostate cancer stages, we used two types of prostate cancer cell lines, LNCaP and PC-3. LNCaP cells demonstrate the characteristics of prostate cancer in early stages of malignancy and were used to evaluate the potential role of topotecan metronomic schedule in the treatment of early stage of prostate cancer [43]. In contrast, PC-3 cells were used to evaluate changes associated with different topotecan dosing regimens on advanced prostatic cancer [44]. Data reported above suggest that metronomic dosing schedules increased the efficacy of topotecan in both local and advanced prostate cancer, and may be effective at treating metastatic spread. The fact that metronomic dosing increased the efficacy of topotecan in both LNCaP and PC-3 cells suggests that metronomic dosing increases efficacy using mechanisms that are independent of androgen-signaling, p53 status, or its known antiangiogenic effects.

We also showed that metronomic dosing of topotecan increased significantly the percentage of PC-3 cells in G₂/M of PC-3 cells, while only slight differences in cell cycle were observed in LNCaP cells. It should be noted that metronomic dosing increased potency in LNCaP cell greater than PC-3 cells (4.5 and 18 versus 2.9 and 8.6 fold at 48 and 72 hr) and that this may be related to differences in cell cycle alterations. Alterations in p53 expression cannot explain this observation because neither treatment schedule, nor cell line had observable differences in the expression of this protein, as determined by immunoblot.

cDNA array analysis showed an increase in the expression level of various important regulatory cancer genes following conventional dosing of topotecan in comparison to untreated control, including p21. This increase was only found following conventional dosing of topotecan and no significant increases in expression of these genes were found following metronomic dosing of topotecan; however, it should be noted that our criteria for increased expression, compared to control was 2.5-fold and that the expression of several genes in metronomic treated cells increased at least 2-fold.

We hypothesized that metronomic dosing may mediate direct antitumor effects in addition to its documented antiangiogenic activity. Expression of p21 plays important roles in regulating cell cycle and its over expression results in G₂/M arrest [45]. Increases in p21 expression are associated with earlier clinical stages of pancreatic adenocarcinoma and enhanced survival rate [46]. Another study suggests p21 expression improved survival in prostate cancer patients and is a better prognostic factor for advanced gastric carcinoma [47, 48]. Thus, it's possible that, in addition to inhibition of angiogenesis, increases in efficacy induced by metronomic dosing can be mediated by increased p21

expression. It is also possible that p21 alterations are induced by the same mechanism that mediates antiangiogenic activity. Further studies are needed to test these hypotheses.

The mechanisms by which metronomic dosing regimens increase p21 expression are still under study. Increases in p21 protein were observed after both conventional and metronomic treatments, they were just higher in metronomic treated cells. This suggests that metronomic dosing enhanced a pathway activated directly by topotecan. cDNA array analysis showed that conventional doses resulted in larger increases in p21 gene transcription than metronomic doses. This suggests that the mechanisms involved in increased p21 protein expression after metronomic dosing is not mediated by increase in transcription. Further, increases were also detected in PC-3 cells, which are p53-null, so the mechanism of induction probably isn't mediated by p53. This hypothesis is supported by the fact that greater increases in p21 expression were seen in PC-3 cells based on both cDNA array and immunoblot analysis.

One possible mechanism by which metronomic dosing increases p21 expression in these studies is post-translational modifications. These include altering mRNA stability, inhibiting degradation by ubiquitin and microRNA [49]. miRNA are small non-coding RNA that negatively interfere with mRNA function through specific cleavage of mRNA which can inhibit translation [50, 51]. Recent evidence suggests roles for various tumor miRNAs in the induction p21 in prostate cancer [52]. Specifically, studies showed that miRNA-106b and miRNA-93 promote cell proliferation by altering p21 translation [53]. Studies also suggested roles for miRNA in chemoresistance in PC-3 cells [54]. None of these studies tested the effect of metronomic dosing regimens on p21 expression and miRNA, which is a subject of future work.

We demonstrated that low-dose, daily administration of topotecan enhanced its antitumor activity in a model of human prostate cancer after direct tumor injection and continuous systematic exposure. Our data also supports previous studies that have demonstrated conventional high-dose administration of topotecan is only marginally effective compared to control tumor growth. However, the antitumor activity of topotecan administered at lower doses was highly efficacious and appeared to have no statistically significant effect on body weight, a gross measure of systemic toxicity. We believe that these data are the first to demonstrate such a finding in prostate cancer for topotecan. Thus, these data will now serve as benchmarks to determine optimal doses for further preclinical testing and translation to the clinical setting.

It is also interesting to note that histopathological analysis of tumors from animals treated with intra-tumor conventional, high-dose treatment, had evidence of necrosis compared to the groups treated following a metronomic schedule. According to the Gleason score, histopathological evidence of necrosis is correlated with increased tumor malignancy and poor prognosis [55]. This further suggests that metronomic dosing altered tumor growth phenotype and decreased its malignancy compared to control and conventional treatment. Tumor tissue staining for CD31, suggest that topotecan will maintain its angiogenic inhibition in prostate cancer.

Data reported herein show that metronomic dosing increases the efficacy of topotecan both *in vitro* and *in vivo*. These results support existing preclinical and clinical studies that have shown metronomic dosing of topotecan orally in non-prostate cancer models increases efficacy and is well tolerated with lower side effects compared to conventional administration [56]. However, to our knowledge, this is first time

metronomic dosing of topotecan has been shown to increase efficacy against prostate cancer cells *in vitro* and an *in vivo* model. These data suggest that metronomic dosing of topotecan may be useful for treatment of prostate cancer and supports further investigation.

In conclusion, we showed that low-dose frequent administration of topotecan increased its anticancer efficacy in both *in vitro* and *in vivo* models of prostate cancer. Data in this study also demonstrate that the observed increase in efficacy was independent of the androgen receptivity of the prostate cancer as well as its p53 status. Immunoblot analysis showed that metronomic dosing increased p21 expression, compared to conventional dosing regimens, suggesting that differential effects of metronomic dosing in cancer cell growth compared to conventional dosing may be mediated by this protein.

ACKNOWLEDGEMENTS

This research was funded in part by an UGA Faculty Research Grant, an Interdisciplinary Toxicology Program equipment grant and Georgia Cancer Coalition Distinguished Scholar Grants to BSC and RDA, a Saudi Arabian Cultural Mission Fellowship to IAA, and graduate stipend support to JM funded by a grant from the NIH, NIBIB-EB008153 to RDA/BSC).

Table 2-1. Effect of treatment and time of exposure on topotecan potency (IC₅₀).

Time (hr)	PC-3			LNCaP		
	Conventional (nM)	Metronomic (nM)	Change (fold)	Conventional (nM)	Metronomic (nM)	Change (fold)
24	183 ± 53	N.A.	N.A.	58.3 ± 10.6	N.A.	N.A.
48	133 ± 16	46.0 ± 10.5*	2.9	24.7 ± 4.3	5.45 ± 0.75*	4.5
72	79.6 ± 10.2	9.3 ± 1.5*	8.6	26 ± 6	1.42 ± 0.23*	18

Data are presented as mean ± S.E.M. (n=5) of at least three independent studies. Values noted with (*) are significantly ($p \leq 0.05$) different in comparison to conventional determined by MTT.

Table 2-2. Alteration in mRNA expression (fold regulation) in comparison to control for key regulatory genes. PC-3 and LNCaP cells exposed to different treatment protocols of topotecan for 48 and 72 hr.

Gene	PC-3				LNCaP			
	Conv.	Metro.	Conv.	Metro.	Conv.	Metro.	Conv.	Metro.
	(80 nM)	(10 nM)	(80 nM)	(10 nM)	(30 nM)	(2 nM)	(30 nM)	(2 nM)
	48 Hr		72 Hr		48 Hr		72 Hr	
ITGB3	9.36	1.48	1.23	1.87	-1.87	-1.40	1.03	1.22
CDKN1A	7.71	1.41	10.1	1.46	11	1.7	9.84	2.04
IL8	4.88	2.23	2.74	1.87	-2.39	-1.39	-1.98	1.12
MMP2	4.02	1.37	-1.21	1.02	-1.05	-1.22	-1.07	1.15
TERT	4.02	1.37	-1.21	1.13	-1.05	-1.22	-1.07	1.17
TIMP3	4.02	1.37	-1.21	1.02	-1.05	-1.22	-1.07	1.15
FGFR2	3.99	1.36	-1.21	1.02	2.34	1.40	2.39	1.09
GZMA	3.77	2.26	1.71	1.29	-2.29	-2.05	-1.17	1.40
FOS	3.47	1.9	7.29	-1.16	2.09	-1.42	1.49	-1.03
IFNB1	3.22	1.75	3.33	-1.32	-1.05	-1.05	-1.02	1.15
MTSS1	3.11	1.33	2.6	2.12	-1.05	-1.02	1.46	1.29
IGF1	2.98	1.79	-1.94	-1.39	-2.42	-1.48	-2.81	-1.08
SNCG	2.56	-1.04	1.46	1.43	-1.58	-1.31	-1.39	1.27
THBS1	2.54	1.63	-1.42	1.04	1.75	1.19	1.55	1.39
TNF	1.22	-1.36	2.69	1.02	3.54	-1.3	14.3	1.79
VEGFA	1.18	1.27	2.51	1.1	-1.09	-1.18	-1.32	-1.14
SERPINB5	2.49	-1.04	1.63	-2.07	10.8	1.66	8.68	1.59
FAS	2.06	-1.17	2.46	2.42	4.61	1.08	4.52	1.21
ANGPT2	1.09	1.52	1.53	-1.12	2.82	1.14	4.82	1.53
MDM2	-1.14	1.29	-1.63	-1.16	2.82	1.1	2.29	1.24
ITGA3	-1.76	1.61	-1.48	1.28	2.67	1.05	1.9	1.52
JUN	-2.02	1.36	-1.33	1.07	2.61	1.32	1.91	1.69
PLAU	-1.36	1.17	-1.42	1.22	-1.45	1.01	2.67	1.47

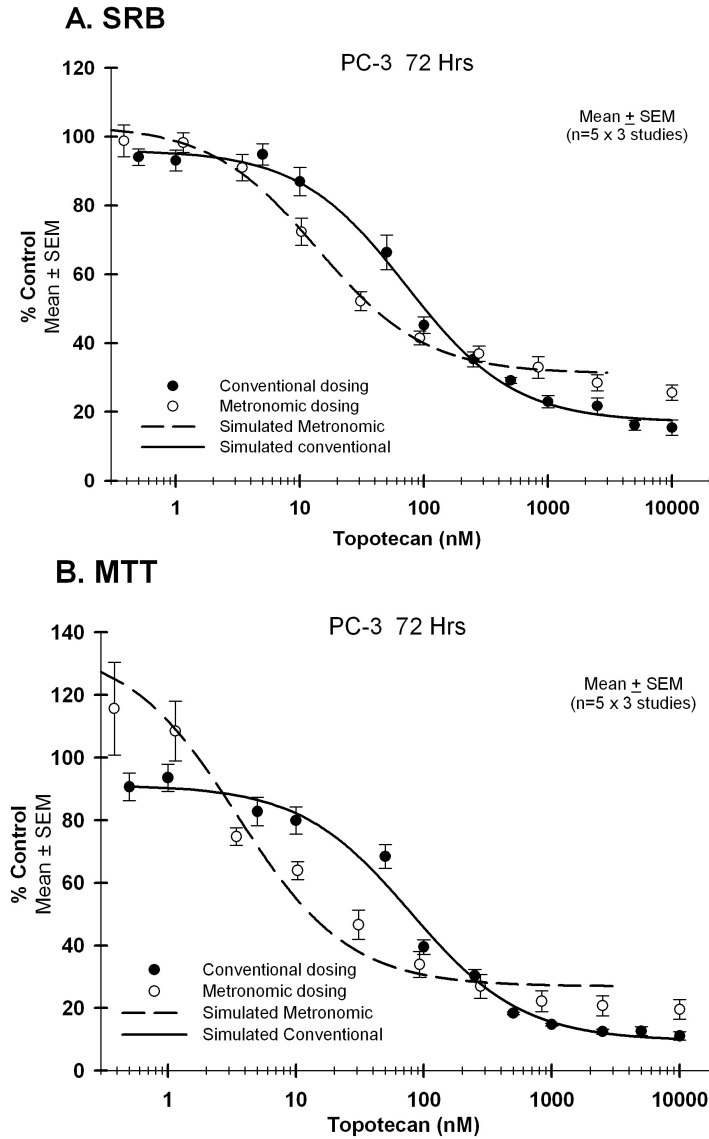


Figure 2-1. Effect of topotecan on the growth of prostate (PC-3) cells *in vitro*. A concentration-dependent decrease in **A.** protein staining (SRB) and **B.** mitochondrial activity (MTT) was observed following increasing drug concentrations. Changing the media/drug daily (to mimic metronomic dosing) achieved an IC_{50} of ~ 10 nM, compared to 80 nM following single exposure after 72 hr. Data are presented as mean \pm S.E.M. (n=5) of at least three independent studies.

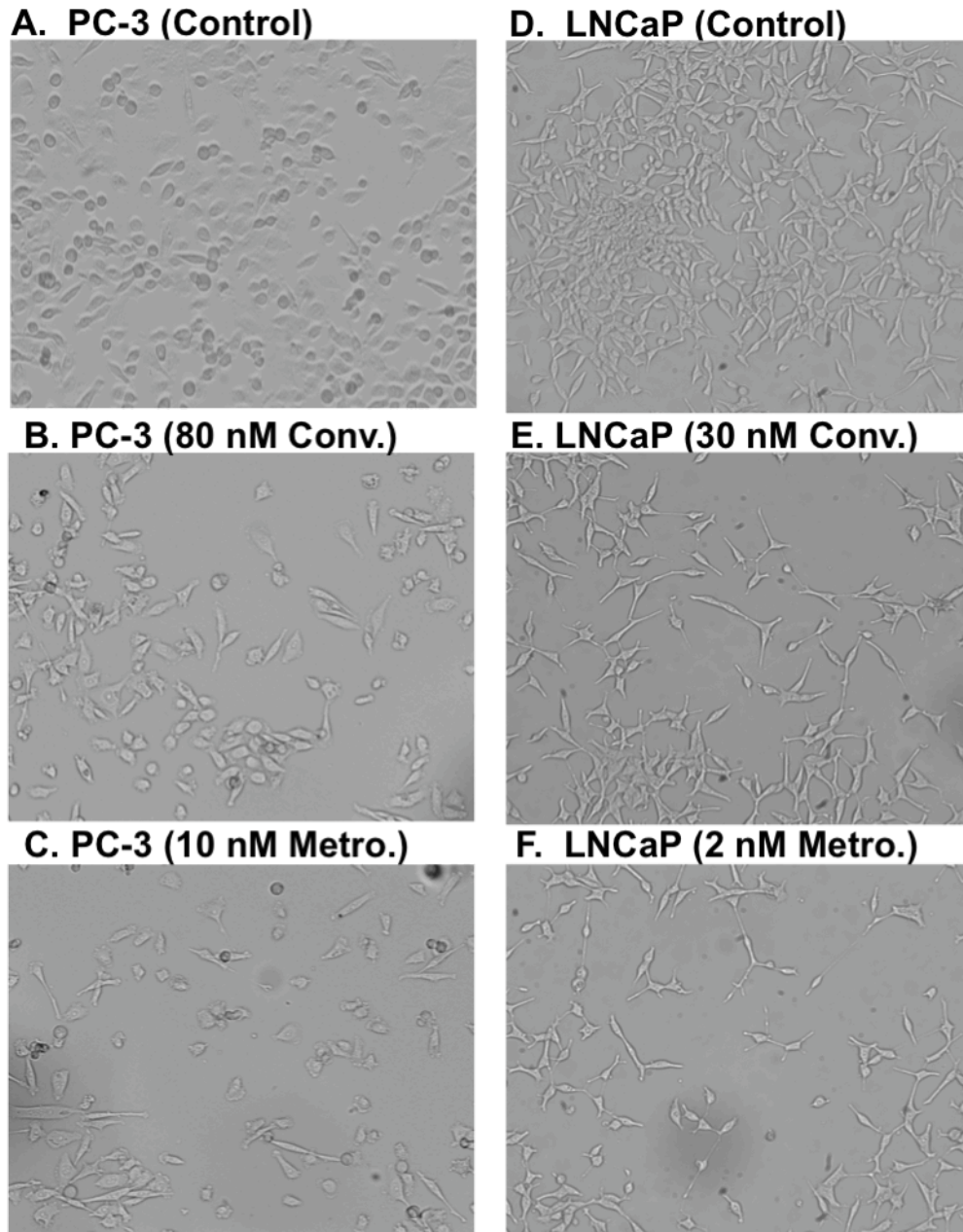


Figure 2-2. Effect of different dosing regimens of topotecan on cellular morphology.

Phase contrast images were captured after treatment with different dosing regimen of topotecan at the calculated IC_{50} . PC-3 and LNCaP cells were seeded in 6 well plates, after 24 hr media was replaced with fresh media containing the concentrations of topotecan representing the conventional IC_{50} (80 nM for PC-3 and 30 nM for LNCaP) or the

metronomic IC_{50} (10 nM for PC-3 and 2 nM for LNCaP). Media with fresh drug was changed daily to simulate metronomic dosing.

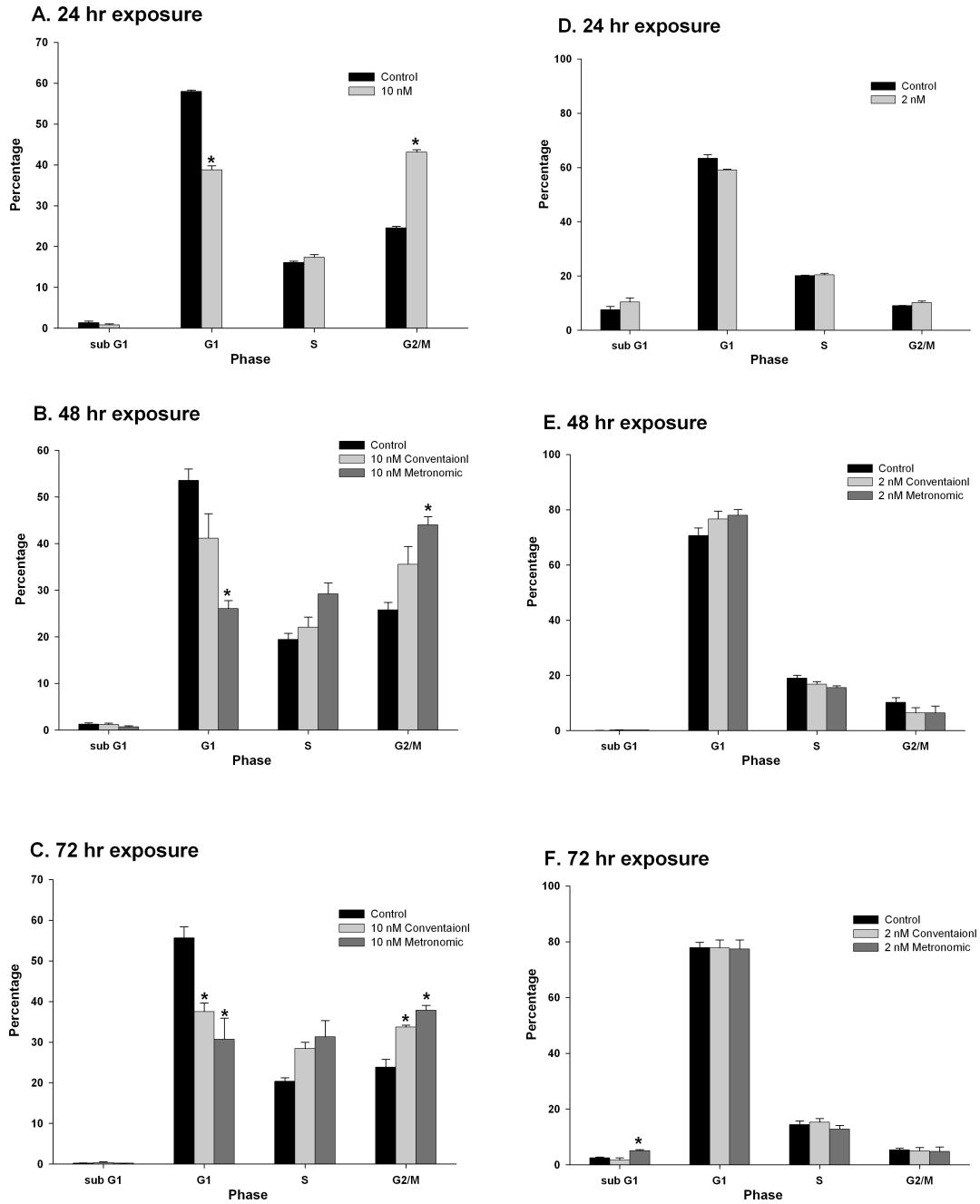


Figure 2-3. Effect of topotecan on PC-3 and LNCaP cell cycle. PC-3 cells were exposed to 10 nM topotecan using different protocols (conventional vs. metronomic) for 72 hr and LNCaP cells were exposed to 2 nM topotecan. Media containing fresh topotecan was changed daily to simulate metronomic dosing. At each time point, cells

were harvested and stained with PI and cell cycle phases were assessed by flow cytometry. Data are presented as the mean \pm S.E.M. of three separate experiments. Means noted with (*) are significantly ($p \leq 0.05$) different in comparison to control.

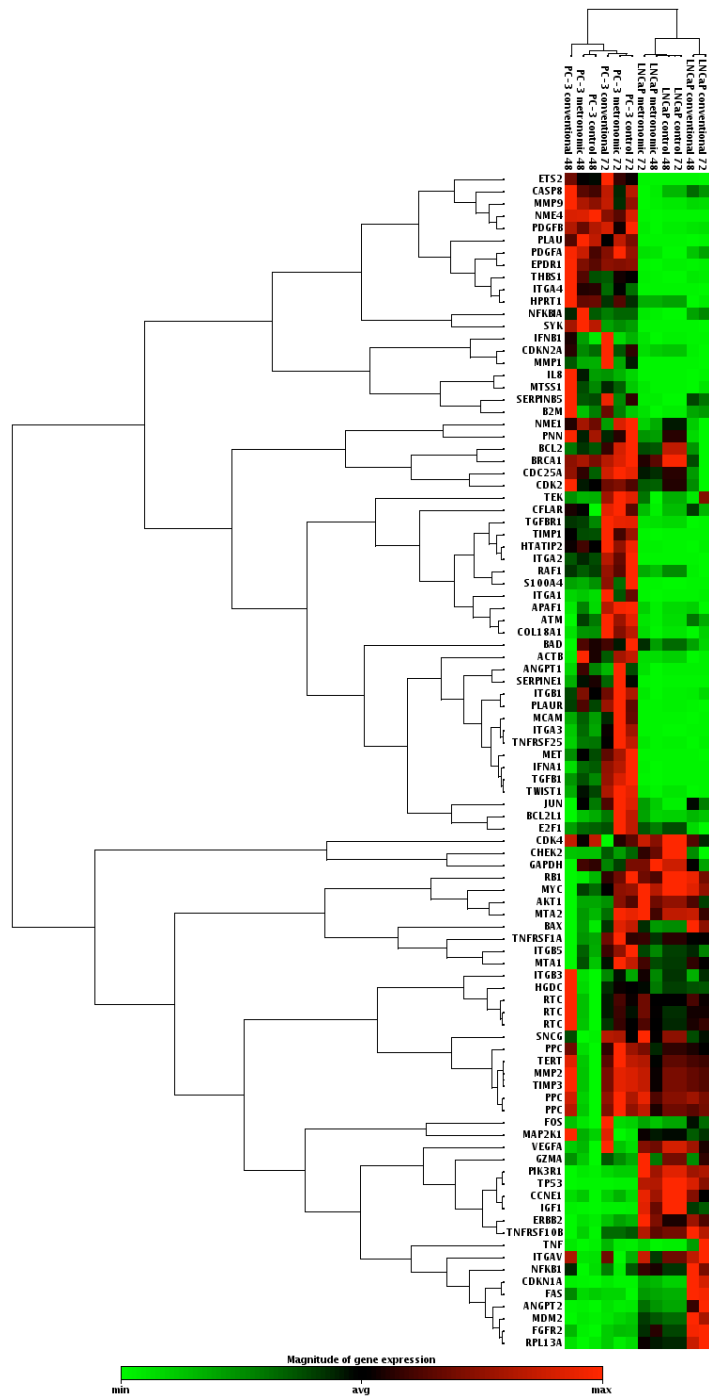


Figure 2-4. Gene expression profiling by RT-PCR array of PC-3 and LNCaP cells exposed to metronomic or conventional treatment of topotecan. Each treatment schedule was based on the calculated IC_{50} for each treatment protocol after 72 hr exposure.

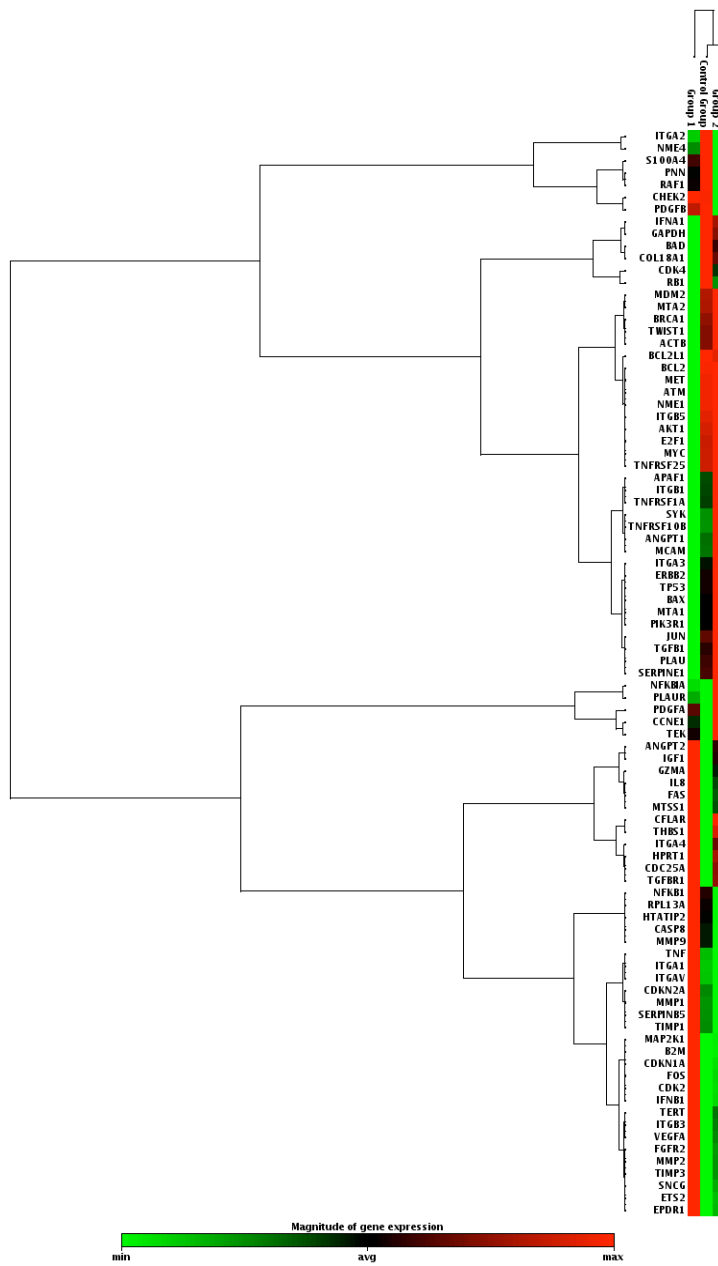


Figure 2-5. Gene expression profiling by RT-PCR array of PC-3 cells exposed to metronomic or conventional treatment of topotecan. Groups were formed based on treatment cohort. Each treatment schedule was based on the calculated IC_{50} for each treatment protocol after 72 hr exposure (Group 1=Conventional and Group 2=Metronomic).

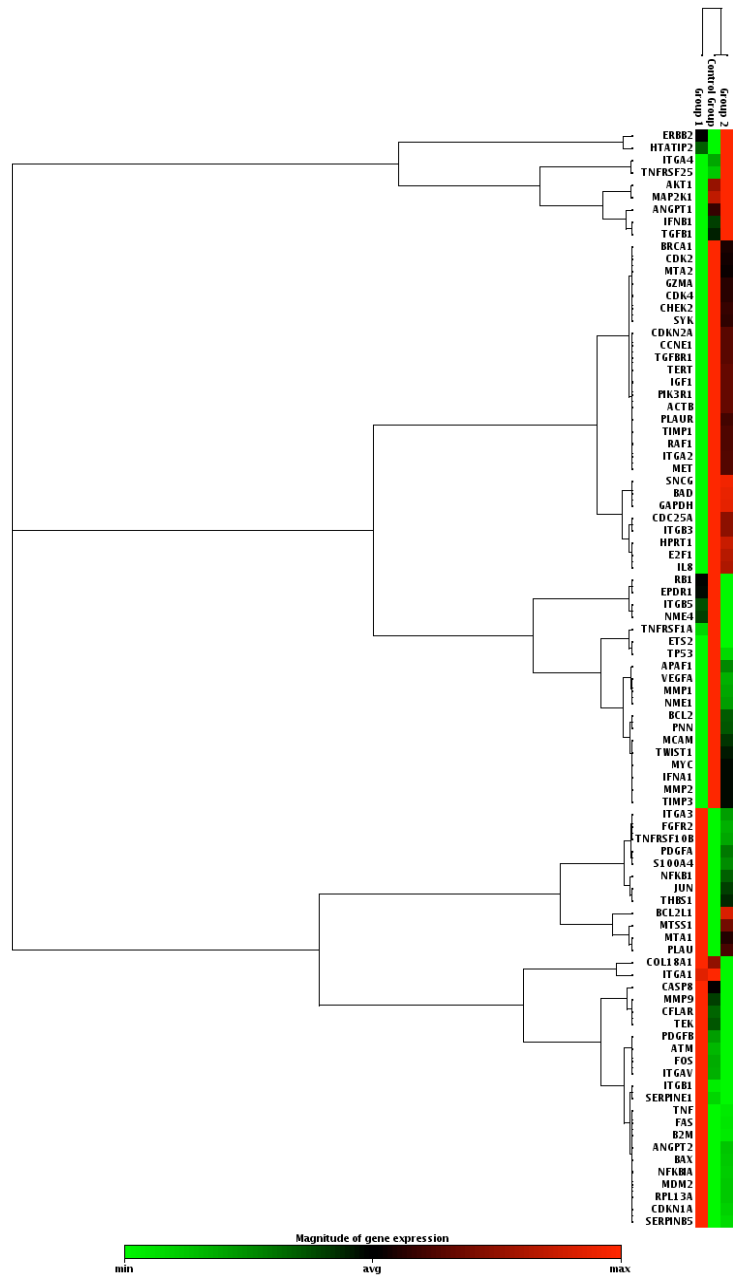


Figure 2-6. Gene expression profiling by RT-PCR array of LNCaP cells exposed to metronomic or conventional treatment of topotecan. Groups were formed based on treatment cohort. Each treatment schedule was based on the calculated IC_{50} for each treatment protocol after 72 hr exposure (Group 1=Conventional and Group 2=Metronomic).

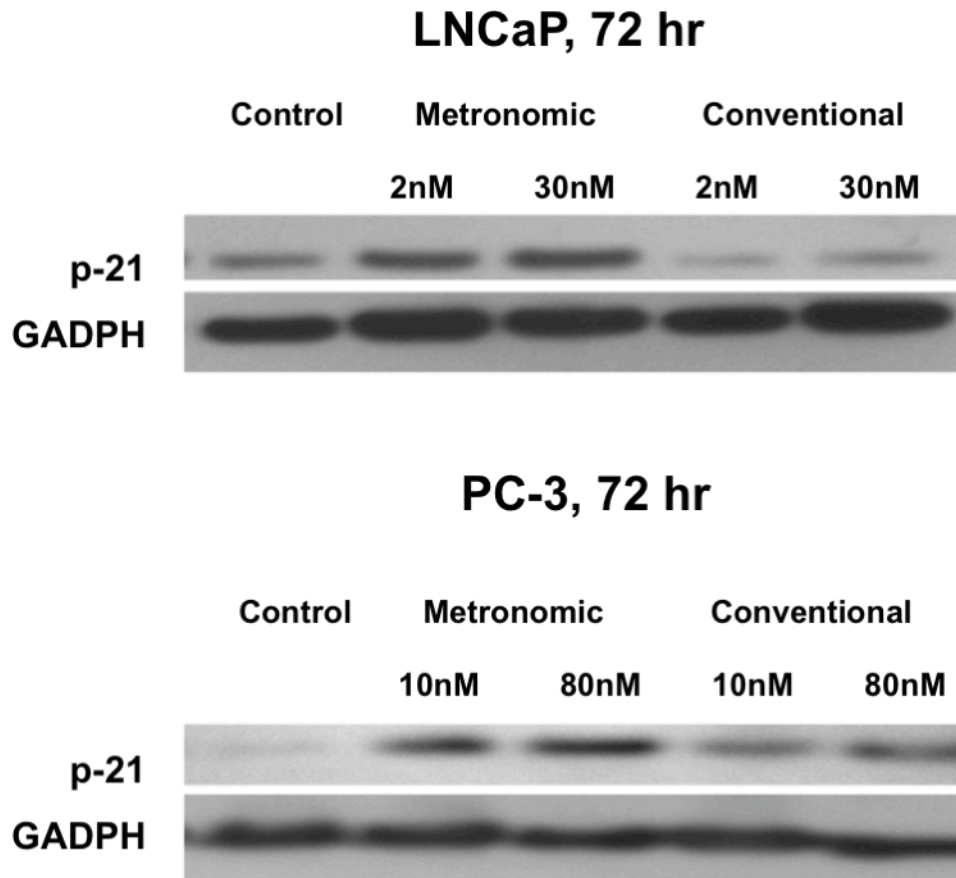


Figure 2-7. Effect of topotecan on p21 expression in LNCaP and PC-3 cells. Both cells were exposed to topotecan at the calculated IC_{50} for each treatment protocol (conventional vs. metronomic) at 72 hr. For conventional exposure, media containing topotecan was not changed after initial exposure. For metronomic exposure, media containing topotecan was changed daily to simulate metronomic dosing. The expression of glyceraldehyde 3-phosphate dehydrogenase (GAPDH) is shown as a loading control. All blots are representative of at least three different experiments.

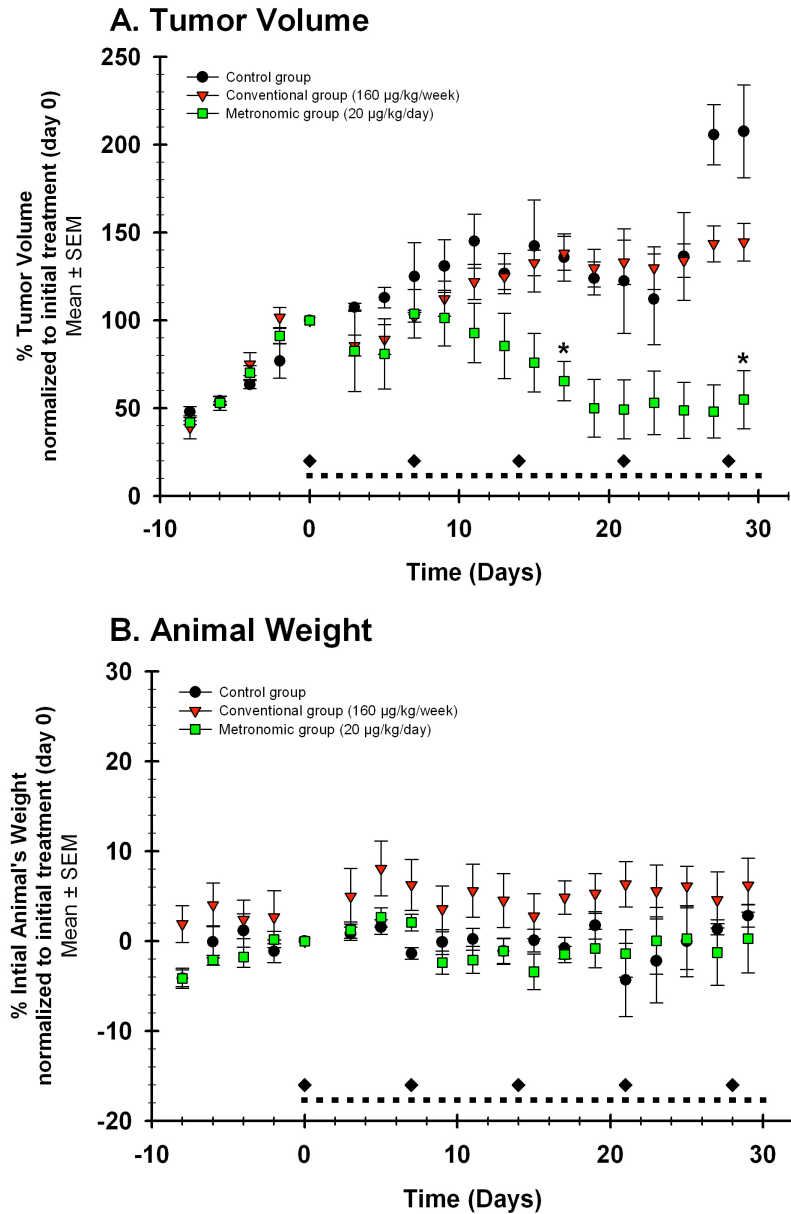


Figure 2-8. Effect of topotecan *in vivo* using xenograft model of human prostate cancer. A. Tumor volume. Effect of topotecan dosing on tumor volume in NCr nude mice implanted subcutaneously with prostate (PC-3) cells. Topotecan was administered intra-tumorally following a conventional (160 mg/kg/week \times 5, represented by diamonds on x-axis) or metronomically (20 mg/kg/day \times 30, represented by squares along x-axis) schedule. A significant ($p \leq 0.05$) reduction in tumor volume was observed following

metronomic exposure of topotecan vs. control and conventional treatments. **B.** Animal weight. Change in percentage of animal weight was observed as a gross measurement of toxicity; no significant change in percentage of initial animal weight was associated with all treatment protocols. Data are presented as the mean \pm S.E.M. (n=5). Means noted with (*) are significantly ($p \leq 0.05$) different in comparison to control.

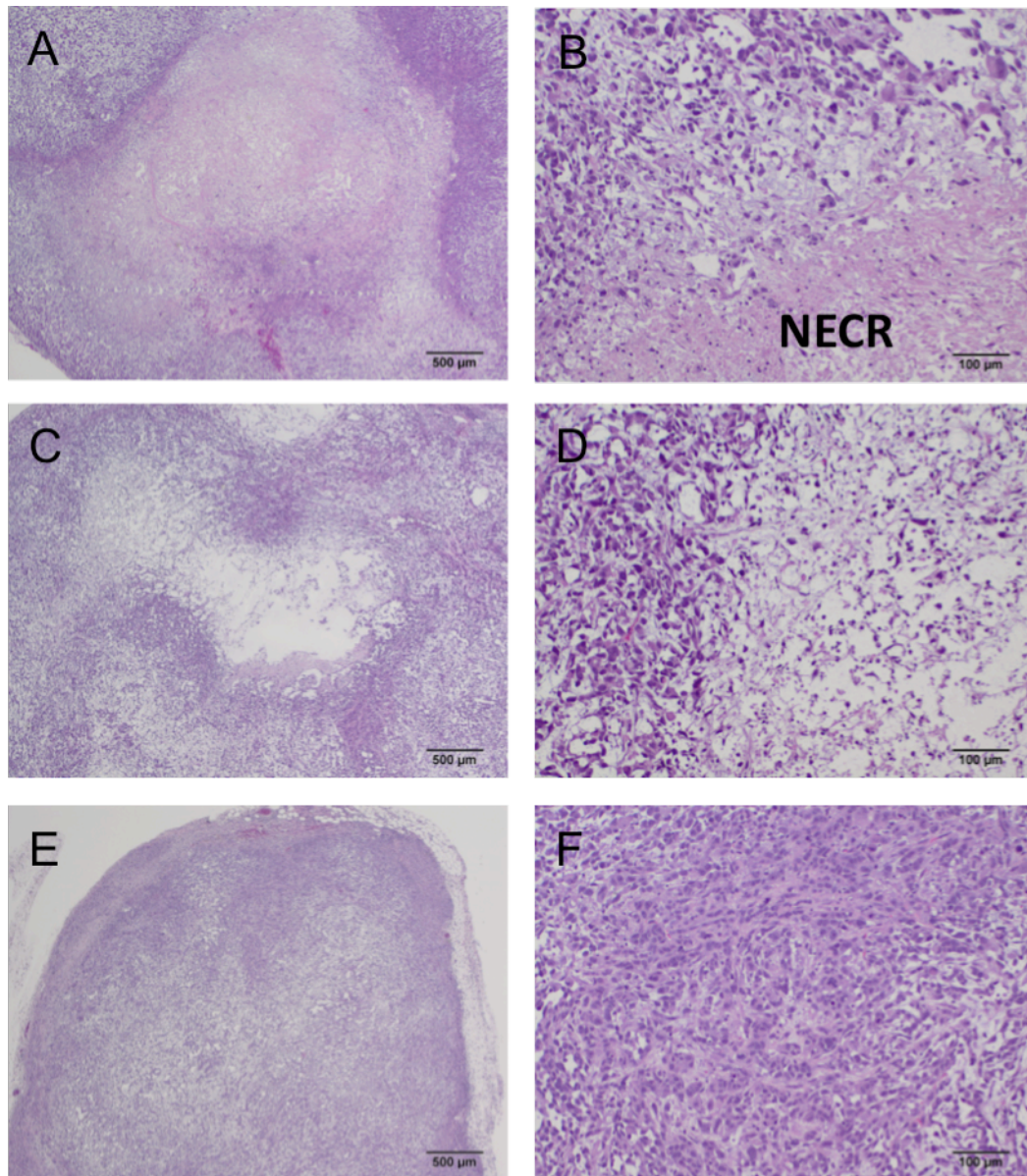


Figure 2-9. Representative histological images of mouse PC-3 tumor xenografts treated with different dosing regimens of topotecan and stained with hematoxylin and eosin (H&E). When tumors reached 400 mm³ mice were treated with intra-tumor injections of topotecan 20 mg/kg/day × 30 (metronomic) or 160 μg/kg/week × 5 (conventional dosing); control groups received no treatment. Micrographs of representative tumor sections at low (20×, **A, C, E**: scale bars = 500 mm) and high (100×,

B, D, F: scale bars = 100 mm) magnification were examined three days after the last treatment. Control tumors had large areas of necrosis within the tumor (**A**). The necrotic area (NECR) is clearly distinct from the viable tissue and characterized by hypereosinophilia and loss of tissue architecture (**B**). Conventionally treated tumors had evidence of necrosis (**C, D**). Note the necrotic area in the center of the image characterized by hypereosinophilia and loss of tissue architecture. Metronomically treated tumors had no appreciable necrosis visible within the tumor (**E, F**). Metronomically treated tumor cells were arranged in haphazard fashion (including looser arrangement on the right side of the image), but with no evidence of necrosis.

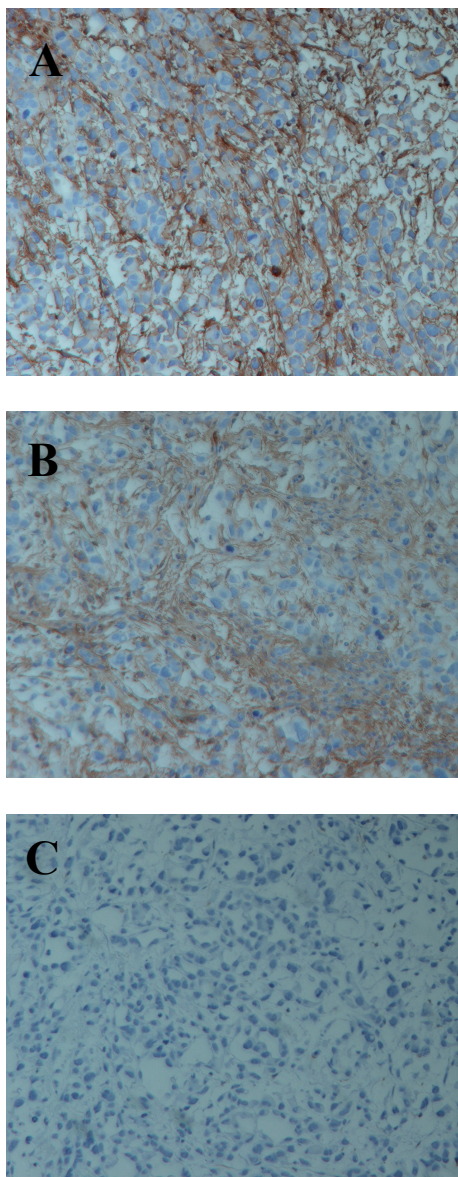


Figure 2-10. Representative histological images of mouse PC-3 tumor xenografts treated with different dosing regimens of topotecan and stained for CD31. Micrographs of representative tumor sections were examined three days after the last treatment. **A.** Control tumors and **B.** conventionally treated showed a moderately strong and consistent staining for CD31, a vascular marker. While for metronomic dosing **C.**, had limited staining for endothelial cells.

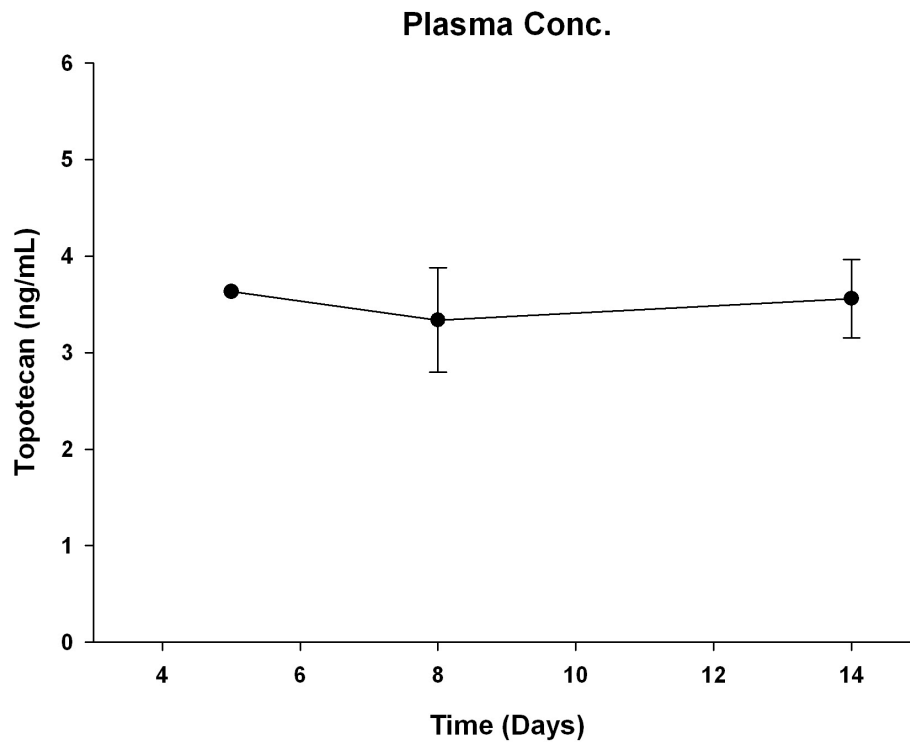


Figure 2-11. Effects of continuous topotecan exposure on topotecan plasma concentration. Animals received subcutaneous implants of ALZET[®] micro-osmotic pumps (model 1004), which delivered topotecan at a dose of 2.45 mg/kg/day for 28 days. This dose was able to achieve a plasma concentration close to the calculated IC₅₀ of topotecan against PC-3 cells (4.57 ng/mL).

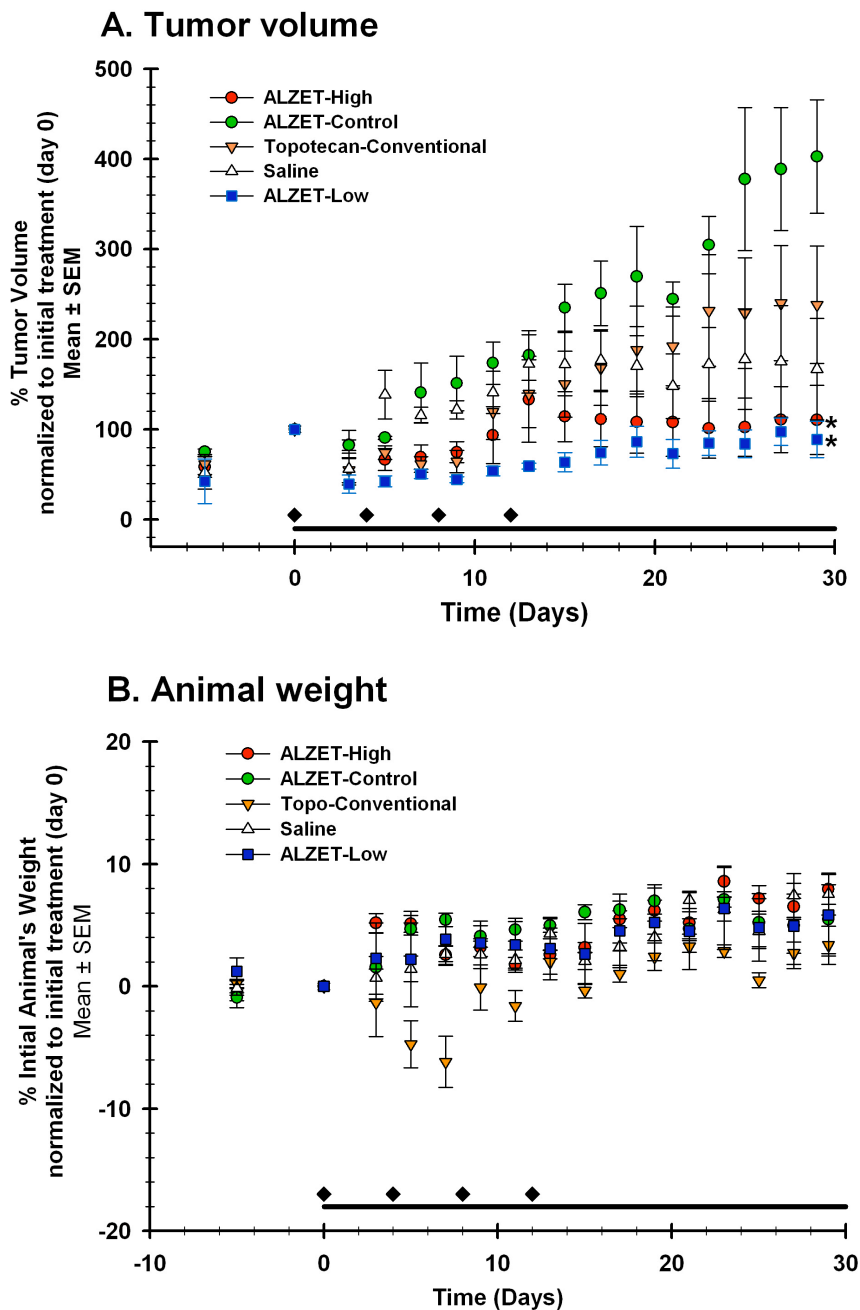


Figure 2-12. Effect of continuous topotecan systemic exposure *in vivo* using xenograft model of human prostate cancer. A. Tumor volume. Effect of topotecan dosing on tumor volume in NCR nude mice implanted subcutaneously with prostate (PC-3) cells. Topotecan was administered continuously using ALZET[®] micro-osmotic pumps

(with high dose (2.45 mg/kg/day) continuous exposure of topotecan or low dose (0.10 mg/kg/day) continuous exposure of topotecan, represented by a line along x-axis) or conventional high dose I.V. (4 mg/kg, q4day, represented by diamonds on x-axis) or no treatment (I.V. with normal saline). A significant ($p \leq 0.05$) reduction in tumor volume was observed following metronomic exposure of topotecan (High and Low dosing) vs. ALZET[®] control. **B.** Animal weight. Change in percentage of animal weights was observed as a gross measurement of toxicity, no significant change in percentage of initial animal weight was associated with all treatment protocols. Data are presented as the mean \pm S.E.M. n=4.

REFERENCES

1. Gulley, J. and W. Dahut, *Novel clinical trials in androgen-independent prostate cancer*. Clin Prostate Cancer, 2002. **1**(1): p. 51-57.
2. Thompson, I., et al., *Guideline for the management of clinically localized prostate cancer: 2007 update*. J Urol, 2007. **177**(6): p. 2106-31.
3. Jani, A.B., *Management strategies for locally advanced prostate cancer*. Drugs Aging, 2006. **23**(2): p. 119-29.
4. Rumohr, J.A. and S.S. Chang, *Current chemotherapeutic approaches for androgen-independent prostate cancer*. Curr Opin Investig Drugs, 2006. **7**(6): p. 529-33.
5. Feldman, B. and D. Feldman, *The development of androgen-independent prostate cancer*. Nature Reviews Cancer, 2001. **1**(1): p. 34-45.
6. Go, R.S. and A.A. Adjei, *Review of the comparative pharmacology and clinical activity of cisplatin and carboplatin*. J Clin Oncol, 1999. **17**(1): p. 409-22.
7. Sakura, M., et al., *Successful therapy of a malignant phyllodes tumor of the prostate after postoperative local failure*. Urology, 2006. **67**(4): p. 845.e11-845.e13.
8. Watanabe, J., et al., *Dicoumarol potentiates cisplatin-induced apoptosis mediated by c-Jun N-terminal kinase in p53 wild-type urogenital cancer cell lines*. Oncogene, 2006. **25**(17): p. 2500-2508.
9. Gandhok, N. and O. Sartor, *Unexpected response of hormone-refractory prostate cancer to treatment with an antileukemic chemotherapy regimen*. Urology, 2004. **64**(4): p. 807-809.

10. Danai D. Daliani, V.A., Shi-Ming Tu, Christos N. Papandreou, Lance C. Pagliaro, Tammy Holtkamp, Xumei Wang, Peter F. Thall, Christopher J. Logothetis,, *Phase II trial of cyclophosphamide, vincristine, and dexamethasone in the treatment of androgen-independent prostate carcinoma*. *Cancer*, 2003. **97**(3): p. 561-567.
11. Kerbel, R.S. and B.A. Kamen, *The anti-angiogenic basis of metronomic chemotherapy*. *Nat Rev Cancer*, 2004. **4**(6): p. 423-36.
12. Kerbel, R.S., et al., *Continuous low-dose anti-angiogenic/ metronomic chemotherapy: from the research laboratory into the oncology clinic*. *Ann Oncol*, 2002. **13**(1): p. 12-5.
13. Jain, R.K., *Barriers to drug delivery in solid tumors*. *Sci. Am.*, 1994. **271**(1): p. 58-65.
14. Berry, W. and M. Eisenberger, *Achieving treatment goals for hormone-refractory prostate cancer with chemotherapy*. *Oncologist*, 2005. **10 Suppl 3**: p. 30-9.
15. Lennernäs, B., et al., *Antiangiogenic effect of metronomic paclitaxel treatment in prostate cancer and non-tumor tissue in the same animals: a quantitative study*. *Apmis*, 2004. **112**(3): p. 201-209.
16. Vogt, T., et al., *Antiangiogenic therapy with pioglitazone, rofecoxib, and metronomic trofosfamide in patients with advanced malignant vascular tumors*. *Cancer*, 2003. **98**(10): p. 2251-2256.
17. Colleoni, M., et al., *Metronomic low-dose oral cyclophosphamide and methotrexate plus or minus thalidomide in metastatic breast cancer: antitumor activity and biological effects*. *Annals of Oncology*, 2006. **17**(2): p. 232.

18. Kamat, A., et al., *Metronomic chemotherapy enhances the efficacy of antivascular therapy in ovarian cancer*. *Cancer Research*, 2007. **67**(1): p. 281.
19. Bocci, G., et al., *Antiangiogenic and anticolorrectal cancer effects of metronomic irinotecan chemotherapy alone and in combination with semaxinib*. *British Journal of Cancer*, 2008. **98**(10): p. 1619-1629.
20. Wang, J., et al., *Paclitaxel at ultra low concentrations inhibits angiogenesis without affecting cellular microtubule assembly*. *Anti-Cancer Drugs*, 2003. **14**(1): p. 13.
21. Fontana, A., et al., *Clinical and Pharmacodynamic Evaluation of Metronomic Cyclophosphamide, Celecoxib, and Dexamethasone in Advanced Hormone-refractory Prostate Cancer*. *Clinical Cancer Research*, 2009. **15**(15): p. 4954.
22. Bocci, G., K. Nicolaou, and R. Kerbel, *Protracted low-dose effects on human endothelial cell proliferation and survival in vitro reveal a selective antiangiogenic window for various chemotherapeutic drugs*. *Cancer research*, 2002. **62**(23): p. 6938.
23. Miller, K., C. Sweeney, and G. Sledge Jr, *Redefining the target: chemotherapeutics as antiangiogenics*. *Journal of Clinical Oncology*, 2001. **19**(4): p. 1195.
24. Doloff, J., et al., *Increased Tumor Oxygenation and Drug Uptake During Anti-Angiogenic Weekly Low Dose Cyclophosphamide Enhances the Anti-Tumor Effect of Weekly Tirapazamine (Supplementary Material)*. *Current Cancer Drug Targets*, 2009. **9**(6): p. 777-788.

25. O'Leary, J.J., et al., *Antiangiogenic effects of camptothecin analogues 9-amino-20(S)-camptothecin, topotecan, and CPT-11 studied in the mouse cornea model.* Clin Cancer Res, 1999. **5**(1): p. 181-7.
26. Clements, M.K., et al., *Antiangiogenic potential of camptothecin and topotecan.* Cancer Chemother Pharmacol, 1999. **44**(5): p. 411-416.
27. Petrangolini, G., et al., *Antiangiogenic effects of the novel camptothecin ST1481 (gimatecan) in human tumor xenografts.* Mol Cancer Res, 2003. **1**(12): p. 863-70.
28. Hsiang, Y. and L. Liu, *Identification of mammalian DNA topoisomerase I as an intracellular target of the anticancer drug camptothecin.* Cancer Research, 1988. **48**(7): p. 1722.
29. Hudes, G., et al., *Phase II study of topotecan in metastatic hormone-refractory prostate cancer.* Investigational New Drugs, 1995. **13**(3): p. 235-240.
30. Klein, C.E., et al., *SWOG-9510: evaluation of topotecan in hormone refractory prostate cancer: a Southwest Oncology Group study.* Prostate, 2002. **52**(4): p. 264-8.
31. NCT00382733, *Oral Topotecan, Utilization for a Metronomic Dosing Schedule to Treat Recurrent or Persistent Solid Tumors (ClinicalTrials.gov Identifier: NCT00382733).*
32. NCT00800345, *A Phase I Trial of Oral Metronomic Topotecan in Combination With Oral Pazopanib Utilizing a Daily Dosing Schedule to Treat Recurrent or Persistent Gynecologic Tumors (ClinicalTrials.gov Identifier: NCT00800345).*

33. Mosmann, T., *Rapid colorimetric assay for cellular growth and survival: application to proliferation and cytotoxicity assays*. J Immunol Methods, 1983. **65**(1-2): p. 55-63.
34. Skehan, P., et al., *New colorimetric cytotoxicity assay for anticancer-drug screening*. J Natl Cancer Inst, 1990. **82**(13): p. 1107-12.
35. Providence, R., *Targeting human prostatic carcinoma through basic fibroblast growth factor receptors in an animal model: characterizing and circumventing mechanisms of tumor resistance*. The Prostate, 1999. **40**: p. 178-191.
36. Geran, R., et al., *Protocols for screening chemical agents and natural products against animal tumors and other biological systems*. Cancer Chemother Rep, 1972. **3**(2): p. 1-103.
37. Chen, J. and J.P. Balthasar, *High-performance liquid chromatographic assay for the determination of total and free topotecan in the presence and absence of anti-topotecan antibodies in mouse plasma*. J Chromatogr B Analyt Technol Biomed Life Sci, 2005. **816**(1-2): p. 183-92.
38. Zastre, J., et al., *Irinotecan-cisplatin interactions assessed in cell-based screening assays: cytotoxicity, drug accumulation and DNA adduct formation in an NSCLC cell line*. Cancer chemotherapy and pharmacology, 2007. **60**(1): p. 91-102.
39. Sun, B., et al., *Inhibition of Ca²⁺-independent phospholipase A2 decreases prostate cancer cell growth by p53-dependent and independent mechanisms*. J Pharmacol Exp Ther, 2008. **326**(1): p. 59-68.

40. Sun, B., et al., *Inhibition of calcium-independent phospholipase A2 activates p38 MAPK signaling pathways during cytostasis in prostate cancer cells*. *Biochem Pharmacol*, 2010. **79**(12): p. 1727-35.
41. Kaiser, M., et al., *Tissue distribution and antitumor activity of topotecan delivered by intracerebral clysis in a rat glioma model*. *Neurosurgery*, 2000. **47**(6): p. 1391.
42. Soffer, S., et al., *Novel use of an established agent: Topotecan is anti-angiogenic in experimental Wilms tumor* I*. *Journal of Pediatric Surgery*, 2001. **36**(12): p. 1781-1784.
43. Horoszewicz, J., et al., *LNCaP model of human prostatic carcinoma*. *Cancer Research*, 1983. **43**(4): p. 1809.
44. Kaighn, M., et al., *Establishment and characterization of a human prostatic carcinoma cell line (PC-3)*. *Investigative Urology*, 1979. **17**(1): p. 16.
45. Niculescu III, A., et al., *Effects of p21Cip1/Waf1 at both the G1/S and the G2/M cell cycle transitions: pRb is a critical determinant in blocking DNA replication and in preventing endoreduplication*. *Molecular and Cellular Biology*, 1998. **18**(1): p. 629.
46. Dergham, S., et al., *The clinical significance of p21WAF1/CIP-1 and p53 expression in pancreatic adenocarcinoma*. *Cancer*, 2000. **80**(3): p. 372-381.
47. Aaltomaa, S., et al., *Prognostic value and expression of p21 (waf1/cip1) protein in prostate cancer*. *The Prostate*, 1999. **39**(1): p. 8-15.
48. Gomyo, Y., et al., *Expression of p21 (waf1/cip1/sdi1), but not p53 protein, is a factor in the survival of patients with advanced gastric carcinoma*. *Cancer*, 2000. **79**(11): p. 2067-2072.

49. Gartel, A. and S. Radhakrishnan, *Lost in transcription: p21 repression, mechanisms, and consequences*. *Cancer Research*, 2005. **65**(10): p. 3980.
50. Bartel, D., *MicroRNAs:: Genomics, Biogenesis, Mechanism, and Function*. *Cell*, 2004. **116**(2): p. 281-297.
51. Lewis, B., C. Burge, and D. Bartel, *Conserved seed pairing, often flanked by adenosines, indicates that thousands of human genes are microRNA targets*. *Cell*, 2005. **120**(1): p. 15-20.
52. Ambs, S., et al., *Genomic profiling of microRNA and messenger RNA reveals deregulated microRNA expression in prostate cancer*. *Cancer Research*, 2008. **68**(15): p. 6162.
53. Petrocca, F., et al., *E2F1-Regulated MicroRNAs Impair TGF [beta]-Dependent Cell-Cycle Arrest and Apoptosis in Gastric Cancer*. *Cancer Cell*, 2008. **13**(3): p. 272-286.
54. Fujita, Y., et al., *Effects of miR-34a on cell growth and chemoresistance in prostate cancer PC3 cells*. *Biochemical and Biophysical Research Communications*, 2008. **377**(1): p. 114-119.
55. Humphrey, P.A., *Gleason grading and prognostic factors in carcinoma of the prostate*. *Mod Pathol*, 2004. **17**(3): p. 292-306.
56. Tillmanns, T., et al., *Daily oral topotecan: Utilization of a metronomic dosing schedule to treat recurrent or persistent solid tumors*. *Chemotherapy* (Presented at American Society of Clinical Oncology Annual Meeting), 2008. **3**(3): p. 19.

CHAPTER 3
EFFECT OF TUMOR MICROENVIRONMENT ON ANTI-CANCER ACTIVITY
OF TOPOTECAN

Ibrahim A. Aljuffali¹ and Robert D. Arnold¹

To be submitted to the Journal of Cancer Biology and Therapy

¹ Department of Pharmaceutical and Biomedical Sciences, College of Pharmacy,
University of Georgia

ABBREVIATIONS

SRB	sulforhodamine B
MTT	3-(4,5-Dimethylthiazol-2-yl)-2,5-diphenyltetrazolium bromide
PC-3	androgen-independent human prostate cancer epithelial cells
DMEM	dulbecco's modified eagle medium
FBS	fetal bovine serum
DMSO	dimethyl sulfoxide
TRIS	tris (hydroxymethyl) aminomethane buffer
TCA	trichloro acetic acid
HPLC	high-performance liquid chromatography
SSL	sterically-stabilized liposomes
DMSO	dimethyl sulfoxide

ABSTRACT

Objective: Our goal was to exploit differences in tumor microenvironment to develop a new drug-targeting strategy. We determined the antitumor activity of topotecan in prostate cancer cells grown chronically in an acidic microenvironment or acutely in reduced oxygen level. **Methods:** Human prostate adenocarcinoma cells (PC-3, androgen-independent) were used to determine the effect of topotecan on cells grown chronically in an acidic microenvironment (pH 6.8) or acutely under hypoxia (2 % O₂). Cytotoxicity of topotecan was determined using mitochondrial enzymatic activity (MTT) assay and total protein concentration (SRB). The effect of pH on the extracellular and intracellular concentrations of topotecan was measured by high performance liquid chromatography

(HPLC) in PC-3 cells. A prototype formulation encapsulated with the inactive carboxylate-ion form of topotecan was developed and its release profile was examined *in vitro*. **Results:** A concentration dependent increase in cytotoxicity was observed following topotecan exposure. Cells grown chronically in acidic media were more sensitive to topotecan ($p \leq 0.05$, IC_{50} of 9.48 ± 1.61 nM) in comparison to tumor cells grown at pH of 7.4 (IC_{50} of 79.6 ± 10.2 nM). The increase in topotecan cytotoxicity is believed to be related to the increase in the concentration of the active, lactone form of topotecan, in the acidic microenvironment. An increase in topotecan potency was also observed in cells exposed to acute hypoxia (IC_{50} of 18.4 ± 2.3 nM) vs. normoxia (IC_{50} of 79.6 ± 10.2 nM). These data were used to develop a prototype liposome formulation loaded with the inactive form of topotecan. This formulation had a prolonged release profile of topotecan *in vitro* at 37 °C. **Conclusions:** In this study, we demonstrated that chronic exposure of PC-3 cells to acidic microenvironment or acute hypoxia can increase topotecan's cytotoxicity against human prostate cancer cells *in vitro* in comparison to normal physiological conditions. A new topotecan formulation was developed to exploit the differences in tumor microenvironment to increase topotecan activity and reduce non-target tissue toxicity.

INTRODUCTION

Prostate cancer represents the most frequent form of malignancy and the second leading cause of non-cutaneous cancer related deaths in men [1]. Several strategies are used to treat prostate cancer including: surgical resection, radiotherapy, hormonal ablation, antiangiogenic drugs and chemotherapy [2, 3]. Understanding the role of

pathological factors that impact the activity of chemotherapeutic agents can result in optimal dose selection to increase clinical therapeutic benefits.

The vascular system of advanced tumors are known to be heterogeneous depending on the type, stage and location of the tumor. To serve fast growing tumors, tumor endothelial cells will grow rapidly to meet the increasing demand for nutrients and oxygen [4]. Incomplete angiogenesis due to fast vascular growth results in the formation of tumors with heterogeneous distribution of blood vessels [5]. This can result in some tumor regions that are well-perfused and others with poor-perfusion.

Tumor microenvironment is known to be different from other non-malignant tissues. We focused on two aspects of tumor microenvironment, shift in extracellular pH and increased tumor hypoxia (*i.e.*, low oxygen tension). Solid tumors are characterized by regions that have different levels of oxygenation [6-8]. The direct cause of hypoxia is an increase in the tumor growth and demand for oxygen with restricted blood supply due to irregular vascular architecture that results from rapid and incomplete angiogenesis [9]. Adaptation of tumor cells to the hypoxia can result in malignant and metastatic phenotype that are resistant to chemotherapy [10-12]. Furthermore, tumor hypoxia can result in a shift to anaerobic glycolysis (Warburg effect), increase production of lactic acid causing a shift in tumor pH [13-15].

Several tumor tissues (including prostate and breast cancer) are known to have acidic microenvironment in comparison to other non-malignant tissues [15-17]. This shift in pH is caused by anaerobic production of lactic acid and hydrolysis of ATP under tumor hypoxic conditions. Inefficient tumor vasculature and poor lymphatics limit the removal of acidic waste from tumor tissues and further contributes to the acidification of

the tumor [18]. Although the external pH is known to be lower than physiological level, intracellular pH of tumor cells is unchanged [19].

The differences between the extracellular and intracellular environment may lead to pH gradients within solid tumors. We hypothesized that this gradient may be used to increase the intracellular uptake of weakly acidic drugs in tumor selectively, while limiting other tissue uptake.

Topotecan (**Figure 3-1**) is a clinically approved chemotherapeutic agent for the treatment of relapsed small cell lung cancer, metastatic carcinoma of the ovary and carcinoma of the cervix. Topotecan cytotoxic activity is mediated by the inhibition of topoisomerase-I [20]. Topotecan undergoes spontaneous reversible non-enzymatic hydrolysis of its biologically active lactone ring to an inactive carboxylate-ion species at physiological pH (7.4) [21]. Stabilization of the lactone form is important for topotecan activity and for passive diffusion through cellular membrane [22].

Differences in tumor pH within cancer tissue may enhance topotecan activity by shifting the equilibrium toward the active lactone form for extended periods of time. However, a previous published report had shown that topotecan activity was lower in acidic microenvironment in comparison to physiological environment [23]. This result contradicts the hypothesis that relatively acidic microenvironment will increase topotecan activity. It should be noted that cells were not chronically maintained in acidic media but rather exposed to acute acidification. Other reports have indicted increased and decreased cytotoxic activity of topotecan activity under acidic microenvironment in various cancer models [24]. For PC-3 cells, a metastatic prostate cancer cell line, other camptothecin analogues activity was similar at different tumor microenvironments (7.4 or 6.8) [25].

Determining the impact of tumor microenvironment on chemo-sensitivity of topotecan is necessary to develop an effective treatment for prostate cancer.

The aims of this research were to determine the chemo-sensitivity of topotecan against metastatic prostate cancer cell *in vitro* under chronic acidification and acute hypoxia; and to exploit differences in tumor microenvironment to develop a novel drug-carrier that exploit tumor microenvironment to develop effective targeting strategy (Figure 3-2).

MATERIALS AND METHODS

Chemicals and Reagents

DMEM (Dulbecco's modified eagle medium), FBS (defined fetal bovine serum) and Trypsin (0.25 %) were purchased from Hyclone (Rockford, IL). Topotecan was purchased from 21st Century Global E-Commerce Network (East Sussex, UK). DMSO (dimethyl sulfoxide), SRB (sulforhodamine B), TRIS buffer, glacial acetic acid, ammonium sulfate, acetonitrile, ethanol, chloroform, trichloroacetic acid, methanol, sodium acetate, sodium borate and ammonium acetate were obtained from Thermo Fisher Scientific Inc. (Rockford, IL). MTT (3-(4,5-Dimethylthiazol-2-yl)-2,5-diphenyltetrazolium bromide) reagent and cholesterol were purchased from Sigma-Aldrich Inc. (St. Louis, MO). Distearoylphosphatidylcholine (DSPC) and distearoylphosphatidylethanolamine coupled to 2000 Da methoxy-polyethyleneglycol (DSPE-PEG) were purchased from Avanti Polar Lipids (Alabaster, AL). Spectro/Por[®] membrane (molecular weight cutoff: 12-14,000) was purchased from Spectrum Laboratories Inc. (Rancho Dominguez, CA).

Cell Lines

Human prostate adenocarcinoma cells (PC-3) were obtained from American Type Culture Collection (ATCC, Rockville, MD). PC-3 cells were maintained in 10 % (v/v) FBS supplemented DMEM at 37 °C, 21 % O₂ and 5 % CO₂ in a humidified incubator from NuAire Inc. (Plymouth, MN).

Exposure to Topotecan at Normal and Acidic Microenvironment (pH 7.4 and 6.8)

The effect of acidic tumor microenvironment on topotecan sensitivity was determined after adapting PC-3 cells to acidified media (pH 6.8) for 60 days prior to treatment. Acidic media was prepared by dissolving powdered DMEM media in sterile water, buffered with 50 mM PIPES (pKa 6.8) and adjusted to pH of 6.8 with 0.1M NaOH. PC-3 cells were seeded in 96-well plates in a 10 % (v/v) FBS supplemented DMEM media. Plates were then incubated for 24 hr at 37 °C, 90 % humidity, 21 % O₂ and 5 % CO₂. After 24 hr, the medium was replaced with fresh media containing different concentrations of topotecan (0.04-10,000 nM). Plates were incubated at the same conditions for 24, 48 and 72 hr post topotecan addition.

Exposure to Topotecan at Acute Hypoxic Microenvironment (2 % O₂)

PC-3 cells were seeded in 96-well plates in a 10 % (v/v) FBS supplemented DMEM media. Plates were incubated for 24 hr at 37 °C, 90 % humidity, 21 % O₂ and 5 % CO₂. To determine the effect of acute exposure to low oxygen tension (2 % O₂) on the activity of topotecan, the media of plated cells was replaced with media that was pre-conditioned in the hypoxic chamber (2 % O₂) for 24 hr prior to drug addition. Increased concentrations of topotecan (0.04-10,000 nM) were added to cells and plates were

incubated at the hypoxic microenvironment (37 °C, 90 % humidity, 2 % O₂ and 5 % CO₂) for 24, 48 and 72 hr post topotecan addition.

Growth Inhibition and Viability Assessment

Antitumor effects were assessed enzymatically by measuring mitochondrial function using MTT assay and sulphorhodamine B (SRB) staining as an indication of cellular protein. SRB and MTT assays were performed as described previously [26, 27]. Briefly, MTT reagent was added to each well and plates were incubated at the same conditions for 2 hr. Media was aspirated and the resulted formazan crystals were dissolved in 200 µL of DMSO and solution absorbance was measured at 550 nm using Synergy HT Microplate Reader from BioTek Instruments, Inc (Winooski, VT). SRB staining was performed by fixing treated cells in 10 % (w/v) TCA for one hr at 4 °C. Fixed cells were then washed five times with tap water and stained with SRB for 5 min. Excess SRB staining was removed with 1 % (v/v) acetic acid, and SRB dye that is bound to cellular protein was dissolved in 200 µL of 10 mM TRIS. Absorbance was measured at 490 nm using Synergy HT Microplate Reader.

Extracellular Concentration of Topotecan

The effect of cell culture media pH on the ratio of the lactone and carboxylate forms of topotecan was determined. Cells were seeded in 6-well plates (8×10^4 cells/well) and exposed to topotecan at high (500 ng/ml), medium (50 ng/ml) and low (10 ng/ml) concentrations in media at pH 6.8 or 7.4. At 24, 48 and 72 hr post topotecan addition, cell culture media was aspirated and diluted with ice cold methanol and acetonitrile mixture

(1:1, v/v) and centrifuged (10,000 x g for 10 min) at 4 °C. Samples were stored in -80 °C until analysis.

Intracellular Accumulation of Topotecan

Intracellular accumulation of topotecan was determined over 24 hr exposure to topotecan at pH 6.8 or 7.4. Cells (5×10^6 cells/tube) were incubated with 1.5 ml of cell culture media containing 10 μ M of topotecan. Tubes were then placed in a tumble shaker at 37 °C, 90 % humidity, 21 % O₂ and 5 % CO₂. At each time point (0.5, 1, 4 and 24 hr), tubes were centrifuged (600 x g for 3 min) at 4 °C and cell pellets were washed three times with ice-cold PBS. Cell pellets were then lysed with 750 μ L of 1 % Triton[®] X-100 (at 4 °C for 5 min) followed by centrifugation (10,000 x g for 5 min) at 4 °C. Ice-cold methanol and acetonitrile (1:1, v/v) mixture was added to the supernatant (1:1, v/v) and vortexed vigorously. The mixture was incubated on ice for 5 min followed by centrifugation (10,000 x g for 5 min) at 4 °C. The supernatants (20 μ L) were injected onto the HPLC for the detection of lactone and carboxylate forms as described in the detection method. Intracellular accumulation of topotecan was normalized to total protein concentration which was quantified using BCA Protein Assay Kit (Thermo Scientific, Rockford, IL)

Measurement of Topotecan Concentration

Quantification of the lactone and carboxylate forms of topotecan was achieved using a modified high performance liquid chromatography (HPLC) method that was published previously [28]. Measurement of carboxylate and lactone forms of topotecan

was performed on an Agilent 1100 HPLC system coupled to fluorescence detector (Santa Clara, CA). The supernatant (20 μ L) was injected onto the HPLC for the detection of lactone and carboxylate forms. Topotecan forms were separated on a Harmony Secure C18 column (5 μ m, 250 \times 4.6 mm) from ES Industries (West Berlin, NJ) equipped with a Phenomenex Security C18 guard column (4.0 \times 3.0 mm). Analytes were eluted from the column using a gradient elution. Mobile phase A was composed of 75 mM ammonium acetate and 5 mM tetrabutylammonium bromide with pH adjusted to 6.4 using glacial acetic acid. Acetonitrile was used as mobile phase B. Gradient elution started from 10 % B and reached 30 % B at 15 min at a flow rate of 1 ml/min. Analytes signals were measured with fluorescence detector (at excitation/emission wavelengths of 370/520 nm). Inter-conversion rate was reduced by extraction using ice-cold solvent and maintaining samples in a refrigerated (4 $^{\circ}$ C) autosampler [28]. A standard curve of topotecan lactone form was prepared in 100 mM sodium acetate buffer, methanol and acetonitrile (2:1:1, v/v/v adjusted to pH of 4.0). For topotecan carboxylate form, a standard curve was prepared in 100 mM sodium borate buffer, methanol and acetonitrile (2:1:1, v/v/v adjusted to pH of 9.0). A concentration range of 1000 to 4.11 ng/mL of topotecan was used to construct the standard curves (with $1/y^2$ weighting scheme) where accuracy of \pm 15 % theoretical values and precision of CV % \leq 15 %.

Measurement of Extracellular pH

PC-3 cells were seeded in 96-well plates in a 10 % FBS supplemented DMEM media or slightly acidified DMEM media (pH 6.8). Plates were incubated for 24 hr at 37 $^{\circ}$ C, 90 % humidity, 21 % O₂ and 5 % CO₂. After 24 hr, the medium was replaced with

fresh media containing high (500 ng/mL), medium (50 ng/mL) or low concentration (10 ng/mL) of topotecan. Plates were incubated at the same conditions for 24, 48 and 72 hr post topotecan exposure. Extracellular pH was monitored directly using Accumet[®] AB15 Basic benchtop pH meter with micro-glass probe from Thermo Fisher Scientific Inc. (Rockford, IL).

Preparation of Topotecan Liposomes

Topotecan containing liposomes were prepared from DSPC, cholesterol and DSPE-PEG in a molar ratio of 9:5:1 using a remote loading procedure as described previously [29, 30]. Phospholipids were dissolved in chloroform, mixed and dried under vacuum at 60 °C for 25 min using a rotary evaporator from Büchi Laboratoriums-Technik (Flawil, Switzerland). Dry phospholipids films were hydrated with 250 mM ammonium sulfate solution (pH of 7.5). The resulting vesicles underwent five freeze–thaw cycles (liquid nitrogen to 60 °C water bath) and extruded five times through a double-stacked 80 nm polycarbonate membrane at 60 °C using a water-jacketed high-pressure extruder from Northern Lipids (Vancouver, BC). Un-encapsulated ammonium sulfate was removed by dialyzing overnight against sucrose solution (10 % w/v, 3 changes) at 4 °C. Topotecan solutions (10 mg/mL topotecan in 10 % (w/v) sucrose) at different pH value (5.0 or 7.5) were prepared and incubated with liposome preparations for one hr at 65 °C with intermittent mixing. An inorganic phosphate assay was performed to determine total phospholipids concentration [31]. Un-encapsulated topotecan was removed by dialyzing overnight against sucrose solution (10 % w/v, 3 changes) at 4 °C. Standard curve of total topotecan was constructed in acidified ethanol (1:1, v/v ratio of ethanol and 0.3 N HCL)

with a concentration range of 460 to 14.3 ng/mL. Formulations were diluted with acidified ethanol and topotecan total concentrations were determined using a Synergy HT Microplate Reader from BioTek Instruments Inc. (Winooski, VT) at excitation and emission filters of (360/40) and (528/20), respectively.

Determination of Topotecan Release

Release of topotecan from liposome samples in sodium chloride solution (0.9 % w/v) was determined at 37 °C. Total topotecan concentrations were determined using a Synergy HT Microplate Reader at excitation and emission filters of (360/40) and (528/20), respectively. At each time point, liposomes were ruptured using acidified ethanol (1:1, v/v ratio of ethanol and 0.3 N HCl) and percentage of topotecan release was calculated by the following equation:

$$\text{Percentage} = [(C_0 - C_t) / (C_0)] \times 100 \%$$

where, C_t represents topotecan concentration at a time (t), C_0 represents topotecan concentration at time zero.

Statistical and Data Analysis

Topotecan potency (IC_{50}) was calculated by fitting observed data to an inhibitory maximum effect (I_{max}) model with a baseline (E_0) effect parameter ($I = E_0 - (I_{max} \times C) / (C + IC_{50})$), using WinNonlin 5.2 from Pharsight Corporation (Cary, NC). A one-way ANOVA followed by Bonferroni t-test was used to assess differences between calculated IC_{50} . A p -value of ≤ 0.05 was considered statistically significant. Statistical analysis was

performed using SigmaStat for Windows version 3.11 from Systat Software, Inc. (Chicago, IL).

RESULTS

Topotecan Activity in Different Tumor Microenvironment

The effects of topotecan exposure on PC-3 cells were assessed by measurement of MTT and SRB staining after 24, 48 and 72 hr of initial topotecan treatment. PC-3 cells were seeded in 96-well plates and left untreated in the corresponding media (pH of 6.8 or 7.4). After 24 hr, media were aspirated and replaced with fresh media containing different concentration of topotecan. Exposure of PC-3 cells to topotecan resulted in time and concentration dependent decreases in SRB and MTT staining after 24, 48 and 72 hr (**Figure 3-3**). For PC-3 cells that were preconditioned at acidic media (pH 6.8), exposure to topotecan in acidic media increased topotecan cytotoxicity significantly ($p \leq 0.05$) compared to dosing in physiological microenvironment (**Figure 3-4**). This increase in activity was calculated by decrease in IC_{50} value (using MTT assay) from 79.6 nM to 9.48 nM for physiological and acidic microenvironment, respectively (**Table 3-1**).

For acute hypoxic study, PC-3 cells were seeded in 96-well plates and left untreated in conventional media. After 24 hr, media was aspirated and replaced with fresh media contain different concentrations of topotecan. This media was preconditioned for 24 hr in the hypoxic chamber (37 °C, 90 % humidity, 2 % O₂ and 5 % CO₂) prior to drug administration. PC-3 cells exposed to acute hypoxia (2 % O₂) (**Figure 3-5**) showed a time and concentration dependent decreases in SRB and MTT staining after 24, 48 and

72 hr. Calculated IC₅₀ (**Table 3-1**) showed a significant increase ($p \leq 0.05$) in topotecan activity in comparison to dosing at normal condition.

Extracellular Concentration of Topotecan

Extracellular concentrations of topotecan were measured in PC-3 cells exposed to topotecan for 72 hr. A reduction in the lactone form concentration was observed in both media (**Figure 3-6**), while the concentration of the carboxylate form increased in both media (**Figure 3-7, Table 3-2**). However, the ratio of carboxylate (inactive) to the lactone (active) form was significantly ($p \leq 0.05$) different between the two microenvironments (**Figure 3-8**). Cells exposed to conventional media maintained a carboxylate/lactone ratio of 4-6, while cells grow chronically in acidic media maintained a ratio of approximately 1 for 72 hr exposure.

Extracellular pH

The effect of topotecan exposure on extracellular pH was determined for 72 hr at three dose levels. Extracellular pH of normal or physiological microenvironment (pH of 7.4) was not altered in comparison to control (**Figure 3-9**). In conventional media, the control and three topotecan levels pH changed from 7.4 to 7.3. In acidic, pH of 6.8 media, the pH changed from 6.8 to 6.5 in control and all three topotecan concentrations.

Intracellular Accumulation of Topotecan

The intracellular accumulation of topotecan was measured following exposure of PC-3 cells to topotecan at pH 7.4 and 6.8. Cells chronically exposed to acidic media

showed rapid and greater uptake of the lactone form of topotecan (**Figure 3-10, Table 3-3**) compared to conventional media. Maximum level of intracellular accumulation (24.1 pg/ μ g protein) was achieved within 30 min. When topotecan was added to PC-3 cells in pH 7.4 media, the accumulation of the lactone form was significantly ($p \leq 0.05$) reduced (conc. below detection limit) compared to cells incubated at pH 6.8 media.

Topotecan Release from Liposome Formulations

Following the demonstration that a higher ratio of the active lactone-form of topotecan exists in an acidic microenvironment, we purposed to develop a novel nanoparticulate drug-carriers loaded with the inactive form of topotecan. Topotecan (inactive carboxylate-ion form) was encapsulated into the aqueous core of a sterically stabilized liposome (SSL) using a remote loading procedure. The internal pH of the liposome's core was maintained at 7.4 while the loading buffer was adjusted to either 7.4 or 5.0. The release profile of topotecan from the two formulations is presented in **Figure 3-11**. A greater concentration of topotecan was encapsulated successfully into the drug-carriers using the buffer at pH 5.0 vs. 7.4. Release of topotecan was monitored for 72 hr and topotecan concentrations were measured using fluorescence detection. Initial burst release of topotecan was detected for 2 hr followed by prolonged zero-order release for up to 72 hr. When topotecan was loaded using the higher pH buffer, significantly lower concentration of topotecan was loaded into the drug-carrier and the topotecan concentrations were undetected after 24 hr incubation period.

DISCUSSION

The overall goal of this research was to understand the effect of tumor microenvironment on topotecan activity against prostate cancer cells *in vitro*. Other goal was to utilize this knowledge to develop nanoparticulate drug-carriers that can exploit tumor microenvironment as a potential targeting strategy. Topotecan was previously found to have different potency in different microenvironment [23]. Alteration in tumor microenvironment *in vitro* was found to alter topotecan cytotoxicity [25]. However, most of these studies exposed tumor cells to acute acidification to test chemo-sensitivity of topotecan and other camptothecin analogues and it's important to consider that cells within advanced tumors may exposed to acidic microenvironments for extended period of time. In this study, we designed our *in vitro* system for tumor cells to be exposed to acidified media (pH of 6.8) for a prolonged time prior to topotecan efficacy determination.

We have shown that topotecan exhibit a concentration and time dependent cytotoxicity. However, when the culture media was acidified to mimic the acidic microenvironment of solid tumors, topotecan mediated cytotoxicity was markedly enhanced. This effect could be related to the fact that topotecan will be predominantly in the active form (lactone form) at acidic pH. Also, differences in pH may enhance the cellular bioavailability of topotecan (lactone form) and therefore enhance its cytotoxic effect. This finding supports our hypothesis that in order to accurately determine the cytotoxicity of chemotherapeutic agent that are sensitive to pH, cells should be maintained in a tumor-like microenvironment. For acute hypoxic exposure, topotecan showed an increase in potency in comparison to normal condition. These findings also

suggest that the activity of topotecan will not be altered due to intermittent changes in oxygen tension within tumor interstitial tissues that is caused by irregularity in vascular architecture and blood flow.

Liposomes has the ability to stably entrap drug and improve their stability and alter their distribution [32]. It was previously reported that encapsulating topotecan as closed lactone ring in liposomes resulted in high encapsulation efficiency but limited benefit due to rapid release of topotecan from the drug carrier and conversion of the active closed lactone ring to inactive carboxylate-ion form [33]. In this research we hypothesize that the inactive carboxylate-ion form of topotecan could be encapsulated stably within liposomes. We further hypothesized that the acidic microenvironment would facilitate the conversion of the carboxylate-ion form to the active lactone form. This strategy may also minimize uptake of topotecan in other organs and limit non-target tissue toxicity, *i.e.*, the majority of topotecan in the drug carriers will be in the inactive state. Since the inactive form would be expected to diffuse slowly through the lipid bilayer of liposomes, greater drug would be retained and accumulate within the tumor tissue. A prototype formulation was developed, using a modified remote loading procedure and demonstrated that loading topotecan as carboxylate form is a feasible approach and can result in longer retention time within the drug-carrier. We demonstrated that using a loading buffer with a low pH (5.0) while maintaining a core with higher pH (7.5) achieved a greater loading of topotecan in comparison to loading buffer with higher pH (7.5). Maintaining a lower pH in the external buffer will force the equilibrium toward the lactone form. Lactone form can cross the liposome membrane due to its hydrophobic

nature and was converted into the hydrophilic form (carboxylate) once reached the basic liposome core.

In conclusion, we have shown that topotecan cytotoxicity significantly increased in tumor-like microenvironments in comparison to conventional conditions. Increase in topotecan activity in an acidic microenvironment can be related to the increase in the concentration of the active lactone form. We developed a prototype formulation loaded with the inactive carboxylate-ion form of topotecan which showed a prolonged release profile *in vitro*. This newly developed formulation can be exploited to increase topotecan activity and reduce non-target tissue toxicity *in vivo*. This finding supports our hypothesis that the carboxylate-ion form of topotecan can be stably trapped within the basic core of the liposome and this prototype formulation may be used to increase topotecan exposure to the tumor.

ACKNOWLEDGMENTS

This research was funded in part by Georgia Cancer Coalition Distinguished Scholar Grant to RDA and a Saudi Arabian Cultural Mission Fellowship to IAA.

Table 3-1: Effect of tumor microenvironment on topotecan potency (IC₅₀) against androgen-independent human prostate cancer (PC-3).

Time (hr)	Microenvironment		
	Conventional Condition IC ₅₀ (nM)	Acute Hypoxia (2 % O ₂) IC ₅₀ (nM)	Acidic (pH 6.8) IC ₅₀ (nM)
24	183 ± 53	63.3 ± 23.7 *	29.9 ± 9.4 *
48	133 ± 16	41.9 ± 11.5 *	17.8 ± 4.4 *
72	79.6 ± 10.2	18.4 ± 2.3 *`	9.48 ± 1.61 *

Data presented as mean ± S.E.M of three independent studies (n=5). IC₅₀ noted with (*) are significantly ($p \leq 0.05$) different in comparison to conventional condition IC₅₀.

Table 3-2: Extracellular concentrations of topotecan forms after topotecan addition to PC-3 cells in conventional media (pH of 7.4). Data presented as mean (conc. ng/mL) \pm S.E.M.

Concentration of the lactone form at pH of 7.4				
Original topotecan (ng/mL)	Time (hr)			
	0	24	48	72
500	442 \pm 15.4	49.5 \pm 2.4	39.4 \pm 3.7	40.8 \pm 1.3
100	80.5 \pm 2.5	10.8 \pm 0.5	10.5 \pm 0.7	9.79 \pm 0.21
50	41.1 \pm 1.62	#	#	#

Concentration of the carboxylate form at pH of 7.4				
Original topotecan (ng/mL)	Time (hr)			
	0	24	48	72
500	62.8 \pm 10.7	333 \pm 6.0	258 \pm 4	202 \pm 4.0
100	9.83 \pm 1.1	69.1 \pm 3.0	52.8 \pm 1.2	40.4 \pm 1.8
50	#	36.2 \pm 1.3	23.0 \pm 1.0	19.5 \pm 1.4

topotecan form was not detected.

Table 3-3: Extracellular concentrations of topotecan forms after topotecan addition to PC-3 cells in acidic media (pH of 6.8). Data presented as mean (conc. ng/mL) \pm S.E.M.

Concentration of the lactone form at pH of 6.8				
Original topotecan (ng/mL)	Time (hr)			
	0	24	48	72
500	546 \pm 35	172 \pm 9.0	150 \pm 2.5	139 \pm 9
100	91.2 \pm 5.5	33.9 \pm 2.2	27.0 \pm 1.9	28.2 \pm 1.3
50	48.0 \pm 2.5	18.0 \pm 0.9	14.1 \pm 1.3	15.7 \pm 0.5

Concentration of the carboxylate form at pH of 6.8				
Original topotecan (ng/mL)	Time (hr)			
	0	24	48	72
500	#	221 \pm 1.0	178 \pm 5.0	145 \pm 1.0
100	#	44.8 \pm 0.6	34.3 \pm 1.1	25.5 \pm 2.0
50	#	21.7 \pm 1.6	16.1 \pm 1.4	14.3 \pm 0.8

topotecan form was not detected.

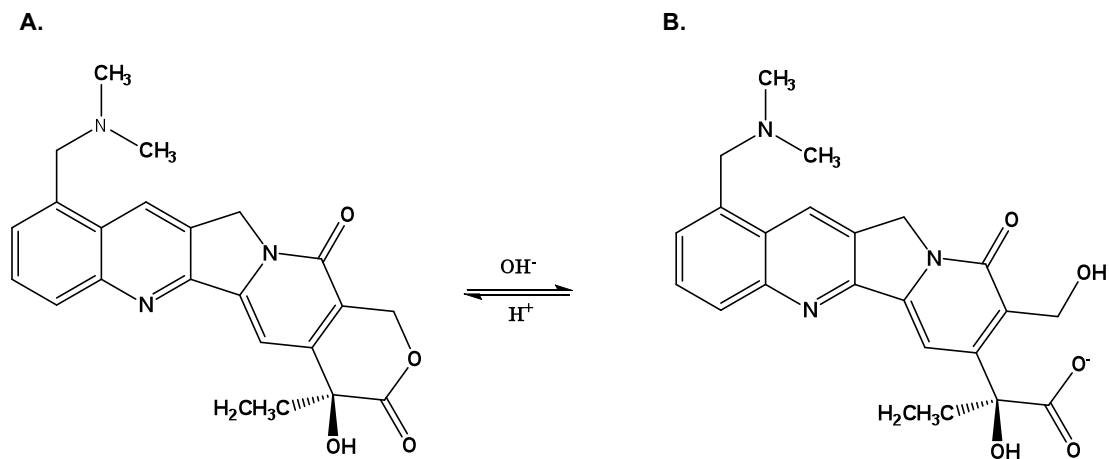


Figure 3-1. Topotecan structure. A. Active α -hydroxy- δ -lactone form, **B.** Inactive carboxylate-ion form.

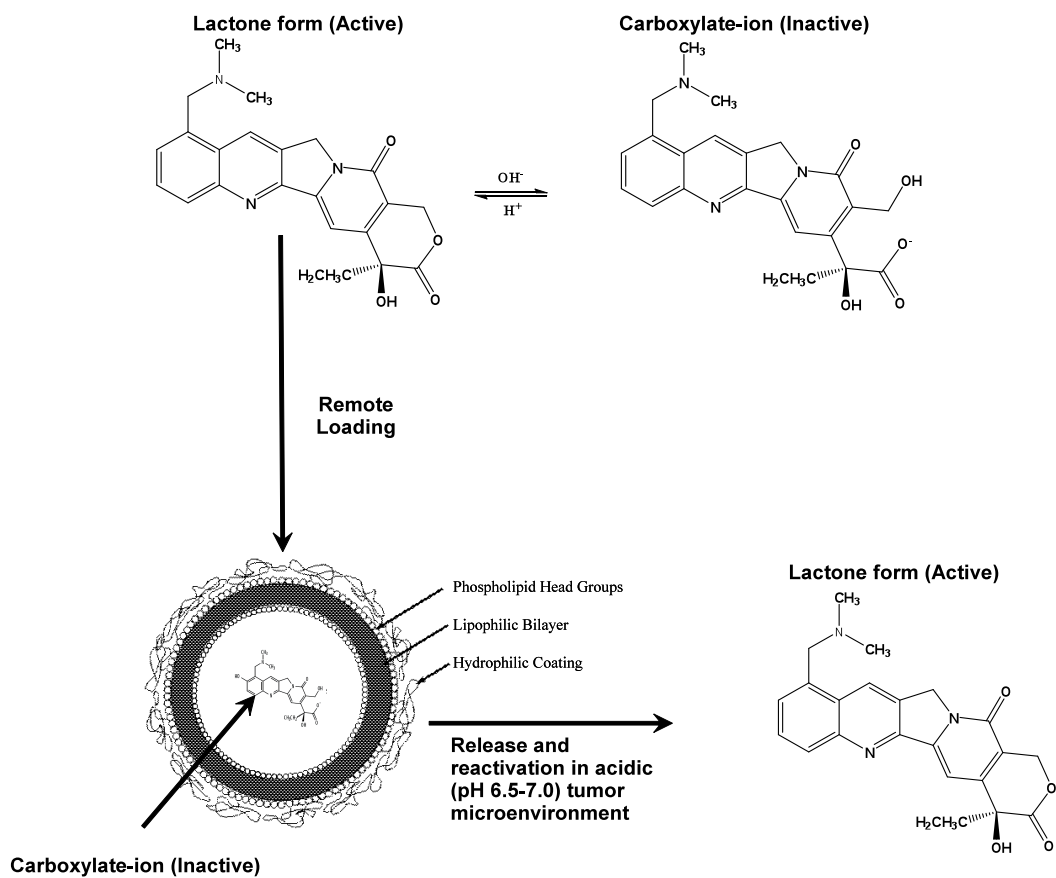


Figure 3-2. Schematic representation of remote loading, entrapment and release of topotecan.

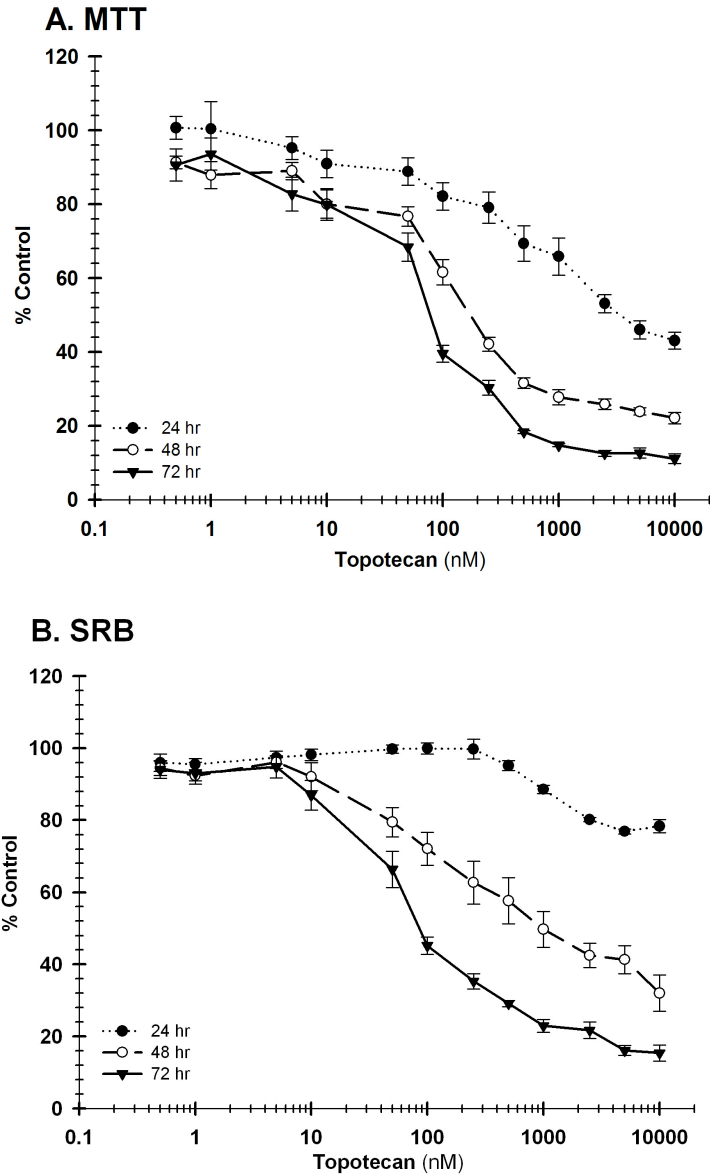


Figure 3-3. Effect of topotecan on growth of prostate cancer cells (PC-3) *in vitro* at pH 7.4. Time and concentration dependent decreases in **A.** mitochondrial activity (MTT) and **B.** protein staining (SRB) were observed following topotecan exposure. Data are presented as mean \pm S.E.M. (n=5) of at least three independent studies.

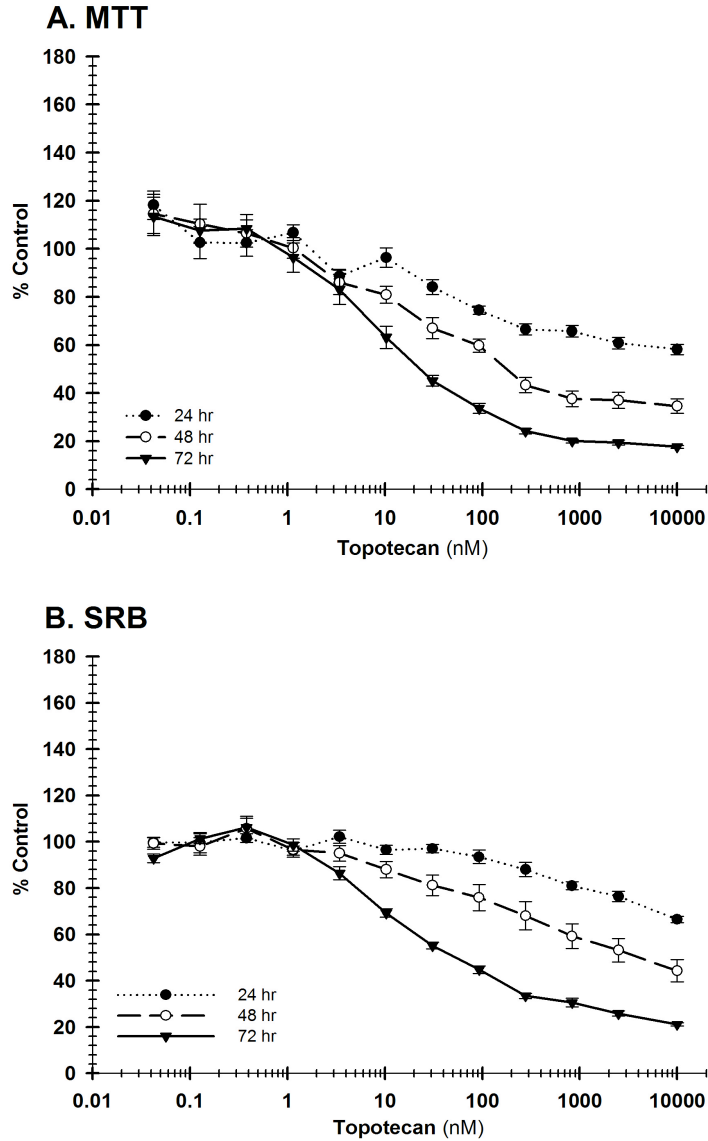


Figure 3-4. Effect of topotecan on growth of prostate cancer cells (PC-3) *in vitro* at pH 6.8. PC-3 cells were maintained chronically at pH of 6.8. Topotecan caused concentration and time dependent decreases in **A.** mitochondrial activity (MTT) and **B.** protein staining (SRB). The observed topotecan potency was greater in comparison to normal condition. Data are presented as mean \pm S.E.M. (n=5) of at least three independent studies.

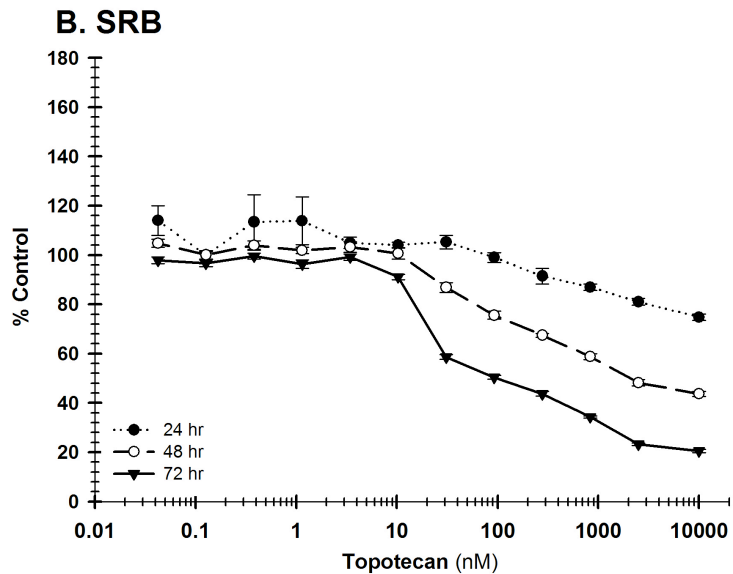
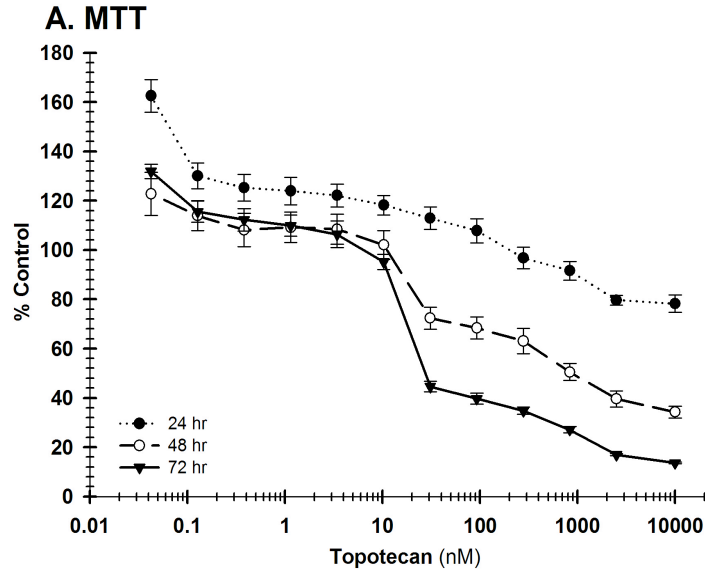


Figure 3-5. Effect of topotecan on growth of prostate cancer cells (PC-3) *in vitro* under acute hypoxia (2 % O₂). Exposing PC-3 cells to hypoxia during topotecan treatment showed concentration and time dependent decreases in **A.** mitochondrial activity (MTT) and **B.** protein staining (SRB). The observed topotecan potency was greater in comparison to conventional media. Data are presented as mean ± S.E.M. (n=5) of at least three independent studies.

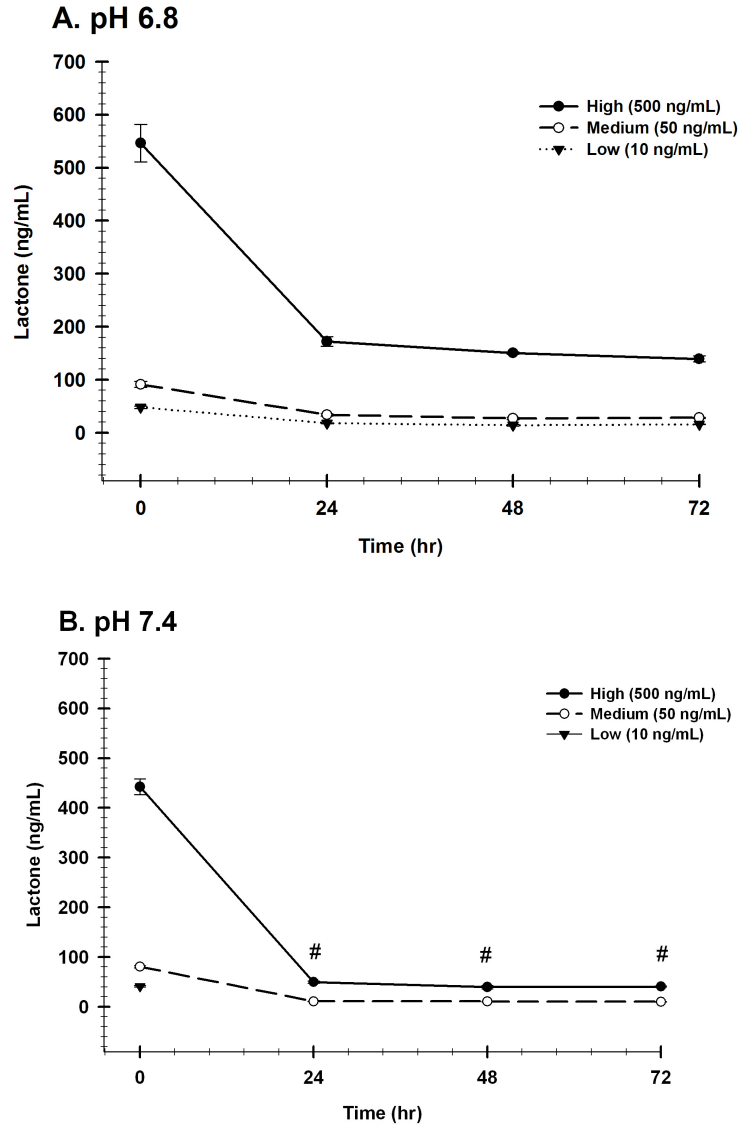


Figure 3-6. Extracellular concentration of topotecan (lactone form) after topotecan addition to PC-3 cells. Extracellular concentrations were determined in either **A.** acidic (pH 6.8) or **B.** normal (pH 7.4) condition. Symbols represent the mean \pm S.D. (n=3).
 # Lactone form of topotecan at low dosing was not detected.

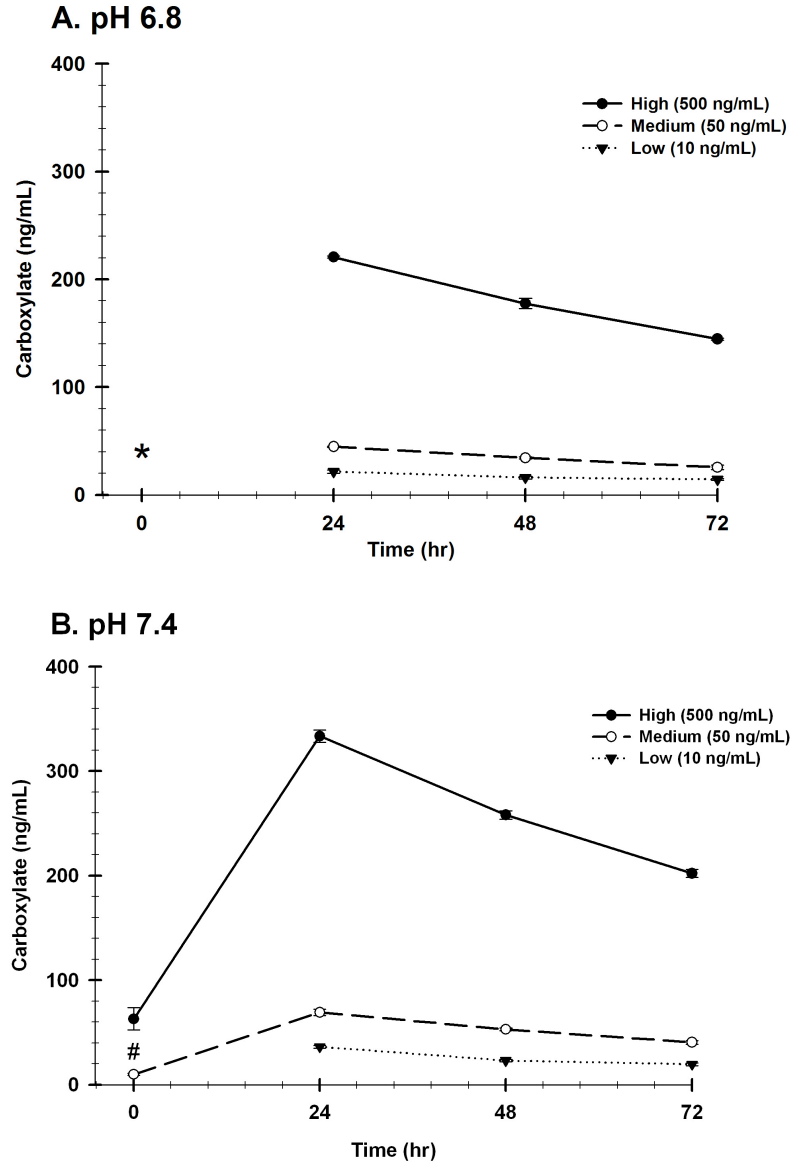


Figure 3-7. Extracellular concentration of topotecan (carboxylate form) after topotecan addition to PC-3 cells. Extracellular concentrations were determined in either **A.** acidic (pH 6.8) or **B.** normal (pH 7.4) condition. Symbols represent the mean \pm S.D. (n=3). # (Carboxylate form of topotecan at low dosing was not detected and ratio cannot be calculated). * (Carboxylate form of topotecan at all doses was not detected).

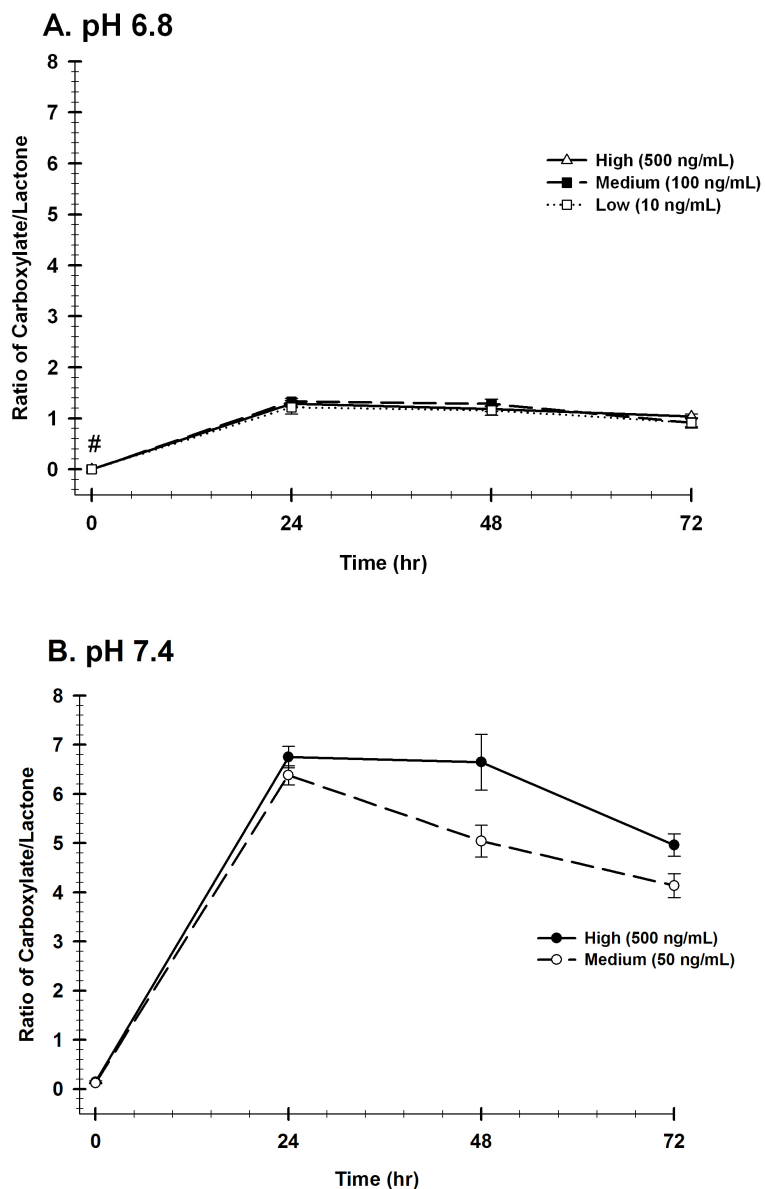


Figure 3-8. Ratio of carboxylate to lactone concentrations of topotecan in extracellular media. Ratio were determined after topotecan addition to PC-3 cells in either **A.** acidic (pH 6.8) or **B.** normal (pH 7.4) condition. Symbols represent the mean \pm S.D. (n=3). # (at time (0), carboxylate form concentration was below detection limit and ratio was set to zero).

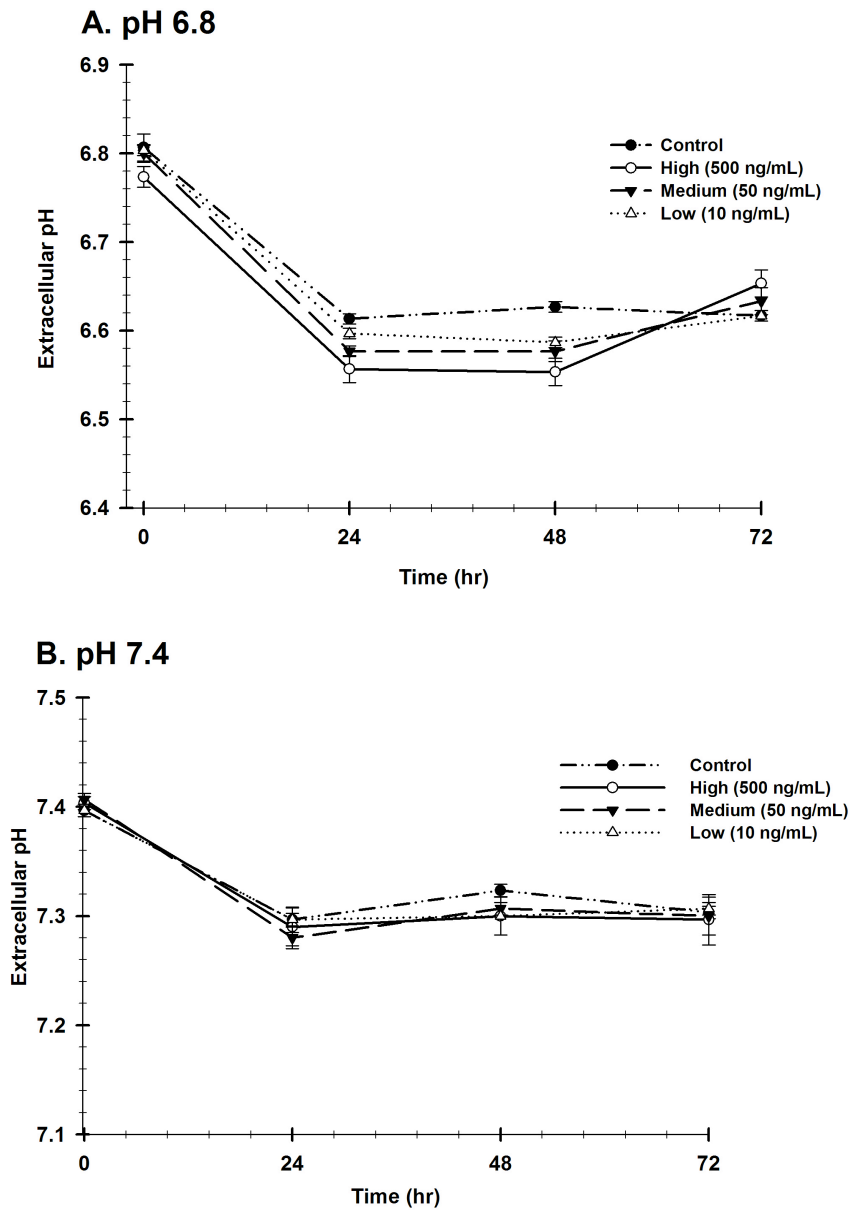


Figure 3-9. Alteration in extracellular pH following treatment with different concentration of topotecan in A. acidic (pH 6.8) and B. normal (pH 7.4) media. Symbols represent the mean \pm S.D. (n=3).

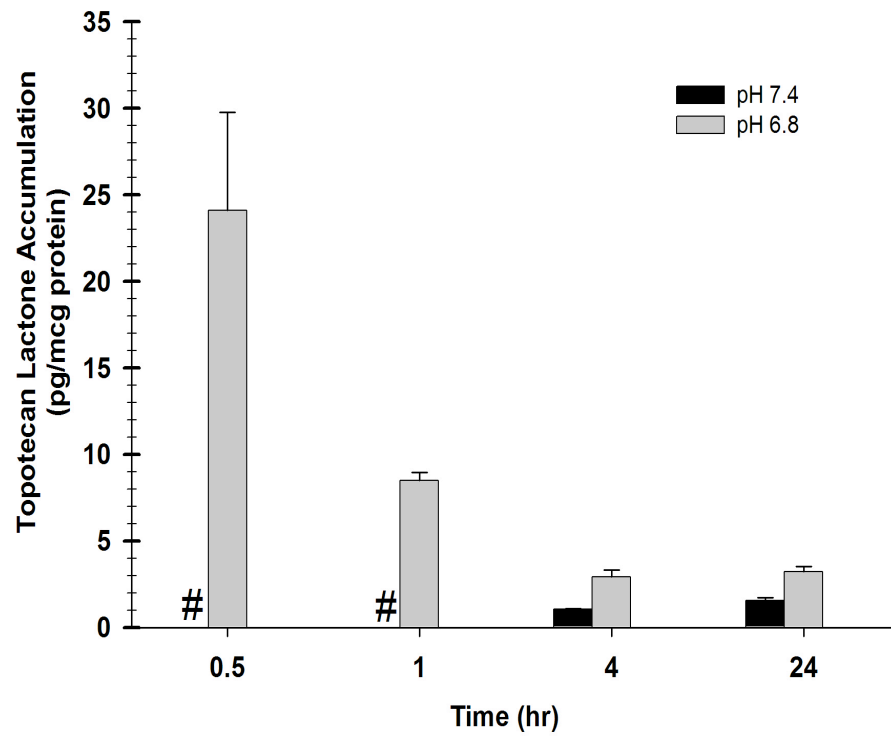


Figure 3-10. Intracellular concentration of the lactone form of topotecan. The effect of topotecan (10 μ M) addition to PC-3 cells in either acidic (pH 6.8) or normal (pH 7.4) condition. Symbols represent the mean \pm S.D. (n=3).

Lactone form not detected at 0.5 and 1 hr time points.

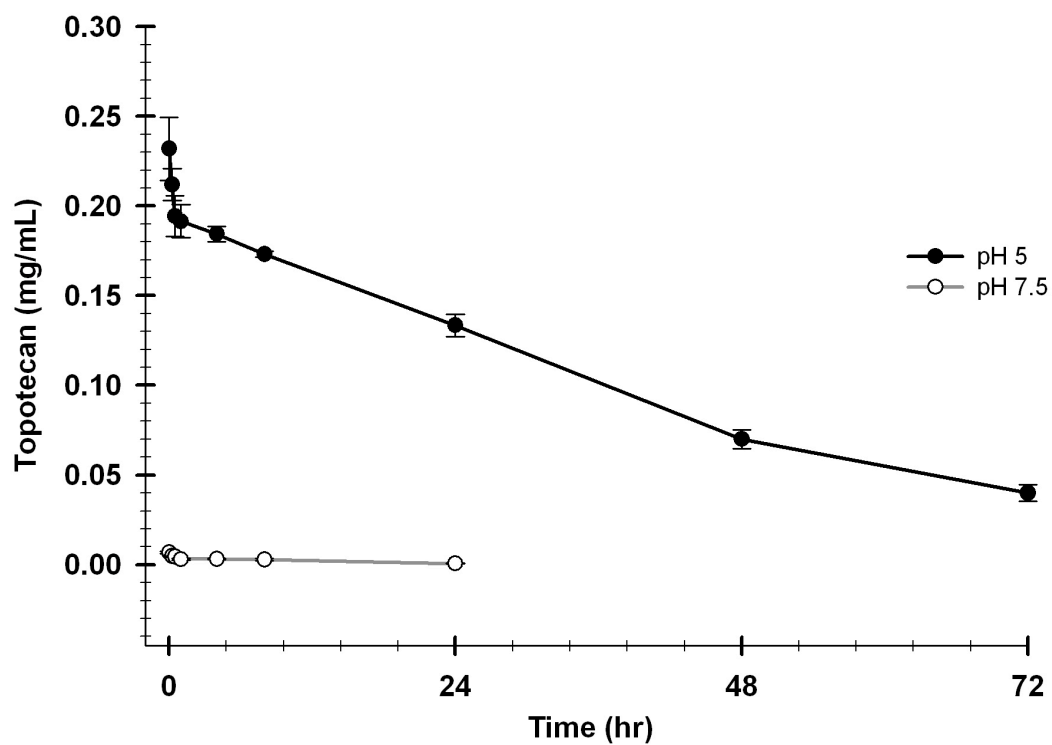


Figure 3-11. *In vitro* release profile of topotecan liposome. Internal liposome core was maintained at a pH of 7.5 while the external pH was adjusted to 5.0 or 7.5. Topotecan release was quantified as total topotecan. Liposome loaded with lower pH buffer (5.0) showed a higher retention of topotecan. Initial burst release was detected followed by prolonged zero-order release for 72 hr. Symbols represent the mean \pm S.D (n=3).

REFERENCES

1. Jemal, A., et al., *Cancer statistics, 2010*. CA: A Cancer Journal for Clinicians, 2010.
2. Mohler, J., *NCCN Clinical Practice Guidelines in Oncology: Prostate Cancer*. National Comprehensive Cancer Network, 2010. **V.2**.
3. Figg, W.D., et al., *Inhibition of angiogenesis: treatment options for patients with metastatic prostate cancer*. Invest New Drugs, 2002. **20(2)**: p. 183-94.
4. Kerbel, R., *Tumor angiogenesis*. New England Journal of Medicine, 2008. **358(19)**: p. 2039.
5. Folkman, J., *Tumor angiogenesis factor*. Cancer research, 1974. **34(8)**: p. 2109.
6. Movsas, B., et al., *Hypoxia in human prostate carcinoma: an Eppendorf PO2 study*. Am J Clin Oncol, 2001. **24(5)**: p. 458-61.
7. Rasey, J.S., et al., *Quantifying regional hypoxia in human tumors with positron emission tomography of [18F]fluoromisonidazole: a pretherapy study of 37 patients*. Int J Radiat Oncol Biol Phys, 1996. **36(2)**: p. 417-28.
8. Movsas, B., et al., *Hypoxic regions exist in human prostate carcinoma*. Urology, 1999. **53(1)**: p. 11-8.
9. Pouyssegur, J., F. Dayan, and N.M. Mazure, *Hypoxia signalling in cancer and approaches to enforce tumour regression*. Nature, 2006. **441(7092)**: p. 437-43.
10. Harris, A., *Hypoxia-a key regulatory factor in tumour growth*. Nature Reviews Cancer, 2002. **2(1)**: p. 38-47.
11. Harris, A., *Hypoxia a key regulatory factor in tumour growth*. Nature Reviews Cancer, 2002. **2(1)**: p. 38-47.

12. Comerford, K., et al., *Hypoxia-inducible factor-1-dependent regulation of the multidrug resistance (MDR1) gene*. *Cancer research*, 2002. **62**(12): p. 3387.
13. Warburg, O., *On the origin of cancer cells*. *Science*, 1956. **123**(3191): p. 309-314.
14. Weinhouse, S., *The Warburg hypothesis fifty years later*. *Journal of Cancer Research and Clinical Oncology*, 1976. **87**(2): p. 115-126.
15. Tannock, I.F. and D. Rotin, *Acid pH in tumors and its potential for therapeutic exploitation*. *Cancer Res*, 1989. **49**(16): p. 4373-4384.
16. Gerweck, L.E. and K. Seetharaman, *Cellular pH gradient in tumor versus normal tissue: potential exploitation for the treatment of cancer*. *Cancer Res*, 1996. **56**(6): p. 1194-1198.
17. Vere, A., et al., *A novel technology for the imaging of acidic prostate tumors by positron emission tomography*. *Cancer research*, 2009. **69**(10): p. 4510.
18. Prescott, D., et al., *The relationship between intracellular and extracellular pH in spontaneous canine tumors*. *Clinical Cancer Research*, 2000. **6**(6): p. 2501.
19. Gerweck, L. and K. Seetharaman, *Cellular pH gradient in tumor versus normal tissue: potential exploitation for the treatment of cancer*. *Cancer research*, 1996. **56**(6): p. 1194.
20. Pommier, Y., *Topoisomerase I inhibitors: camptothecins and beyond*. *Nature Reviews Cancer*, 2006. **6**(10): p. 789-802.
21. Underberg, W., et al., *Equilibrium kinetics of the new experimental anti-tumour compound SK&F 104864-A in aqueous solution*. *Journal of Pharmaceutical and Biomedical Analysis*, 1990. **8**(8-12): p. 681-683.

22. Yao, S., et al., *Topotecan lactone selectively binds to double-and single-stranded DNA in the absence of topoisomerase I*. *Cancer research*, 1998. **58**(17): p. 3782.
23. Vukovic, V. and I. Tannock, *Influence of low pH on cytotoxicity of paclitaxel, mitoxantrone and topotecan*. *British journal of cancer*, 1997. **75**(8): p. 1167.
24. Adams, D., *The impact of tumor physiology on camptothecin-based drug development*. *Current Medicinal Chemistry-Anti-Cancer Agents*, 2005. **5**(1): p. 1-13.
25. Flowers, J., et al., *The activity of camptothecin analogues is enhanced in histocultures of human tumors and human tumor xenografts by modulation of extracellular pH*. *Cancer chemotherapy and pharmacology*, 2003. **52**(3): p. 253-261.
26. Mosmann, T., *Rapid colorimetric assay for cellular growth and survival: application to proliferation and cytotoxicity assays*. *J Immunol Methods*, 1983. **65**(1-2): p. 55-63.
27. Skehan, P., et al., *New colorimetric cytotoxicity assay for anticancer-drug screening*. *J Natl Cancer Inst*, 1990. **82**(13): p. 1107-12.
28. Zastre, J., et al., *Irinotecan-cisplatin interactions assessed in cell-based screening assays: cytotoxicity, drug accumulation and DNA adduct formation in an NSCLC cell line*. *Cancer chemotherapy and pharmacology*, 2007. **60**(1): p. 91-102.
29. Madden, T., et al., *The accumulation of drugs within large unilamellar vesicles exhibiting a proton gradient: a survey*. *Chemistry and physics of lipids*, 1990. **53**(1): p. 37-46.

30. Arnold, R., et al., *Effect of repetitive administration of Doxorubicin-containing liposomes on plasma pharmacokinetics and drug biodistribution in a rat brain tumor model*. Clinical Cancer Research, 2005. **11**(24): p. 8856.
31. Bartlett, G., *Phosphorus assay in column chromatography*. J biol chem, 1959. **234**(3): p. 466-468.
32. Drummond, D., et al., *Optimizing liposomes for delivery of chemotherapeutic agents to solid tumors*. Pharmacological reviews, 1999. **51**(4): p. 691.
33. Burke, T. and X. Gao, *Stabilization of topotecan in low pH liposomes composed of distearoylphosphatidylcholine*. Journal of pharmaceutical sciences, 1994. **83**(7): p. 967-969.

CHAPTER 4

**NON-INVASIVE RELEASE MEASUREMENT OF MAGNETIC
RESONANCE IMAGING PROBE FROM NANOPARTICULATE
DRUG-CARRIERS**

Ibrahim A. Aljuffali¹, Joseph A. Spornyak² and Robert D. Arnold¹

To be submitted to the Journal of Therapeutic Delivery

¹ Department of Pharmaceutical and Biomedical Sciences, College of Pharmacy,
University of Georgia

² Preclinical Imaging Resource, Roswell Park Cancer Institute

ABBREVIATIONS

CaCl ₂	Calcium chloride
D ₂ O	Deuterium Oxide
DSPC	1,2-distearoyl- <i>sn</i> -glycero-3-phosphatidylcholine
DSPE	1,2- distearoyl- <i>sn</i> -glycero-3-phosphatidylethanolamine
DSPE-PEG	1,2-distearoyl- <i>sn</i> -glycero-3-phosphoethanolamine-N-[poly(ethylene glycol) 2000
Gd-DTPA	Gadolinium-diethylenetriaminepentaacetic acid
MRI	Magnetic Resonance Imaging
NMR	Nuclear Magnetic Resonance
R ₁	Relaxation rate
SPL	Secretory Phospholipase A ₂ sensitive Liposomes
sPLA ₂	Secretory Phospholipase A ₂
SSL	Sterically-Stabilized Liposomes

ABSTRACT

Purpose: To develop a technique to prepare and characterize a prototype long circulating liposome formulation encapsulated with gadolinium-DTPA. The overall goal was to facilitate the quantification of drug release *in vivo* and to optimize liposome composition to attain optimum target-site exposure. Determining drug release *in vivo* can aid in designing nanoparticles with optimum release kinetics. **Methods:** Long circulating liposomes (SSL) were encapsulated with gadolinium-DTPA using aqueous capturing. Relaxation rate of liposome formulations or gadolinium-DTPA was determined using

NMR and MRI. Release of gadolinium-DTPA from liposome formulation was also tested *in vitro* over 24 hr incubation. **Results:** A concentration dependent increase in relaxation rate of gadolinium-DTPA was found to be linear in saline and plasma. Long circulating liposomes exhibited an increase in the relaxation rate with increasing concentration, while blank liposomes had no effect on relaxation rates. The relaxation rate of undialyzed and dialyzed liposomes were found to be different. *In vitro* release study showed an initial liposome burst followed by extended release over 24 hr. **Conclusions:** This study showed that liposome encapsulated with gadolinium-DTPA could be used to determine carrier leakiness using magnetic resonance imaging. Further study will follow to optimize drug release *in vitro* and *in vivo* using different liposome formulations.

INTRODUCTION

Nanoparticulate drug carriers, such as long-circulating liposomes, have the potential to stably encapsulate drugs and alter their kinetics and activity [1]. Despite the clinical use of liposomes in the treatment of different malignancies, there is a limited understanding of the processes involved in the carrier degradation and mechanisms of drug release *in vivo*. Correlation of nanoparticles release efficiency at the site of interest with its therapeutic activity *in vivo* is not well understood. A variety of techniques have been tested to facilitate and control drug release *in vivo* [2-4]. The extracellular form of phospholipases A₂ (secretory phospholipases A₂, sPLA₂) was found to be up-regulated in different malignancies [5-7]. We previously showed that altering liposomes composition can be used to increase the release of liposomes when sPLA₂ is present [8]. In order to measure the release profile of these formulations *in vivo*, a non-invasive technique

needed to be developed. However, there are no functional methods that are clinically useful to continuously monitor the rate and extend of release of nanoparticulate drug-carriers *in vivo*.

Frequently applied methods to quantify drug release such as chromatography, microscopy and calorimetric methods require tissue extraction; which typically involve serial sampling on a single subject [9]. In addition, sample preparation may introduce artifacts to the processed samples. Furthermore, it is not feasible to conduct tissue distribution and release studies in humans using the methods described above. Other *in vivo* monitoring techniques with radioactive labeled liposome provide only information concerning the liposomes and do not track the disposition of encapsulated compounds and limit their use in human [10]. Magnetic resonance techniques are appropriate methods for real time serial measurements due to their non-destructive nature. Magnetic resonance techniques use proton resonance to generate a signal. Protons are excited by a radiofrequency pulse and then emit energy in the form of a radiofrequency signal as they return to their magnetization equilibrium. The radiofrequency signal decays in an exponential manner. The time constant for this exponential decay is called the longitudinal or spin-lattice T_1 relaxation time [11].

Gadolinium (Gd^{3+}) is a paramagnetic ion that alters the nuclear spin of adjacent hydrogen ions of surrounding water molecules. Gadolinium (Gd^{3+}) has seven unpaired electrons and strong proton spin-lattice relaxation effects [12]. Gadolinium-based compounds (Gd^{3+} complexes) were used to avoid the high toxicity associated with the use of the free Gd^{3+} ion [13]. Gadolinium-DTPA (Gadolinium diethylenetriaminepentaacetic acid, Magnevist[®]) is the most clinically used contrast agent

[14]. Relaxation rates of the extracellular fluid depend on the concentration of gadolinium present. Gadolinium-based compounds enhance tissue contrast on T₁-weighted images by reducing the T₁ relaxation time [12].

Several methods have used Gd-based compounds to study *in vivo* liposome fate including, accumulation and imaging of radiolabeled liposomes [15], tumor detection and liver specific contrast agents [16, 17]. Other reports utilize Gd-DTPA loaded liposomes as a method to measure liposomes distribution into brain tumors [18]. The overall goal of this project is to develop a multifunctional drug carrier that encapsulates Gd-DTPA, to track the carrier deposition and release non-invasively. The aim was to develop a platform to determine effective liposome release kinetics and optimize dosing schedules *in vivo* (**Figure 4-1**). Our first aim was to encapsulate Gd-DTPA into different liposome formulations; our second aim was to quantify the release of the entrapped Gd-DTPA by MRI and NMR.

MATERIALS AND METHODS

Chemicals and Reagents

DSPC (1,2-distearoyl-*sn*-glycero-3-phosphatidylcholine), DSPE (1,2- distearoyl-*sn*-glycero-3-phosphatidylethanolamine) and DSPE-PEG (1,2-distearoyl-*sn*-glycero-3-phosphoethanolamine- N-[poly(ethylene glycol) 2000) were purchased from Avanti Polar Lipids Inc. (Alabaster, AL). Secretory Phospholipase A₂ Group III (bee venom) was purchased from Cayman Chemical Company (Ann Arbor, MI). Gadolinium-based contrast enhancing agent (Gd-DTPA, Magnevist[®]) was obtained from Berlex Inc. (Montville, NJ). Sucrose, cholesterol and sodium chloride were obtained from Thermo

Fisher Scientific Inc. (Rockford, IL). Spectro/Por[®] membrane (molecular weight cutoff: 12-14,000) was purchased from Spectrum Laboratories Inc. (Rancho Dominguez, CA). Deuterium Oxide (D₂O) was obtained from MP Biomedicals (Solon, OH).

Preparation of Gd-DTPA Liposomes

Two formulations were prepared, sterically stabilized liposomes (SSL) and sPLA₂ sensitive liposomes (SPL). SSL were prepared by mixing DSPC, cholesterol and DSPE-PEG (in a molar ratio of 9:5:1), while SPL was prepared by mixing DSPC, cholesterol, DSPE and DSPE-PEG (in a molar ratio of 8:5:1:1). Phospholipids in chloroform were mixed and dried under vacuum at 60 °C using a Büchi rotavapor from Büchi Laboratoriums-Technik (Flawil, Switzerland). Dry phospholipid films were hydrated with normal saline containing Gd-DTPA. The resulting vesicles underwent five freeze–thaw cycles (in liquid nitrogen and 60 °C water bath) and were extruded five times through a double-stacked 80 nm polycarbonate membrane at 65 °C using a water-jacketed high-pressure extruder from Northern Lipids (Vancouver, BC). Unencapsulated Gd-DTPA was removed by dialyzing against a sucrose solution (10 % w/v, 3 changes) at 4 °C over night.

Sample Preparation

Samples for MRI study were prepared by diluting each preparation (SSL or SPL, loaded with 10 mM Gd-DTPA) in normal saline containing 1 mM CaCl₂ with or without 2.5 µg/mL sPLA₂. Blank formulations were diluted in normal saline containing 1 mM

CaCl₂. Samples for NMR study were prepared by diluting the preparation (SSL loaded with 100 mM Gd-DTPA) in 80 % D₂O.

MRI Study

All MR imaging studies were carried out on a General Electric 4.7T/33 cm horizontal bore magnet (GE NMR instruments, Fremont, CA) incorporating AVANCE digital electronics (Bruker BioSpec platform with ParaVision Version 4.0 acquisition software from Bruker Medical, Billerica, MA). T₁ relaxation rates were measured using an inversion recovery TrueFISP method [19] and calculated using a non-linear fitting routine developed in-house using Matlab Version 7.0 from MathWorks Inc. (Natick, MA). Prior to measuring enzyme kinetics, T₁ relaxivity of Gd-containing liposomes were determined by serially diluting the liposomes and measuring the T₁ relaxation rate at each concentration. We utilized the MRI within the small animal imaging facility at Roswell Park Cancer Institute (Buffalo, NY).

NMR Study

Gd-DTPA liposomes were diluted with 80 % D₂O and loaded into NMR glass tubes for relaxivity measurements. ¹H-NMR spectra were recorded on Varian Inova 500 MHz NMR spectrometer with Varian VNMR software version 6.1. NMR signals were obtained as follow: receiver gain was set to the minimum with standard two-pulse t-measurement sequence; 180 degree pulse was set to 32 μs and the read out pulse was set to 70 degree due to intense water signal causing receiver overflow. The pre-relaxation delay was set to 10 sec and the acquisition time is 1.9 sec. The spectrum window was set

to 2500 and the T_1 -delay varied as 0.125, 0.25, 0.5, 0.75, 1, 2, 4 and 8 sec. The NMR is located at the College of Pharmacy, UGA.

RESULTS AND DISCUSSION

MRI Study

Initial study using MRI suggested that there was no change in sample signal over 24 hr (**Figure 4-2**). Further experiments were carried out to characterize samples signal with different preparation dilutions (**Figure 4-3**). This experiment showed that the formulation exhibited an increase in the relaxation rate with increasing concentration of the formulations (SSL or SPL), while blank liposomes have no effect on the relaxation rates (R_1). Further study will follow to characterize Gd-DTPA formulation using NMR with increasing Gd-DTPA concentration.

NMR Study

The relaxivity of samples using NMR was carried out in similar formulations (SSL) with increased Gd-DTPA concentration (100 mM Gd-DTPA). The relaxation rate (R_1) of un-dialyzed liposomes and liposomes that were dialyzed were found to be different (**Figure 4-4**). This data showed that dialysis removed unencapsulated Gd-DTPA. Relaxivity of dialyzed liposomes ruptured with 1 % Triton-X 100 was similar to un-dialyzed liposomes. This data suggest that encapsulated Gd-DTPA was released upon liposomes digestion which altered the relaxation rate of the sample. Relaxation rate of both samples (encapsulated Gd-DTPA and digested liposomes) were higher than blank (80 % D_2O). Relaxation rates of different dilution factors of the formulation were also

measured (**Figure 4-5**). This data showed that the formulation exhibited an increase in the relaxation rate with increasing concentration of the formulation. Normalizing sample's signal to ruptured liposomes signal showed no difference in ratio with increasing concentration.

Release of Gd-DTPA from SSL formulations was tested *in vitro* over 24 hr incubation. SSL formulations were maintained in a 37 °C water bath. At each time point, sample of the formulation was taken and diluted with 80 % D₂O; relaxivity was measured using a 500 MHz NMR. **Figure 4-6** showed that the formulation had a burst release effect within 3 hr of incubation followed by prolonged and extended release over 24 hr. In order to obtain a concentration-signal curve that can be used to calculate the concentration of Gd-DTPA, relaxivity of free Gd-DTPA was measured using NMR. Several concentrations of Gd-DTPA (50 µL) were diluted with 0.2 mL of normal saline and mixed with 1.25 mL of D₂O. The relationship between the concentration of Gd-DTPA and relaxation rate (R_1) was found to be linear (**Figure 4-7**). This experiment suggests that the concentration of Gd-DTPA can be measured using relaxation rate as a response variable. Further experiments were carried out by analyzing different concentrations of Gd-DTPA (50 µL) that were diluted with 0.2 mL of rat plasma and mixed with 1.25 mL of D₂O. A similar linear relationship was found when rat plasma was used as a vehicle for Gd-DTPA (**Figure 4-8**). These data suggest that this method can be used to measure the concentration of Gd-DTPA in plasma.

CONCLUSION

Nanoparticulate drug-carriers, such as liposomes, continued to be a valuable alternative to conventional chemotherapeutic agents [1]. However, the rate and extent of drug release into the tumor site are not well understood. Determining drug release *in vivo* can aid in designing nanoparticles with optimum release characteristics. This research has developed a technique to quantify the rate and extent of release of Gadolinium-DTPA, a magnetic imaging probe, encapsulated into long-circulating liposomes. MRI, a non-invasive imaging technique, can be used to quantify GD-DTPA release with longitudinal and non-invasive sampling from a single subject. Further study will follow to optimize drug release *in vitro* and *in vivo* of different lipid components to optimize liposome formulation. This research can have broad applications including: optimizing therapy by optimizing drug delivery release non-invasively and can serve as a diagnostic tool for various diseases.

ACKNOWLEDGMENTS

Financial support of this work was provided by the University of Georgia, College of Pharmacy. Special thanks are given to the Department of Pharmaceutical and Biomedical Sciences NMR facility, UGA Bio-Imaging Research Center and Preclinical Imaging Facility at Roswell Park Cancer Institute (Buffalo, NY).

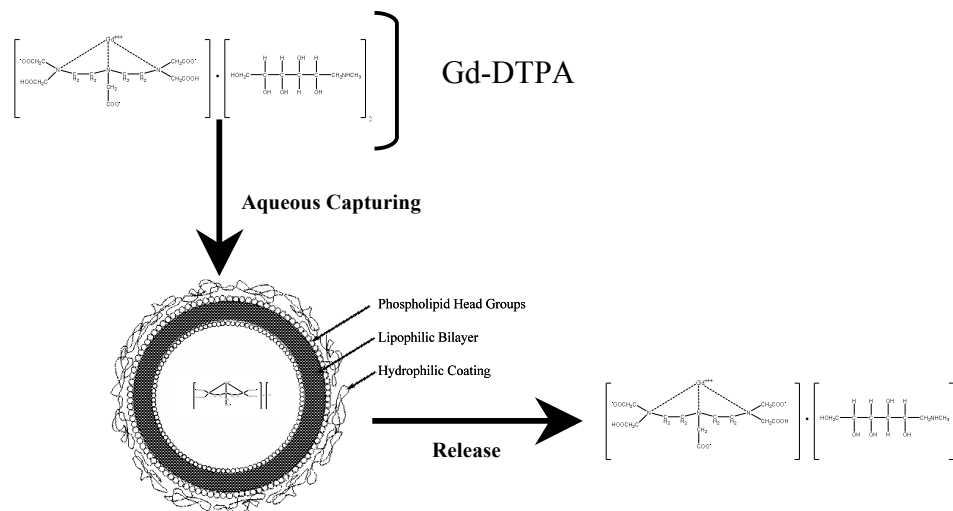


Figure 4-1. Research Hypothesis. We hypothesized that Gd-DTPA can be stably encapsulated into sterically stabilized liposomes (SSL). Upon *in vivo* accumulation, Gd-DTPA will be released and alter the T_1 -relaxation rate of the tissue of interest. Changes in relaxation rate can be used to understand the release kinetics *in vivo*.

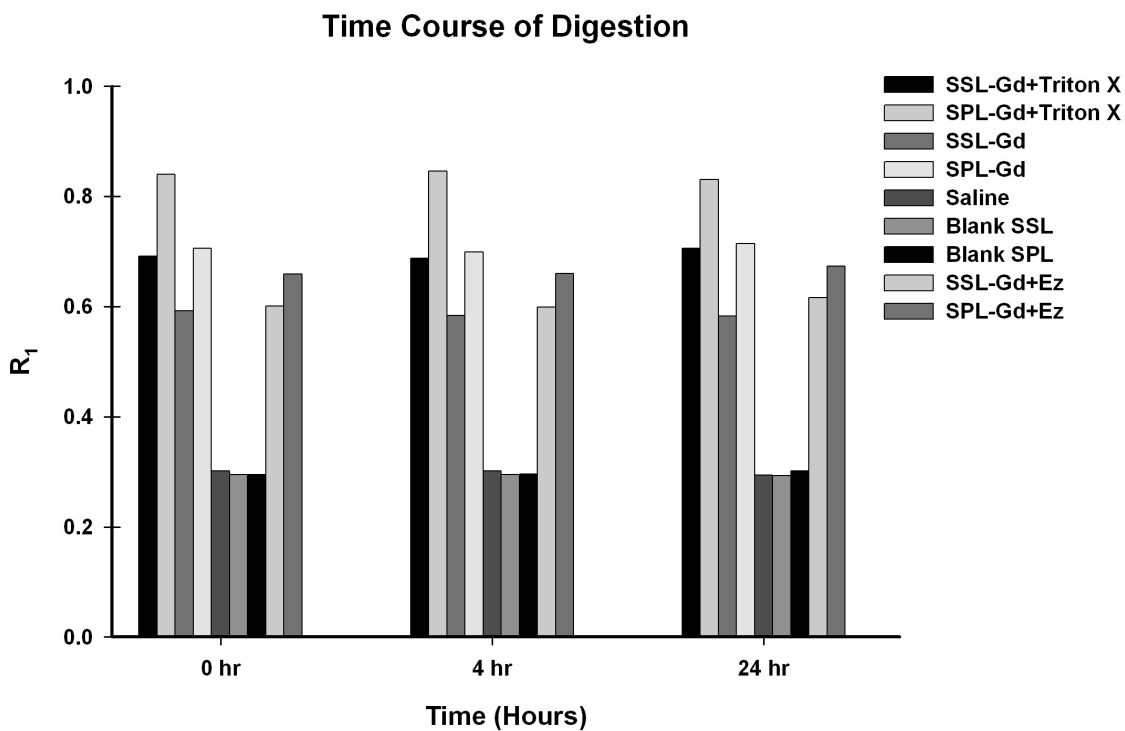


Figure 4-2. Determination of different liposome formulations relaxivity using MRI.

R_1 values were calculated as the inverse of T_1 relaxation times, where T_1 values were determined using a simple algorithm fit to the exponential equation for spin-echo sequence (SSL-Gd= Sterically-Stabilized Liposomes loaded with 10 mM Gd-DTPA, SPL-Gd=Secretory Phospholipase A_2 sensitive Liposomes with 10 mM Gd-DTPA, SSL-Gd-Ez=SSL-Gd incubated with 2.5 $\mu\text{g}/\text{mL}$ sPLA $_2$ and SPL-Gd-Ez=SPL-Gd incubated with 2.5 $\mu\text{g}/\text{mL}$ sPLA $_2$).

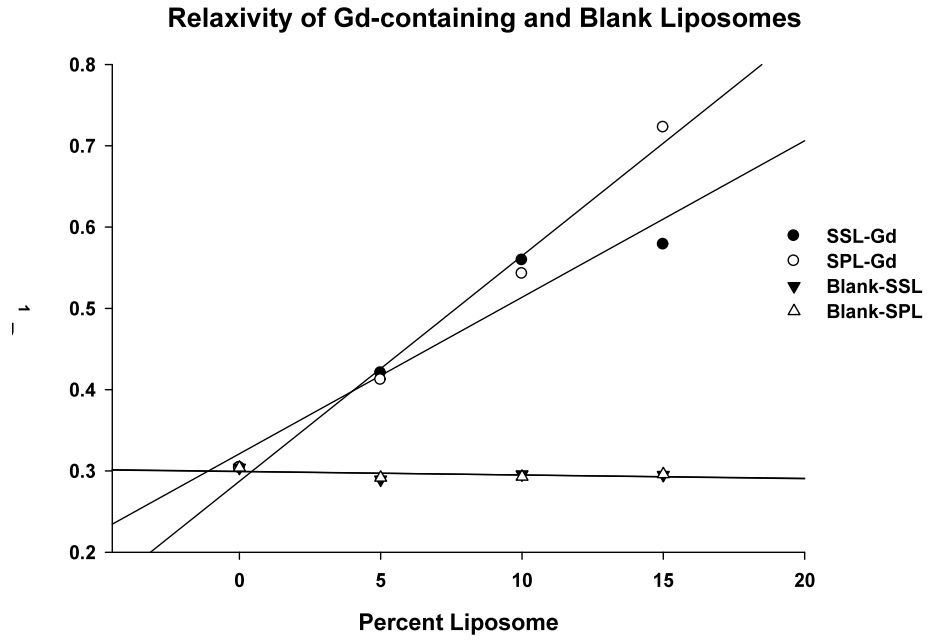


Figure 4-3. R_1 relaxation rate of different liposome-dilution ratio. (SSL= Sterically-Stabilized Liposomes and SPL=Secretory Phospholipase A_2 sensitive Liposomes).

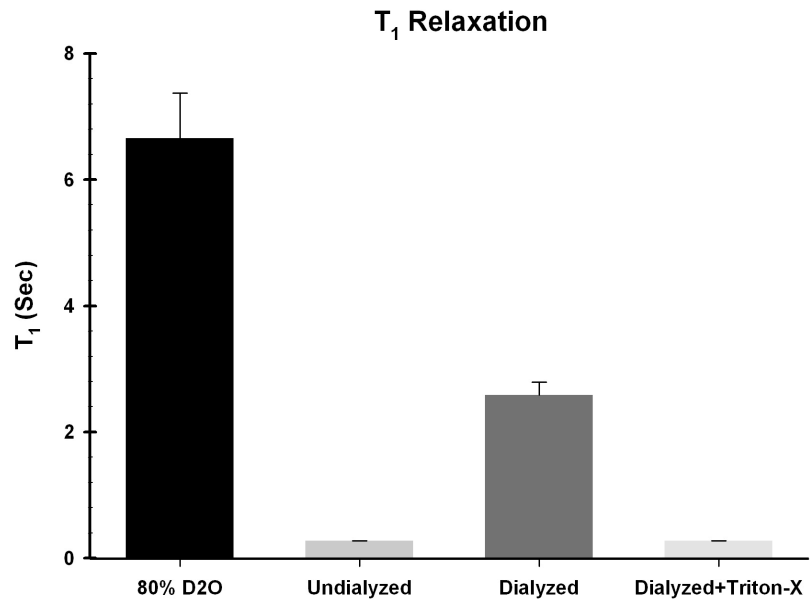


Figure 4-4. Measurement of T₁ relaxation times using NMR.

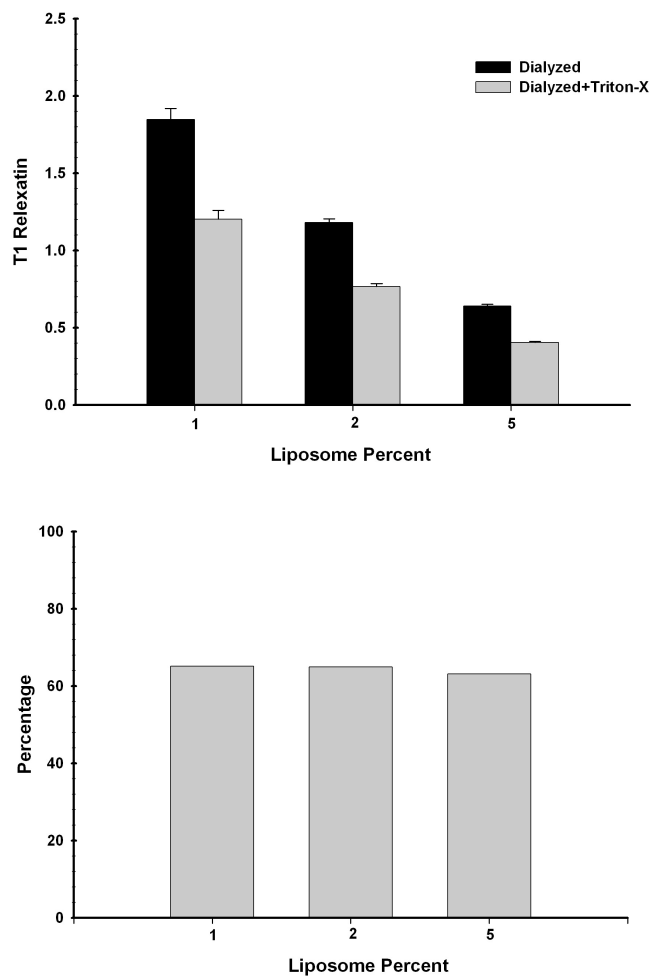


Figure 4-5. Plots of T_1 relaxation time versus Gd-DTPA encapsulated liposome (Gd-lip) of different liposome concentrations. The Gd-lip was prepared using 100 mM Gd-DTPA solution. Different formulation volumes were diluted with 80 % D_2O and relaxivity was measured using NMR.

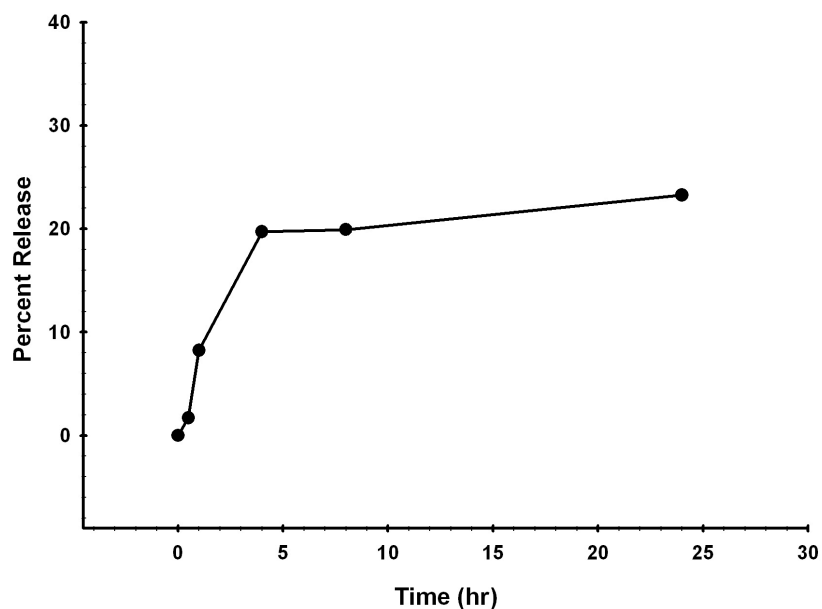


Figure 4-6. Release profile of Gd-DTPA from Gd-liposome. Gd-liposome formulated with DSPC, cholesterol and DSPE-PEG (in a molar ratio of 9:5:1). Plots of percentage versus time for Gd-DTPA liposomes show a burst release of Gd-DTPA followed by prolonged slow release. Signal at each time point was normalized to the signal of ruptured liposomes signal.

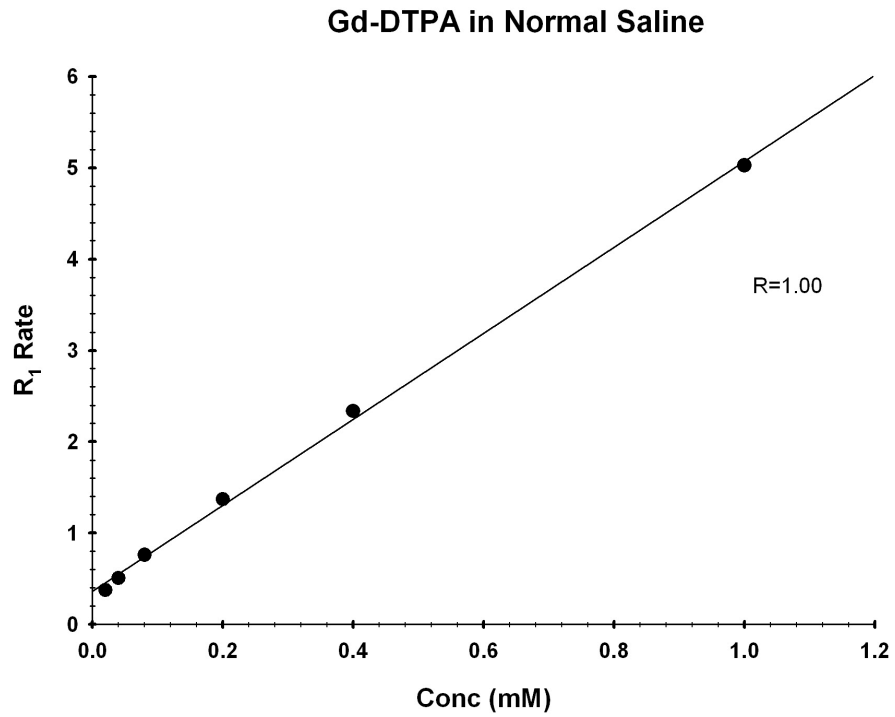


Figure 4-7. Plots of T_1 relaxation rate versus free Gd-DTPA concentrations in normal saline. R_1 values were calculated as the inverse of T_1 relaxation times.

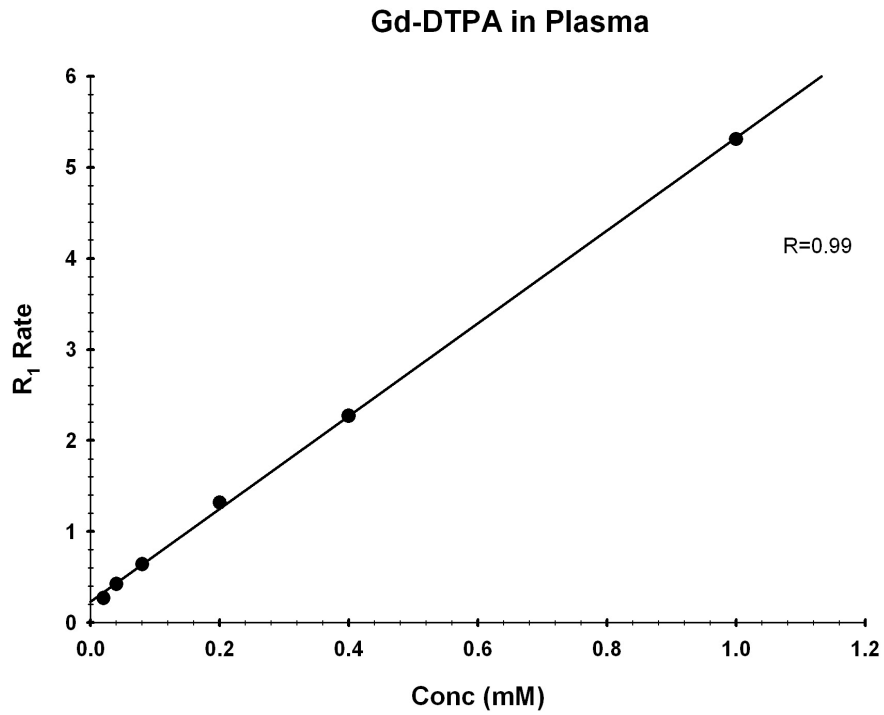


Figure 4-8. Plots of T_1 relaxation rate versus free Gd-DTPA concentrations in rat plasma. R_1 values were calculated as the inverse of T_1 relaxation times.

REFERENCES

1. Drummond, D., et al., *Optimizing liposomes for delivery of chemotherapeutic agents to solid tumors*. Pharmacological reviews, 1999. **51**(4): p. 691.
2. Shum, P., J. Kim, and D. Thompson, *Phototriggering of liposomal drug delivery systems*. Advanced drug delivery reviews, 2001. **53**(3): p. 273-284.
3. Kong, G., et al., *Efficacy of liposomes and hyperthermia in a human tumor xenograft model: importance of triggered drug release*. Cancer research, 2000. **60**(24): p. 6950.
4. Huang, S. and R. MacDonald, *Acoustically active liposomes for drug encapsulation and ultrasound-triggered release*. Biochimica et Biophysica Acta (BBA)-Biomembranes, 2004. **1665**(1-2): p. 134-141.
5. Jiang, J., et al., *Expression of group IIA secretory phospholipase A2 is elevated in prostatic intraepithelial neoplasia and adenocarcinoma*. American Journal of Pathology, 2002. **160**(2): p. 667.
6. Yamashita, S., J. Yamashita, and M. Ogawa, *Overexpression of group II phospholipase A2 in human breast cancer tissues is closely associated with their malignant potency*. British journal of cancer, 1994. **69**(6): p. 1166.
7. Kiyohara, H., et al., *Immunohistochemical localization of group II phospholipase A2 in human pancreatic carcinomas*. International Journal of Gastrointestinal Cancer, 1993. **13**(1): p. 49-57.
8. Zhu Z., A.I.A., Mock J.N., Cummings B.S. and Arnold R.D., *Development of Secretory Phospholipase A2-Targeted Liposomes*. AAPS Journal PharmSci, 11(S2), AAPS National Meeting, Los Angeles, CA. , 2009.

9. Richardson, J., et al., *Pharmaceutical applications of magnetic resonance imaging (MRI)*. *Advanced drug delivery reviews*, 2005. **57**(8): p. 1191-1209.
10. Goins, B. and W. Phillips, *The use of scintigraphic imaging as a tool in the development of liposome formulations*. *Progress in Lipid Research*, 2001. **40**(1-2): p. 95-123.
11. Freeman, R., *Magnetic resonance in chemistry and medicine*. 2003: Oxford University Press, USA.
12. Weinmann, H., et al., *Characteristics of gadolinium-DTPA complex: a potential NMR contrast agent*. *American Journal of Roentgenology*, 1984. **142**(3): p. 619.
13. Caravan, P., et al., *Gadolinium (III) chelates as MRI contrast agents: structure, dynamics, and applications*. *Chem. Rev*, 1999. **99**(9): p. 2293-2352.
14. Bellin, M., M. Vasile, and S. Morel-Precetti, *Currently used non-specific extracellular MR contrast media*. *European radiology*, 2003. **13**(12): p. 2688-2698.
15. Matteucci, M., et al., *Hyperthermia increases accumulation of technetium-99m-labeled liposomes in feline sarcomas*. *Clinical Cancer Research*, 2000. **6**(9): p. 3748.
16. Leander, P., et al., *CT and MR Imaging of the Liver Using Liver-Specific Contrast Media*. *Acta Radiologica*, 1996. **37**(3): p. 242-249.
17. NIESMAN, M., et al., *Liposome encapsulated MnCl₂ as a liver specific contrast agent for magnetic resonance imaging*. *Investigative Radiology*, 1990. **25**(5): p. 545.

18. Saito, R., et al., *Distribution of liposomes into brain and rat brain tumor models by convection-enhanced delivery monitored with magnetic resonance imaging*. Cancer research, 2004. **64**(7): p. 2572.
19. Weidensteiner, C., et al., *Quantitative dynamic contrast-enhanced MRI in tumor-bearing rats and mice with inversion recovery TrueFISP and two contrast agents at 4.7 T*. Journal of Magnetic Resonance Imaging, 2006. **24**(3): p. 646-656.

CHAPTER 5

PHARMACOKINETIC AND PHARMACODYNAMIC ASSESSMENT OF

KETANSERIN IN HORSES, PART I: PHARMACOKINETIC AND

PHARMACODYNAMIC MODELING

Ibrahim A. Aljuffali¹, Benjamin M. Brainard², James N. Moore^{3,4}, Soyoung Kwon^{3,4},
Douglas Allen³, Thomas P. Robertson^{3,4} and Robert D. Arnold^{1*}

Submitted to the Journal of Veterinary Pharmacology and Therapeutics

¹Department of Pharmaceutical and Biomedical Sciences, College of Pharmacy,

²Departments of Small Animal Medicine and Surgery, ³Large Animal Medicine, and

⁴Physiology and Pharmacology, College of Veterinary Medicine, University of Georgia.

ABBREVIATIONS

5-HT	5-hydroxytryptamine (serotonin)
ADP	adenosine diphosphate
NCA	non-compartmental analysis
LC-MS/MS	liquid chromatography tandem mass spectrometry
PK	pharmacokinetics
PD	pharmacodynamic
I.V.	intravenous
AUC	area under the curve
CL	clearance
V _d	volume of distribution
I _{max}	maximum fractional extent on inhibition
IC ₅₀	inhibition constant for 50 % inhibition of maximum function of k _{in}
k _{in}	production (synthesis) rate constant
k _{out}	removal rate constant,
R	response variable
γ	Hill coefficient

ABSTRACT

The purpose of this study was to determine the pharmacokinetics (PK) of a 5-HT receptor antagonist ketanserin in healthy adult horses, and to develop an exposure-response model that could be used to optimize dosing. Plasma concentrations of ketanserin were determined using liquid chromatography with mass spectrometry after

single and multiple I.V. doses were administered to horses. The plasma drug concentration time profiles were analyzed using non-compartmental and compartmental approaches. A linear PK model was used to obtain parameter estimates and examine different dosing schedules. Ketanserin's effects on *in vitro* platelet aggregation responses were monitored as pharmacodynamic (PD) effects of the drug, and a PK/PD model was developed to describe the observed time course of drug effects. A two compartment linear pharmacokinetic model described the plasma concentration-time profile of ketanserin after single and multiple doses in healthy horses; the terminal half-life was 8.25 hr, volume of distribution was 11.6 L, AUC was 5.98 mg•min/liter and clearance was 0.01 L/min. Model simulations predicted multiple doses PK accurately and were used to select optimal dosing based on *in vitro* platelet aggregation data. Ketanserin's PD exhibits a hysteresis and modeling suggested its dynamics could be described using an indirect response model. PK of ketanserin in healthy horses following single and multiple dosing can be described by a two-compartment PK model and alterations in platelet aggregation due to ketanserin can be described using an indirect response model.

INTRODUCTION

Laminitis is a debilitating, painful and crippling condition that affects horses of all breeds. As a clinical condition, laminitis occurs secondary to inflammation of the laminae within the horse's hoof, and results in the separation of epidermal basal cells in the inner hoof from the underlying basement membrane [1, 2]. Laminitis is a multi-factorial disorder that frequently occurs secondary to other systematic disorders, such as inflammatory bowel disease, grain overload and placental retention [3]. Evidence

suggests that disruption in hematological, inflammatory and vascular homeostasis within the horse's digit are involved in the development of laminitis. Pre-existing metabolic imbalances can also contribute to the development of laminitis [4]. Currently, no effective therapy is available for laminitis and treatment modalities include the management of the underlying condition, local and systemic analgesia, and stall rest [5].

The release of vasoactive substances, formation of microthrombi, leukocyte emigration and disruption of blood flow in the equine hoof can induce clinical signs of laminitis [6-8]. 5-HT is a potent vasoconstrictor that can mediate the described alterations in laminar blood flow [9-11]. 5-HT is derived from tryptophan and is present in high concentrations in the central nervous system and the enterochromaffin cells of the gastrointestinal tract. When released into the systemic circulation, 5-HT is sequestered by circulating platelets that regulate circulating concentrations of 5-HT [12, 13]. Upon aggregation and activation, platelets release 5-HT, which intensifies platelet aggregation responses to agonists such as ADP, in addition to causing local vasoconstriction [11]. Selective 5-HT_{2A} receptors antagonists such as ketanserin can block the interaction of 5-HT with the platelet receptors, and potentially result in a decrease in platelet activation and aggregation.

Ketanserin (**Figure 5-1 A**) is a selective and potent antagonist of the vasoconstrictor effects of 5-HT through the antagonistic effect 5-HT receptors subpopulation (5-HT_{2A}) [14]. Studies indicate that small veins in the equine laminar dermis are sensitive to 5-HT [8], which suggests that a 5-HT_{2A} receptor antagonist (e.g. ketanserin) may help to attenuate the alterations in laminar blood flow that occur during development of laminitis by inhibiting platelet activation and subsequent 5-HT release.

The goals of this study were to determine the pharmacokinetics (PK) for ketanserin in healthy horses and develop a pharmacokinetic model that describes the plasma concentrations of ketanserin and its effect on platelet aggregation. The model was used to predict and subsequently describe the pharmacodynamic (PD) effects of ketanserin on equine platelet aggregation. PK/PD modeling is a computational approach that uses mathematical expressions to assess drug deposition and activity and to facilitate rationale dose selection *in vivo* [15]. The developed model can be used to test hypotheses by extrapolating model parameters to predicate changes associated with different doses and/or frequency of administration.

METHODS

Reagents and Materials

Ketanserin (3-(2-[4-(4-fluorobenzyl)-1-piperidinyl]ethyl)-2,4-[1H,3H]-quinazoline-dione), acetic acid, acetonitrile and ammonium acetate were obtained from Thermo Fisher Scientific Inc. (Rockford, IL). Internal standard R-46594 (**Figure 5-1 B**) (3-(2-[4-(4-chlorobenzyl)-1-piperidinyl]ethyl)-2,4-[1H,3H]-quinazoline dione) was obtained from RDI Division of Fitzgerald Industries Intl. (Concord, MA).

Study Design

A dose of 0.1 mg/kg of ketanserin was administered slowly I.V. through a jugular venous catheter to six healthy female adult horses. Blood was obtained for pharmacokinetic analysis by sampling from the jugular catheter. After a 10 mL waste sample, 4 mL of blood were anticoagulated with EDTA. This blood sample was

centrifuged within 5 minutes of collection at 1500 x g, after which plasma was collected and stored frozen at -80°C until analysis. Samples were collected from each horse at t=15, 30 min, and 1, 2, 4, 8, 12 and 24 hr.

Based on initial PK calculations, a multiple-dose model for ketanserin was derived. Three healthy horses (all female) not previously treated were administered ketanserin at a dose of 0.3 mg/kg I.V. through a 14 g 5 ½” jugular venous catheter every 8 hr for a total of 3 doses. Blood was collected from the jugular catheter using the techniques described above at baseline (t=0) and at 4, 8, 12, 16, and 24 hr after the initial dose.

Drug Quantification

The concentration of ketanserin in equine plasma was determined using a liquid chromatography tandem mass spectrometry (LC-MS/MS). Ketanserin was extracted from EDTA-anticoagulated plasma (200 µL) using protein precipitation with ice-cold acetonitrile (1:2 v/v); R-46594 (**Figure 5-1 B**) was used as an internal standard. Extracted samples were centrifuged (4 °C at 3,220 × g for 10 min) and the resultant supernatants were transferred to glass vials and capped. Calibration standards were prepared in drug-free equine plasma and extracted as described above. The ratios of ketanserin to the internal standard were used to prepare calibration curves. A concentration range of 111 to 0.5 ng/mL of ketanserin was used to construct the standard curve where accuracy of ± 15 % theoretical values and precision of CV % ≤ 15 %. The limit of quantification was determined as the minimum concentration where the signal was three times greater than the baseline value with CV ≤ 20 % and accuracy of ± 20 %.

Instrumentation

The analytes were separated on an Agilent Eclipse XDB C18 column (30×2.1 mm i.d., 3.5 μm) equipped with a Phenomenex Security Guard C18 guard column (4.0×3.0 mm). Analytes were eluted from the column using isocratic mobile phase consisting of 10 mM ammonium acetate buffer adjusted to pH of 5 with glacial acetic acid and acetonitrile (1:1, v/v). LC-MS/MS measurement of ketanserin and the internal standard was performed on an Agilent 1100 HPLC system coupled to Agilent XCT Ultra Plus ion-trap mass spectrometer (Santa Clara, CA). The samples were introduced into the MS with flow rate of 0.25 ml/min using an Electrospray Ionization (ESI) source. Nitrogen gas was used as desolvation gas (flow rate of 9 L/min at 350 °C) and as nebulizer gas (40 psi) and helium was used as a collision gas. Capillary voltage was set at 3500 V, skimmer was set at 40 V and cap exit was set at 120.6 V. Mass spectra were acquired in positive-ion mode and mass transitions were monitored using multiple-reaction monitoring (MRM). MRM transitions from m/z 395 → 189 (for ketanserin) and 411 → 189 (for the I.S.) were used for analyte quantification.

Pharmacokinetics Analysis and Modeling

Noncompartmental analysis

Noncompartmental analysis of ketanserin's concentration after single dose was performed using a nonlinear regression program (WinNonlin Version 5.2, Pharsight Corp., Cary, NC). Variables include maximum plasma concentration (C_{max}), time at maximum plasma concentration (T_{max}), area under the plasma concentration-time curve (AUC), terminal half-life ($t_{1/2}$), apparent volume of distribution (V) and total systemic

clearance (CL). AUC after single I.V. dose was estimated using the log-trapezoidal method [16].

Pharmacokinetics Modeling

Pharmacokinetics modeling was performed using a nonlinear regression analysis program (WinNonlin Version 5.2, Pharsight Corp., Cary, NC). Individual animal data were analyzed using naïve pooled data (NPD), and individual plasma concentration-time profiles (**Figure 3-A**) were fitted to a two-compartment linear pharmacokinetic model described by the following explicit equation:

$$C = Ae^{-\alpha t} + Be^{\beta t} \quad \text{Eq 1.}$$

where C is the drug plasma concentration, A and B are the mass constant that represent the ordinate intercepts for the distribution and elimination phases; α and β are the slopes of the distribution and elimination phases. Model fitting was discriminated based on goodness of fit (visual inspection), the Akaike's Information Criterion (AIC) and the sum of squares [17, 18]. The resulting model was used to predict drug concentration-time profile following multiple dosing of ketanserin *via* simulation of different doses and frequency of administration.

Multiple Dose PK

The goal of the PK modeling was to capture the PK behavior in healthy horses and to predict optimal dosing schedules for future studies, based on preliminary *in vitro* studies that suggested an effective concentration of 3 ng/mL. After model simulations

were conducted, a PK study was performed, 0.3 mg/kg I.V. q8h×3, in three untreated horses to assess model validity following multiple dosing.

Ketanserin Pharmacodynamic Modeling

Pharmacological data used for current modeling were obtained from the other study (**Appendix A**) [19]. Ketanserin's effects were analyzed using a basic inhibitory indirect response model to describe the relationship between a drug concentration in the plasma and its *ex vivo* measured effects [20]. The model was then simulated to predict ketanserin's effects at different doses. Pharmacodynamic modeling was performed using WinNonlin Professional (v5.2, Pharsight Corp.). The indirect response model (**Figure 5-2**) was described by the following equation:

$$\frac{dR}{dt} = k_{in} \cdot \left(1 - \frac{I_{max} \cdot C_p^\gamma}{IC_{50}^\gamma + C_p^\gamma} \right) - k_{out} \cdot R \quad \text{Eq. 2}$$

where, k_{in} is production (synthesis) rate constant, k_{out} is the removal rate constant, R is the response variable, I_{max} is the maximum fractional extent on inhibition, γ is the Hill coefficient, IC_{50} is the inhibition constant for 50 % inhibition of maximum function of k_{in} and C_p is plasma drug concentration.

RESULTS

Pharmacokinetics Analysis

Figure 5-1 A presents the individual horse plasma drug concentration-time profiles after a single dose of ketanserin (0.1 mg/kg I.V.). Ketanserin PK exhibited multi-exponential drug disposition and was best described by a linear two-compartment PK

model (**Figure 5-2**). A non-compartmental approach was used to obtain initial PK parameter estimates from the naïve pooled data (NPD), **Table 5-1**.

Data from all horses were used during the PK modeling using a NPD approach. A two-compartment model with a linear 1st order elimination rate was used to estimate pharmacokinetics parameters (**Figure 5-3 A**). Improved fit of data was achieved after curve weighting by the inverse of the squared model predicted drug concentration ($1/\hat{y}^2$). Estimated parameters from single dose ketanserin administration are listed in **Table 5-2**.

Multiple Dose PK

To estimate the PK parameters after multiple doses, parameters were fixed and simulations with different dosing regimens were performed. Five different multiple dosing schedules were simulated, 1.0, 0.5, 0.3, 0.1 and 0.05 mg/kg/q8h over a 48 hr time period. **Figure 5-4 A** presents the resulting model simulation plasma concentration–time profiles after multiple I.V. doses. The effect of dosing frequency was simulated for 0.3 mg/kg administered every 6, 8, 12 and 24 hr. The simulated plasma drug concentration–time profiles for different dosing frequencies are presented in **Figure 5-4 B**.

Based on PK model prediction, a dose of 0.3 mg/kg/q8h was selected and administered to three adult horses. Plasma samples were collected, analyzed by LC-MS/MS and the plasma concentration-time profiles analyzed using a two-compartment model (**Figure 5-4 C**). Ketanserin disposition followed a similar kinetics profile and the estimated parameters from multiple doses of ketanserin are listed in **Table 5-2**.

Pharmacodynamic Modeling

A model linking the PK data with the pharmacological responses (platelet aggregation) was developed. Based on the observed hysteresis of the effects of ketanserin on platelet aggregation responses, an indirect response PD model (**Figure 5-2**) was used to describe the observed effects of ketanserin over time. PK parameters were fixed and used as a driving function for the PD model. The maximum fractional extent of inhibition (I_{\max}) was fixed at 1, assuming complete inhibition can be achieved, and the Hill coefficient (γ) was set to 2. The Hill coefficient was used in the model to describe the shape and steepness of the fitted curve. Averaged activity data was fitted to the proposed PD model; parameter estimates and their variation (CV %) are provided in **Table 5-3**. **Figure 5-6 A and C** present the model fitting to the observed activity data. The resulting parameters were used to simulate average drug response profiles for several dosage regimens, 0.5, 0.3, 0.1, 0.05 and 0.01 mg/kg. **Figure 5-6 B and D** illustrate the simulated average drug response profiles for ketanserin dosing. It was predicted that the lowest dose (0.01 mg/kg) would produce an insignificant pharmacological response and a 0.3 mg/kg dose would reduce platelet aggregation by approximately 50 % within 8 to 16 hr post injection. At all doses simulated, the response returned to baseline value at 24 hr.

DISCUSSION

This study utilizes the application of PK/PD modeling for the selection of an effective dosing regimen of ketanserin for subsequent clinical evaluation in horses. Knowledge of drug concentration-effect relationships can provide valuable insights into

mechanisms of drug action [21, 22] and can be used to optimize dosing regimen and rational dose selection [22].

In this study, I.V. administration of ketanserin (0.1 mg/kg) was well tolerated by all six horses. The single I.V. dose of ketanserin in healthy horses was best described by a two-compartment model, a pharmacokinetic profile similar to that reported for dogs [23], but different from humans in which plasma concentration–time data were best fitted to a 3-compartment model [24]. The estimated terminal $t_{1/2}$ of 11.5 h after a single I.V. dose in healthy horses corresponded well with elimination half-lives reported after I.V. dosing in healthy human subjects (14.3 ± 4.4 h) [24] or in patients with essential hypertension (9.6 ± 1.27 h) [25]. However, terminal $t_{1/2}$ was longer in horses in comparison to other animal species (rats, rabbit and dogs) [23]. In this study, plasma ketanserin concentrations after I.V. dosing remained for approximately 8 h above the 3 ng/mL value that had been calculated as the IC_{50} from the proposed pharmacodynamic model.

Repeated (multiple) doses of ketanserin can also be explained by a two-compartment model. Dosing of healthy horses with 0.3 mg/kg I.V. ketanserin q8h showed a similar profile to the one that was observed following single dose. Good agreement between the observed and predicted values was achieved. Thus, the present model can be used for optimizing therapeutic regimens of ketanserin.

Optical aggregometry was used to quantify the platelet response to ketanserin in equine platelet rich plasma by monitoring changes in light transmittance after stimulation by ADP or collagen. After a single dose of ketanserin (0.1 mg/kg I.V.), platelet responses to both ADP and collagen decreased [19]. An indirect response model was devised to capture the temporal delay in ketanserin's effects on platelet aggregation. The PK/PD

model was also used for simulating several dosage regimens that could be used to assist in dose selection for future clinical studies.

The present results suggest that the proposed indirect response model provided a good prediction of the time course of ketanserin's pharmacological activity. An important issue regarding mechanistic PD models is the ability to explain the underlying mechanism of the drug response. Ligands that interact with a corresponding receptor have gained considerable interest to optimizing therapeutic use. In this study, we assumed that binding of ketanserin with 5-HT₂ receptor is a zero-order process with a rate constant (K_{in}), whereas drug-receptor dissociation is a first-order process with a rate constant (K_{out}). Ketanserin induces platelets aggregation through binding with 5-HT₂ receptor with an inhibition value of IC_{50} .

The initial decline in platelet aggregation reflected the inhibition of K_{in} values, whereas the return to baseline was controlled by the disappearance of ketanserin from the plasma[19]. Platelet aggregation returned to basal levels over a relatively long time in comparison to the drug-receptor interaction. This may be attributed to strong drug receptor binding, as well as slow dissociation from the receptor. In addition, the long duration of the pharmacological effect was justified by the finding that the IC_{50} of ketanserin was low, which suggested that ketanserin is a potent, long acting inhibitor of platelet aggregation.

A two-compartment PK model was used to describe the PK of ketanserin in healthy horses after single and multiple doses. Ketanserin activity as reflected by changes in optical platelet aggregation, exhibits hysteresis and preliminary studies suggest that

ketanserin PD's can be described using an indirect response model. Model simulations are currently being used to predict PK/PD of ketanserin to support clinical studies.

ACKNOWLEDGMENTS

These studies were funded in part by a Grayson Jockey Club Research Foundation Inc. I.A. is funded, in part, by Saudi Arabian Cultural Mission Fellowship.

Table 5-1. Pooled non-compartmental pharmacokinetic parameter estimates of six healthy adult horses after a single ketanserin I.V. dose of 0.1 mg/kg to 6 horses.

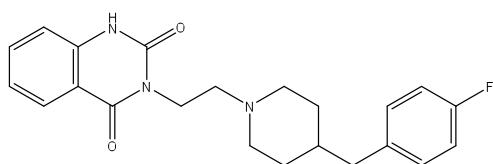
Parameter (units)	Estimate
C_{\max} (ng/mL)	15.6
T_{\max} (hr)	0.25
AUC (0- ∞) (hr•ng/mL)	99.6
$t_{1/2}$ (hr)	8.8
V (L/kg)	11.3
CL (L/hr/kg)	0.89

Table 5-2. Pharmacokinetics parameters obtained by compartmental analysis after single I.V. dose (0.1 mg/kg, n=6) or multiple doses (0.3 mg/kg, n=3). Two-compartment model with 1st order elimination was used to estimate these parameters.

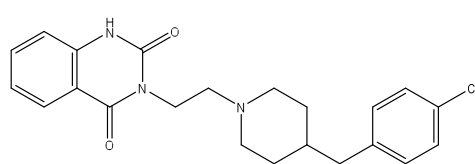
Parameter (units)	Single Dose (0.1 mg/kg)		Multiple Doses (0.3 mg/kg/q8h)	
	Estimate	CV %	Estimate	CV %
A (ng/mL)	11.2	24.9	33.6	55
B (ng/mL)	4.49	71.4	13.4	101
Alpha (hr ⁻¹)	0.28	41.5	0.32	76.8
Beta (hr ⁻¹)	0.06	49.4	0.07	43.1
AUC (hr•ng/mL)	115	8.42	286	12.1
K10- t _{1/2} (hr)	5.07	12.9	4.2	27.5
Alpha- t _{1/2} (hr)	2.47	41.6	2.17	76.7
Beta- t _{1/2} (hr)	11.5	49.3	9.3	43
K10 (hr ⁻¹)	0.14	13	0.16	27.5
K12 (hr ⁻¹)	0.08	46.3	0.08	129
K21 (hr ⁻¹)	0.12	77.6	0.14	105
V1 (L/kg)	6.37	7.5	6.38	28.3
CL (L/hr/kg)	0.87	8.5	1.05	12.1
Vss (L/kg)	10.5	21.1	10.1	20.1
V2 (L/kg)	4.17	48.5	3.74	54.3

Table 5-3. Pharmacodynamic parameters for platelet aggregation after single I.V dose of ketanserin (0.1 mg/kg) in healthy adult horses.

Parameter (units)	ADP		Collagen	
	Estimate	CV %	Estimate	CV %
K_{in} (hr ⁻¹)	7.12	26.4	9.85	24
K_{out} (hr ⁻¹)	0.09	22.4	0.12	19.9
IC ₅₀ (ng/mL)	3.68	21.7	3.7	20.1
R (% aggregation)	76.3	7.70	81.2	8.3

A

(3-(2-[4-(4-fluorobenzyl)-1-piperidinyl]ethyl)-2,4-[1H,3H]-quinazolin-2(1H)-one)

B

(3-(2-[4-(4-chlorobenzyl)-1-piperidinyl]ethyl)-2,4-[1H,3H]-quinazolin-2(1H)-one)

Figure 5-1. Ketanserin structure. Chemical structure of **A.** ketanserin and **B.** R-46594, the internal standard.

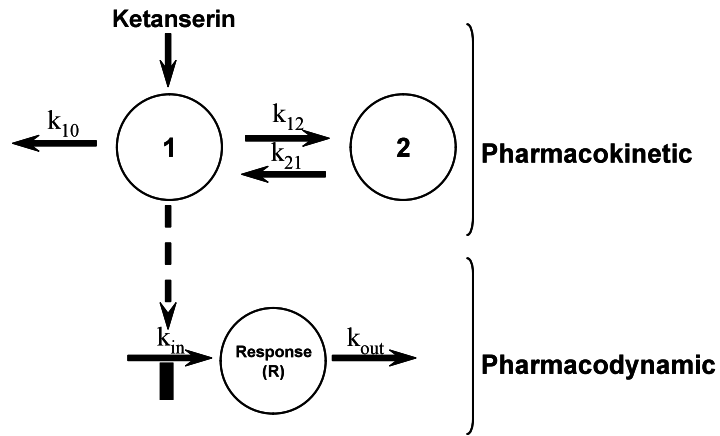


Figure 5-2. Diagram of pharmacokinetic/pharmacodynamic model used to describe ketanserin deposition and *ex vivo* platelets aggregation activity after single and multiple dose administration.

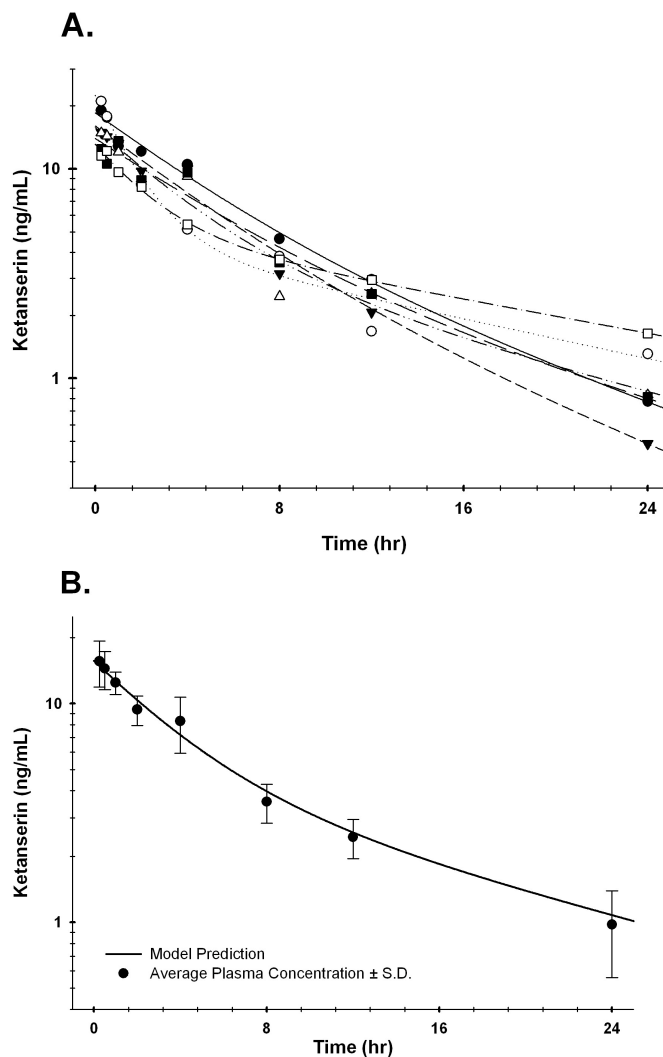


Figure 5-3. Pharmacokinetic profiles of ketanserin in healthy horses after a single dose (0.1 mg/kg I.V.). **A.** Pharmacokinetic profiles of individual observed plasma concentrations of ketanserin in individual healthy horses after a single dose (0.1 mg/kg I.V.). **B.** Naïve pooled data of all six horses were used in the pharmacokinetic modeling of ketanserin. All data were analyzed simultaneously and fitted to a two-compartment pharmacokinetics model. Symbols represent mean data \pm S.D (n=6).

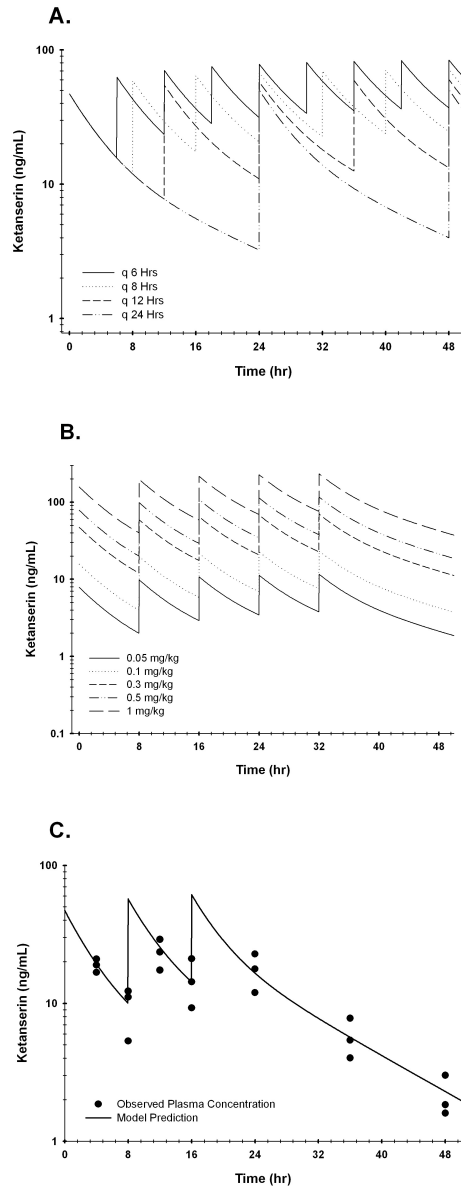


Figure 5-4. Model simulation with different dose and dosing schedules. A. Simulated plasma concentration–time profiles of ketanserin with a 0.3 mg/kg at q6h, q8h, q12h and q24h. **B.** Simulated plasma concentration–time profiles of ketanserin with a 1.0, 0.5, 0.3, 0.1 and 0.05 mg/kg/q8h doses. **C.** Ketanserin (0.3 mg/kg/q8h I.V.) was administered to three adult healthy horses. Data were analyzed simultaneously (pooled data) and fitted to a two-compartment pharmacokinetic model. Solid line represents the model fit.

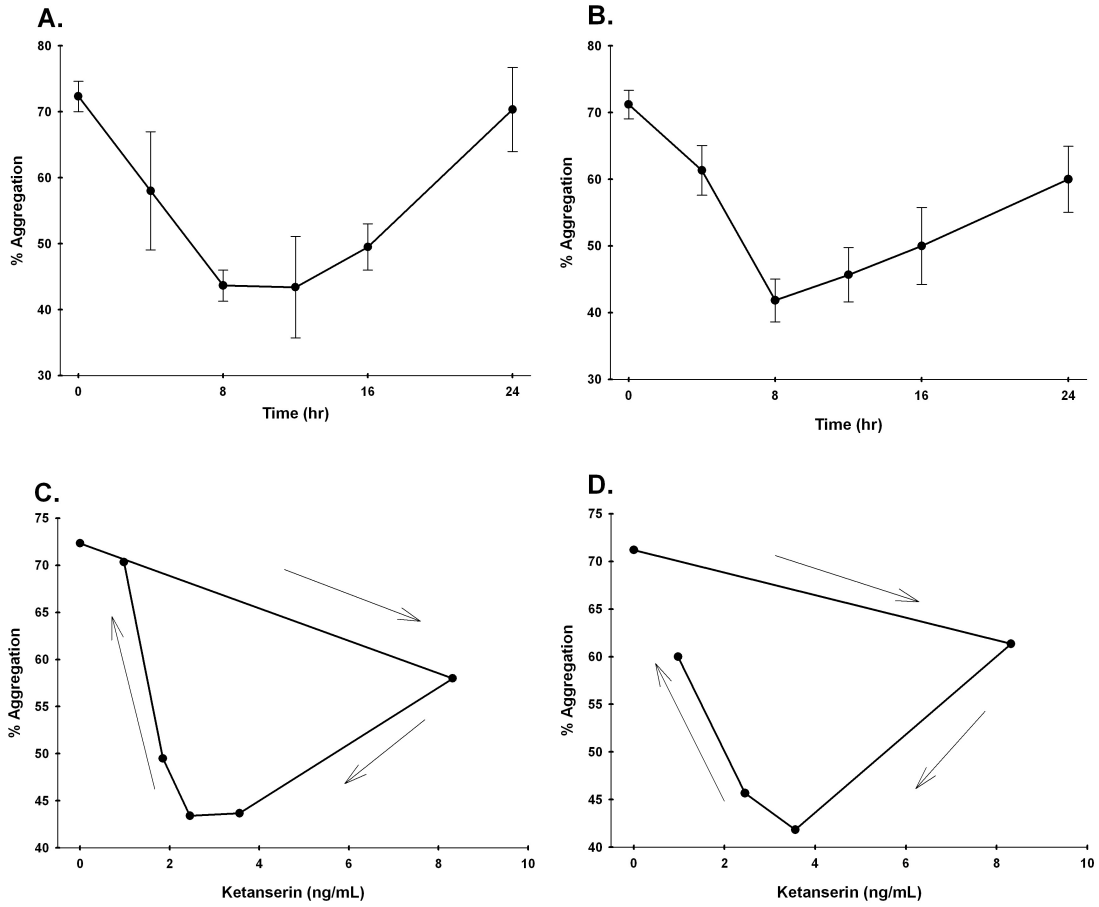


Figure 5-5. Time course of *ex vivo* platelets aggregation induced using two methods to stimulate platelet aggregation. First method by 15 μ M ADP (**A**) and the second method by using 15 μ g/mL collagen (**B**) after administration of a single dose of ketanserin. The plot of effect versus plasma concentration (**C** and **D**) results in a hysteresis curve for the two methods.

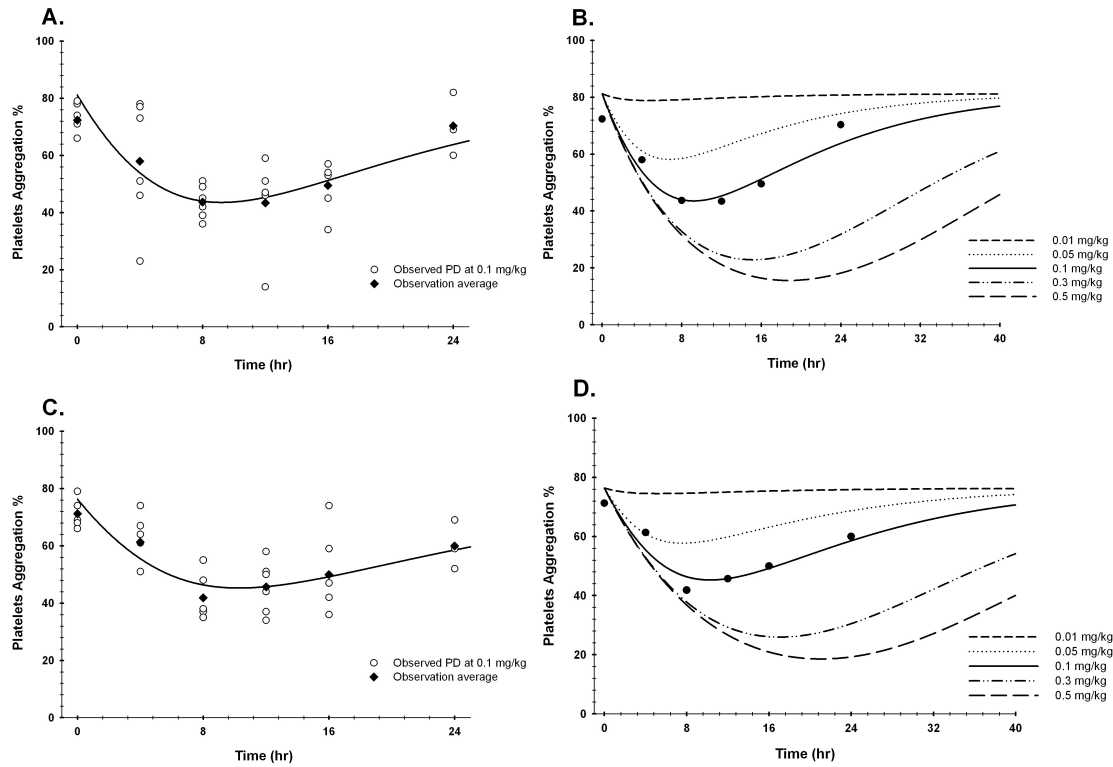


Figure 5-6. *Ex vivo* platelets aggregation data fitted using indirect response pharmacodynamic model (A and C). Model was sufficient to capture platelet aggregation mediated by ADP and Collagen. Model simulation of different doses was performed to predict platelet aggregation with different doses of ketanserin (B and D).

REFERENCES

1. Pollitt, C., *Basement membrane pathology: a feature of acute equine laminitis*. Equine veterinary journal, 1996. **28**(1): p. 38-46.
2. Pollitt, C. *Equine laminitis: a revised pathophysiology*. in *Proceedings of the Annual Convention of the AAEP*. 1999.
3. Eades, S., A. Holm, and R. Moore. *A review of the pathophysiology and treatment of acute laminitis: pathophysiologic and therapeutic implications of endothelin-1*. in *Proceedings of the Annual Convention of the AAEP*. 2002.
4. Robertson, T., S. Bailey, and J. Peroni, *Equine laminitis: A journey to the dark side of venous*. Veterinary immunology and immunopathology, 2009. **129**(3-4): p. 164-166.
5. Carter, D. and B. Renfroe, *A Novel Approach to the Treatment and Prevention of Laminitis: Botulinum Toxin Type A for the Treatment of Laminitis*. Journal of Equine Veterinary Science, 2009. **29**(7): p. 595-600.
6. Black, S., et al., *Leukocyte emigration in the early stages of laminitis*. Veterinary immunology and immunopathology, 2006. **109**(1-2): p. 161-166.
7. Weiss, D., et al., *Evaluation of platelet activation and platelet-neutrophil aggregates in ponies with alimentary laminitis*. American journal of veterinary research, 1997. **58**(12): p. 1376.
8. Peroni, J., et al., *Predisposition for vasoconstriction in the equine lamellar dermis: implications in equine laminitis*. Journal of Applied Physiology, 2006. **100**(3): p. 759.

9. Elliott, J., Y. Berhane, and S. Bailey, *Effects of monoamines formed in the cecum of horses on equine digital blood vessels and platelets*. American journal of veterinary research, 2003. **64**(9): p. 1124-1131.
10. Weiss, D., et al., *Effect of a competitive inhibitor of platelet aggregation on experimentally induced laminitis in ponies*. American journal of veterinary research, 1998. **59**(7): p. 814.
11. Vanhoutte, P., *Vascular effects of serotonin and ischemia*. Journal of cardiovascular pharmacology, 1990. **16**: p. S15.
12. Vane, J., *The release and fate of vaso-active hormones in the circulation*. British Journal of Pharmacology, 1969. **35**(2): p. 209.
13. De Meyer, S., et al., *Antiplatelet drugs*. British journal of haematology, 2008. **142**(4): p. 515-528.
14. Van Nueten, J., et al., *Vascular effects of ketanserin (R 41 468), a novel antagonist of 5-HT₂ serotonergic receptors*. Journal of Pharmacology and Experimental Therapeutics, 1981. **218**(1): p. 217.
15. Toutain, P., *Pharmacokinetic/pharmacodynamic integration in drug development and dosage-regimen optimization for veterinary medicine*. The AAPS Journal, 2002. **4**(4): p. 160-188.
16. Gibaldi, M. and D. Perrier, *Pharmacokinetics. 2nd*. Drugs and the pharmaceutical sciences. New York, NY: Marcel Dekker, 1982.
17. Yamaoka, K., T. Nakagawa, and T. Uno, *Application of Akaike's information criterion (AIC) in the evaluation of linear pharmacokinetic equations*. Journal of Pharmacokinetics and Pharmacodynamics, 1978. **6**(2): p. 165-175.

18. Gabrielsson, J. and D. Weiner, *Pharmacokinetic/pharmacodynamic data analysis: concepts and applications*. Fourth Edition ed. 2007.
19. Brainard, B., Aljuffali, I., Moore, J., Kwon, S., Allen, D., Robertson, T., and Arnold, R., *Pharmacokinetic and Pharmacodynamic Assessment of Ketanserin In Horses, Part II: In vivo and Ex Vivo Effects on Equine Platelet Function*. J Vet Pharm Ther, 2010.
20. Dayneka, N., V. Garg, and W. Jusko, *Comparison of four basic models of indirect pharmacodynamic responses*. Journal of Pharmacokinetics and Pharmacodynamics, 1993. **21**(4): p. 457-478.
21. Landoni, M., F. Cunningham, and P. Lees, *Pharmacokinetics and pharmacodynamics of ketoprofen in calves applying PK/PD modelling*. Journal of veterinary pharmacology and therapeutics, 1995. **18**(5): p. 315-324.
22. Lees, P., et al., *PK/PD integration and PK/PD modelling of nonsteroidal anti-inflammatory drugs: principles and applications in veterinary pharmacology*. Journal of veterinary pharmacology and therapeutics, 2004. **27**(6): p. 491-502.
23. Michiels, M., et al., *Pharmacokinetics and tissue distribution of ketanserin in rat, rabbit and dog*. Arzneimittel-Forschung, 1988. **38**(6): p. 775.
24. Heykants, J., et al., *Pharmacokinetics of ketanserin and its metabolite ketanserinol in man after intravenous, intramuscular and oral administration*. European journal of clinical pharmacology, 1986. **31**(3): p. 343-350.
25. Hedner, T., B. Persson, and G. Berglund, *Ketanserin, a novel 5-hydroxytryptamine antagonist: monotherapy in essential hypertension*. British journal of clinical pharmacology, 1983. **16**(2): p. 121.

CHAPTER 6

SUMMARY

The overall goal of this dissertation was to exploit differences in tumor microenvironment (pH and hypoxia), develop dosing schedules to facilitate optimization of drug-carriers, and use pharmacokinetic-pharmacodynamic modeling to improve therapy. In **Chapter 2** we determined the effect of metronomic dosing on the activity of topotecan in *in vitro* and *in vivo* models of human prostate cancer. We found that topotecan exhibits schedule-dependent anticancer activity, cell cycle alterations and differences in p21 expression following metronomic-like exposure *in vitro*. Specifically, the metronomic schedule significantly ($p \leq 0.05$) increased topotecan activity (8-20 fold) against PC-3 and LNCaP human prostate cancer cells. mRNA expression between PC-3 and LNCaP were markedly different. Further, the levels of numerous cancer regulatory genes were altered with different exposure profiles. Increase in topotecan potency was also observed *in vivo* using a xenograph model of human prostate cancer in nude mice following metronomic dosing in comparison to conventional dosing or to untreated controls. These findings support our hypothesis that metronomic dosing of topotecan can increase its potency compared to conventional dosing and also suggests that the enhanced antitumor activity of topotecan following fractionated dosing correlated with cell cycle arrest and increased expression of p21.

Solid tumors exhibit spatial differences in oxygenation status and acidity within the extracellular fluid that can impact treatment outcome. In **Chapter 3** we determined the

antitumor activity of topotecan in PC-3 cells grown under a tumor-like microenvironment (chronic acidification and acute hypoxia) *in vitro*. We have shown that topotecan cytotoxicity increased significantly ($p \leq 0.05$) in the tumor-like microenvironment in comparison to a more physiological condition. Increases in topotecan activity in an acidic microenvironment can be correlated to the increase in the concentration of the active form (lactone). We also determined that topotecan cytotoxicity increases due to acute hypoxic exposure. Another aim of this chapter was to develop a new nanoparticulate drug-carrier by exploiting pH differences of tumor tissues. We developed a prototype formulation loaded with the inactive carboxylate-ion form of topotecan that had a prolonged release profile *in vitro*. This newly developed formulation can be exploited to increase topotecan activity and reduce non-target tissue toxicity *in vivo*.

To better understand and characterize the release of nanoparticulate drug-carriers *in vivo*, we encapsulated Gd-DTPA, a paramagnetic agent, into liposome formulations. Our goal was to non-invasively examine the release of this compound from different lipid compositions and tumor microenvironments. In **Chapter 4**, we developed a technique to quantify the rate and extent of release of Gadolinium-DTPA encapsulated into long-circulating liposomes. Determining drug release *in vivo* can aid in designing nanoparticles with optimum release kinetics. Further study will follow to optimize drug release *in vitro* and *in vivo* with different liposome formulations.

In **Chapter 5**, we utilized pharmacokinetic and pharmacodynamic modeling techniques to optimize dosing of ketanserin in animal model of equine laminitis. We determine the pharmacokinetics of ketanserin, a 5-HT receptor antagonist, in healthy adult horses. Other goal was to develop an exposure-response model that could be used to

describe the observed effect of ketanserin (platelets aggregation). We utilized liquid chromatography with tandem mass spectrometry (LC-MS/MS) to determine ketanserin plasma concentrations. A two-compartment linear pharmacokinetic (PK) model was used to describe ketanserin plasma kinetics, and this model was used to simulate different dosing scenarios. This model was able to capture ketanserin plasma kinetics following multiple dosing. Furthermore, ketanserin's activity on platelet aggregation was obtained, and the observed time course of drug effect was sufficiently characterized by an indirect response model.

APPENDIX A

**PHARMACOKINETIC AND PHARMACODYNAMIC ASSESSMENT OF
KETANSERIN IN HORSES, PART II: *IN VIVO* AND *EX VIVO* EFFECTS ON
EQUINE PLATELET FUNCTION**

Benjamin M. Brainard², Ibrahim A. Aljuffali¹, James N. Moore^{3,4}, Soyoung Kwon^{3,4},
Douglas Allen³, Thomas P. Robertson^{3,4} and Robert D. Arnold¹

Submitted to the Journal of Veterinary Pharmacology and Therapeutics

¹Department of Pharmaceutical and Biomedical Sciences, College of Pharmacy,

²Departments of Small Animal Medicine and Surgery, ³Large Animal Medicine, and

⁴Physiology and Pharmacology, College of Veterinary Medicine, University of Georgia.

ABBREVIATIONS

5HT	5-hydroxytryptamine (serotonin)
ADP	adenosine diphosphate
CBC	complete blood count
IV	intravenous
PK	pharmacokinetics
PD	pharmacodynamics
PRP	platelet rich plasma
PPP	platelet poor plasma

ABSTRACT

Serotonin (5HT) released from platelets augments platelet activation and vasoconstriction. Ketanserin, a 5HT_{2A} receptor antagonist, was studied for its effects on platelet aggregation in horses. *In vitro* addition of two concentrations of ketanserin (200 ng/mL and 1 mg/mL) to equine platelet rich plasma (PRP) resulted in a significant decrease in ADP-induced (but not collagen-induced) platelet aggregation after a 60 min incubation (66.0 ± 9.8 % to 46.3 ± 9.6 % or 46.8 ± 5.6 , $p=0.001$, respectively). Based on these findings, ketanserin was administered IV at a dose of 0.1 mg/kg to six healthy adult horses, and alterations in *ex vivo* platelet aggregation were monitored. Administration of ketanserin resulted in a significant decrease in *ex vivo* platelet aggregation induced by both ADP and collagen 4-12 hr after administration (71.2 ± 5.3 % to a nadir of 41.8 ± 7.9 % for ADP, and 72.3 ± 5.7 % to a nadir of 43.4 ± 17.2 % for collagen, both $p<0.001$). In a subsequent study, administration of 0.3 mg/kg ketanserin IV q8h to seven different

adult horses did not result in a significant decrease in either ADP- or collagen-induced platelet aggregation. In three of these horses, ketanserin did not have an effect on serum or plasma 5HT concentrations. Ketanserin has an inconsistent effect on platelet aggregation in the horse, meriting further study prior to clinical use.

INTRODUCTION

Serotonin (5HT) released from platelet dense granules plays an important role in platelet aggregation, as well as in the vasoactive changes that occur after platelet activation [1]. Release of 5HT from platelets serves to activate additional platelets at sites of vascular injury by interacting with the platelet 5HT_{2A} receptor. Activation of the 5HT_{2A} receptor on platelets results in Gq- mediated activation of phospholipase C and subsequent calcium signaling, platelet shape change, and granule secretion. 5HT causes weak reversible platelet aggregation in human platelets, and is important as a synergistic activator of aggregation in combination with more common stimuli such as ADP and collagen [2, 3]. The same appears to be true in horses [4]. Platelets cannot synthesize 5HT de novo, but rather have specific pumps for the uptake of 5HT from the bloodstream and subsequent sequestration in dense granules [5]. In the majority of vascular beds, vasoconstriction is the primary effect of 5HT release, which can also serve to promote hemostasis at areas of vascular injury [6].

The vasoactive properties of serotonin (released from platelets or generated elsewhere) purportedly play a role in the pathophysiology of many animal diseases. Collateral blood flow in areas of arterial thrombosis (such as feline aortic thromboembolism) is decreased with exposure to 5HT [7-9], and dogs with chronic

valvular disease have increased concentrations of 5HT in circulation [10]. Increased circulating concentrations of 5HT have been identified in horses with recurrent airway obstruction [11], and a steady increase in serum 5HT concentration has also been documented in horses with carbohydrate overload-induced laminitis [12]. Digital laminar vessels (specifically veins) [13, 14] and smaller laminar vessels [15] in horses with experimental laminitis are exquisitely sensitive to serotonin-induced vasoconstriction. Increased equine digital laminar vessel reactivity after endotoxin exposure may also be a result of exposure to products of platelet activation such as 5HT and thromboxane A₂ (TXA₂) [16]. Serotonin-like products may also be produced as the result of bacterial fermentation in the equine gastrointestinal tract, and may contribute to laminar vasoconstriction [17, 18]. These products also may inhibit platelet reuptake of 5HT, resulting in the progressive increase in serum 5HT in the prodromal stages of carbohydrate overload-induced laminitis [19].

In addition to the increase in circulating concentrations of 5HT in horses with experimental laminitis, there is also evidence that platelet reactivity is increased in these animals, and may be both the source of and result of the increased 5HT concentrations. Weiss et al. reported that platelets are in a hyperactive state in the prodromal stages of carbohydrate overload-induced laminitis in ponies and horses [20, 21]. This hyperactivity is characterized by a magnification of the response of platelets to thrombotic stimuli and by an increased tendency to aggregate spontaneously. Increased circulating platelet-neutrophil aggregates and microthrombi in the small veins of the laminar dermis were also identified in horses administered excessive amounts of carbohydrate. The formation of platelet aggregates within the veins of the digit can result in a localized increase in

5HT concentration, which could result in vasoconstriction of the laminar veins and progression towards laminitis.

Because 5HT receptor antagonists may attenuate both the vasoconstriction and platelet aggregation resulting from 5HT exposure, they are attractive candidates for study in horses that are at risk of laminitis. Ketanserin is an antagonist at the 5HT_{2A} receptor, and has been used mainly as an antihypertensive agent in human medicine [22]. Studies on human and feline platelets indicate that ketanserin decreases platelet aggregation [23]. In humans, cats, dogs, and rabbits, the administration of ketanserin specifically attenuates the secondary aggregation response to agonists such as ADP, collagen, and TXA₂, and is hypothesized to be mediated by the antagonism of 5HT release from platelet dense granules [3, 24-26]. The effects of ketanserin on platelet function in the horse have not been studied.

Because of the role that 5HT plays in the reactivity of digital laminar vessels during the development of laminitis, and because of the possible role of platelet activation or formation of platelet thrombi in this condition, we investigated the pharmacodynamics of ketanserin on *in vitro* and *ex vivo* equine platelet aggregation. Our hypothesis was that equine platelets exposed *in vitro* to ketanserin would have decreased aggregation responses to both ADP and collagen, and that this decreased aggregation would be demonstrable after IV administration of ketanserin.

MATERIALS AND METHODS

Animals

A total of 13 adult horses owned and cared for by the College of Veterinary Medicine were used in this study. The horses were deemed to be healthy based on the results obtained from a physical examination, complete blood counts (CBC) and serum chemistry analyses. All procedures were approved by the University of Georgia IACUC.

Preparation of ketanserin solutions

Ketanserin used in the *in vitro* investigations was diluted to appropriate concentrations from a stock solution of 5mM ketanserin in DMSO (Sigma Chemical, St. Louis MO). Dilutions were made using sterile 0.9 % saline for irrigation, and no precipitation of compound was visible with dilution. Ketanserin used for *in vivo* administration was prepared as a stock solution in DMSO to a final concentration of 50 mg/mL, and was diluted to the appropriate dose using 40 mL of sterile 0.9 % saline for injection.

In vitro investigation

Blood was collected from 4 healthy adult horses by clean jugular venipuncture with a 19g butterfly catheter and syringe, and anticoagulated with 3.2 % sodium citrate (Sigma Chemical, St. Louis MO) to a final citrate: blood ratio of 1:9. Anticoagulated blood was transferred to 15 mL conical tubes, and centrifuged at 150 x g at room temperature for 10 min to prepare platelet rich plasma (PRP). After harvesting the PRP, the remainder of the sample was centrifuged at 1500 x g for 10 min to prepare platelet

poor plasma (PPP). PRP samples were adjusted as necessary using PPP to attain a final platelet count between 175,000 and 250,000 platelets/ μ L. After preparation of PRP, all samples rested at least 30 min prior to aggregation analysis, and all analyses were completed within 4 hr of collection.

PRP samples (500 μ L each) were assayed for aggregation responses using a dual-channel optical lumi-aggregometer (Model 700 Whole Blood/Optical Lumi-Aggregometer, Chrono-log, Havertown PA). A dose titration identified the concentration of ADP and collagen (both from Chrono-log, Havertown PA) that would result in aggregation responses between 60 – 80 %. These concentrations were 15 μ M for ADP, and 15 μ g/mL for collagen. Two PRP aliquots were each exposed to ketanserin at two concentrations, 200 ng/mL and 1 mg/mL. After addition of ketanserin, two aliquots were stirred with a silicone-coated magnetic stir bar at 1200 rpm for 10 min at 37 °C, followed by aggregation analysis. The other two aliquots were stirred with a silicone-coated magnetic stir bar at 1200 rpm for 10 min at 37 °C, and subsequently held at 37 °C for 50 more min (without stirring) prior to aggregation analysis.

Because the ketanserin stock solution contained DMSO, an equivalent dilution of DMSO in saline was studied as a control for each dose and time point. DMSO samples were treated identically to the ketanserin samples with regards to temperature, stirring, and rest period. Two baseline samples of PRP without additives were also evaluated for aggregation to both ADP and collagen. The percentage of aggregation after exposure to each agonist was the recorded outcome measure for these assays; aggregation was allowed to progress for 6 min after addition of agonist and the maximum percent aggregation was recorded.

Ex vivo investigations

A dose of 0.1 mg/kg of ketanserin was administered to 6 healthy adult horses by slow intravenous administration (over 2-3 min) through 14g. 5 ½" jugular venous catheters. Horses were monitored during drug administration, and assessed every 15 min after administration for 1 hr, after which they were evaluated after an additional hour, and then every 2 hr for any signs of discomfort, colic, or abnormal rectal temperature. Rectal temperature, heart rate, and respiratory rate were recorded at each evaluation time. Blood was sampled for platelet aggregometry at 6 time points: baseline (time = 0), and 1, 4, 8, 12, and 24 hr after drug administration. Blood was obtained from the jugular venous catheter after 10 mL of blood was aspirated and discarded. 9 mL of whole blood was then drawn directly into a syringe containing 1 mL 3.2 % sodium citrate. This blood was subsequently transferred to 15 mL conical tubes, and was processed into PRP and PPP as described above. Aggregation of these samples was performed using ADP (15 µM) and collagen (15 µg/mL) as agonists. All aggregation analyses were performed in duplicate, and the average percent aggregation for the two trials was used for statistical comparisons. In addition to the aggregation analyses, blood was collected for pharmacokinetic modeling at time 0, 15 min, 60 min, and 2, 4, 8, 12, and 24 hr after drug administration.

The pharmacodynamics of ketanserin were also investigated in a multiple-dose trial in which a different group of 7 healthy horses were equipped as described above with 14 g 5 ½" jugular venous catheters. Based on pharmacokinetic data obtained from the single dose ketanserin study [27], horses were administered ketanserin at a dose of 0.3 mg/kg IV every 8 hr for a total of 3 doses. Doses were given slowly over 2-3 min. Blood

was sampled from the jugular catheter using the techniques described above at baseline (t=0) and at 4, 8, 12, 16, and 24 hr after the initial dose. Blood was evaluated for optical aggregation responses as described above, using ADP (15 μ M) and collagen (15 μ g/mL) as agonists.

One additional EDTA blood tube was collected from all horses 24 hr after dosing for analysis of a complete blood count (CBC) by an automated analyzer, and a blood tube without additive was also collected for analysis of serum chemistry values.

Serum 5HT

Serum 5HT was measured in 3 of the horses involved in the multi-dose ketanserin study. Blood was collected from the jugular catheter as described above, and placed into a siliconized glass tube and allowed to clot for 1 hr. After one hr, the tube was centrifuged at 400 x g, and 4 °C for 10 min, after which the serum was removed and centrifuged again at 1200 x g at 4 °C for 10 min [16]. The serum was removed and frozen in aliquots at -80 deg C for analysis using a commercially available 5HT ELISA kit (5HT ELISA, Immuno-biologic Labs, Minneapolis, MN). These samples were assayed within 4 weeks of collection. At the same time, blood was also collected and placed into a tube containing lithium heparin, clomipramine (1 mM), and phenylzine (0.1 mM) (both Sigma Chemical, St. Louis MO), to inhibit 5HT metabolism and uptake. This tube was centrifuged twice immediately following collection, as described above.

Statistics

Statistics were performed using a commercial statistics program (Sigma-Stat 3.05, Systat, Co, Chicago IL). Aggregation responses for the *in vitro* study were compared using a one-way ANOVA, with a Bonferroni correction for multiple comparisons when significant associations were identified. The aggregation data for the *ex vivo* investigations were compared using a one-way ANOVA for repeated measures, with appropriate post hoc adjustments for multiple comparisons. Significance was set at a $p \leq 0.05$. Normally distributed data (as determined by the Kolmogorov-Smirnov test) are described as mean \pm standard deviation, while non-parametric data are described as median (range).

RESULTS

In vitro investigation

Results of the *in vitro* study are summarized in **Table A-1**. Baseline ADP-induced aggregation was 66.0 ± 9.8 %, and baseline collagen-induced aggregation was 92.0 ± 6.0 %. There was a significant difference between baseline ADP aggregation and the aggregation response after 60 min of incubation with both the low (46.3 ± 5.6 %, $p = 0.002$) and the high concentration (46.8 ± 9.0 %, $p = 0.003$) of ketanserin. There was no difference between the baseline ADP aggregation and the ADP-induced aggregation of samples after 10 min of incubation with either concentration of ketanserin ($p = 0.29$ [low], $p = 0.79$ [high]). There were no differences between the baseline ADP-induced aggregation and the DMSO control samples or between baseline collagen-induced aggregation and any of the experimental samples ($p = 0.361$).

Ex vivo investigation, single dose

Six adult female Quarter horses were studied. Four of these horses were the same horses used for the *in vitro* portion of this experiment. Intravenous administration of ketanserin resulted in sweating in all horses and agitation or ataxia in three horses. These signs lasted for 60 min after injection of drug, and did not recur for the duration of the study. Despite these outward signs, there were no significant differences in heart rate (range 28-52, $p = 0.419$), respiratory rate (range 12-36, $p = 0.199$) or rectal temperature (range: 98.7 – 100.7 °F, $p = 0.830$) between time points. There were no significant changes in complete blood count or serum chemistry results as an effect of treatment. Significant decreases in platelet aggregation were identified at 4, 8, and 12 hr after injection of ketanserin, with a greater than 50 % decrease from baseline aggregation for both ADP and collagen agonists (**Table A-2**). There was no difference in aggregation responses between the 24 hr samples and the baseline samples (**Table A-2**).

In vivo investigation, multiple doses

7 adult horses, all different from the single dose cohort, were studied. Intravenous injection of ketanserin was not associated with any changes in physical exam parameters in this group, and horses tolerated the multiple dose protocol without abnormal physical exam findings. There were no significant differences in aggregation responses using either ADP or collagen as agonists between any time points ($p = 0.207$, $p = 0.200$, respectively). Aggregation data from these horses is summarized in **Table A-3**.

In the three horses in which concentrations of serotonin in either plasma or serum were determined, there were no changes identified as a result of ketanserin therapy.

There was a trend towards a decreased serum serotonin concentration at 12 and 16 hr after the first dose, but these values did not reach statistical significance compared to baseline values ($p = 0.360$, **Table A-4**).

Complete blood count (CBC) data for all 13 horses used in the *ex vivo* study were within institutional reference ranges both before and 24 after drug administration. There were no significant changes in any parameter as a result of either single or multiple drug administration (data not shown).

DISCUSSION

In this study, ketanserin failed to result in a predictable decrease in platelet aggregation. While some horses had a significant decrease in platelet aggregation after a single dose, platelets from other horses, exposed to a more stable plasma concentration of ketanserin by multiple dosing, did not. The lack of effect in the multiple-dose group of horses was surprising, and may have resulted from differences in the 5HT_{2A} receptor between individual horses or horse breeds. Horses whose platelets were responsive to ketanserin may have been inadvertently selected, because some of the same horses used for the *in vitro* study were used for the *in vivo* single-dose study.

Another possible difference between horses whose platelets were affected by ketanserin and those whose platelets were not, may have been the amount of 5HT present in dense granules of the horses investigated. Platelets do not synthesize 5HT, but scavenge it from the circulation via cellular 5HT uptake pumps [5]. Variations between circulating concentrations of 5HT, and thus of platelets, may have resulted in a less obvious effect of 5HT antagonism in the multiple dose group. While a study of horses

with equine Cushing's disease failed to show a circadian or seasonal variation of plasma 5HT [28], different seasons result in different management techniques. It is known that 5HT-like substances can be produced by bacterial fermentation in the cecum [19], and dietary changes between groups may have resulted changes in platelet responsiveness to 5HT_{2A} receptor blockade. Both groups of horses were studied in April (single dose group in 2008, multiple dose group in 2009), and were eating predominantly hay, with some access to new pasture for grazing. Although 5HT release after aggregation was not measured in all groups, this measure could have been used to estimate the relative 5HT release from platelets in each group. Given the trend towards decreased serum 5HT in the multiple dose group after treatment, it is possible that the single dose group may have had lower serum 5HT levels, accounting for the change in aggregation.

In addition to 5HT, platelet dense granules release several other pro-aggregatory products, including TXA₂ and ADP [1]. These additional substances contribute to the wave of secondary aggregation that is potentiated by 5HT [2]. If adequate amounts of these other substances were released, the platelets of the horses studied may have been able to achieve full aggregation without the contribution of 5HT, mitigating any effects of 5HT_{2A} blockade by ketanserin. In addition, relatively high doses of agonist were used in this study; at a concentration of 15 μ M, ADP is able to trigger irreversible aggregation by horse platelets. If a lower concentration of ADP had been studied, the secondary aggregation caused by platelet granule release may have been more obvious, and it may have been easier to elucidate the actual effects of ketanserin in this group.

A pilot study concerning the possible beneficial effects of ketanserin in horses suggested that ketanserin may attenuate laminar venous constriction in carbohydrate

overload-induced laminitis. However, the results of the current study make it difficult to elucidate whether this effect was a direct effect on the vasculature or whether ketanserin prevented platelet activation and subsequent 5HT release in the laminae. At the very least, the effects of ketanserin on equine platelets are unpredictable, and future studies should evaluate both the platelet effects as well as changes in the digital vasculature.

Ketanserin interacts with the 5HT_{2A} receptor, and its binding site may be different between different horses. Variants of both the platelet 5HT transporter as well as the 5HT_{2A} receptor have been investigated in humans with hyperserotonemia syndromes [29] and myocardial infarction [30]. Other studies in humans have shown that the response to clozapine, another 5HT_{2A} antagonist, is variable, depending on the presence of a mutation in the T102 position of the 5HT_{2A} receptor gene [31]. Although these allelic variations have not been identified in the horse, it is likely that some degree of polymorphism exists.

With the exception of the single dose group, no changes in physical exam parameters were noted as a result of administration of ketanserin. The sweating that was seen may be indicative of cutaneous vasodilation, but other physical exam parameters consistent with hypotension (e.g. increase in heart rate, decreased digital pulse pressure) were not noted. Notably, the group that demonstrated sweating was also the same group that demonstrated a decreased *ex vivo* platelet aggregation effect of ketanserin. As the clinical signs rapidly abated, and no other adverse effects were seen in this group, the physiologic cause remains unknown. As the horses that displayed a clinical reaction to ketanserin all received drug from the same lot and preparation, the possibility also exists that this drug may have been contaminated with a compound such as endotoxin that

would cause similar clinical signs. However, while endotoxin may affect platelet aggregation due to direct and indirect mechanisms, the result is usually pro-aggregatory, and endotoxin contamination is not consistent with our findings [32]. The horses that received multiple doses of ketanserin were given drug from two different lots, and concurrent pharmacodynamic analysis confirmed that ketanserin and its metabolite ketanserol were present in the plasma of these horses [27].

Limitations of this study include the small number of horses that were evaluated. Although significant findings were obtained in some horses, if a receptor polymorphism or other phenotypic variation is the cause of the difference in aggregation responses, the response of many more horses would need to be evaluated to fully characterize the pharmacokinetics and pharmacodynamics of ketanserin in specific populations. The possibility also exists of a dose-response variability between different horses; the specific dose used in the multiple-dose study was chosen on the basis of positive results in the single-dose trial. However, if the second group of horses required a higher drug dose to demonstrate platelet aggregation inhibition, this study would not have identified that possibility. Of note, in the *in vitro* studies, the addition of a higher concentration of ketanserin did not result in quantitatively greater inhibition of platelet aggregation. The horses in the second group also displayed a lower platelet aggregation response to ADP; starting with a lower percent aggregation may have limited the degree to which ketanserin-induced changes would be recognized.

This study demonstrates that ketanserin may have an inhibitory effect on equine platelet aggregation responses to ADP and collagen. While this effect was seen in some horses, it was not demonstrated in others, either due to individual characteristics or dose-

dependent actions. Because the pharmacodynamics of this drug with regards to platelet aggregation were variable in this study group, further investigation of this drug at different doses and in different breeds of horses is necessary to truly elucidate the origin of the drug effects.

ACKNOWLEDGMENTS

These studies were funded in part by a Grayson Jockey Club Research Foundation Inc. I.A. is funded, in part, by Saudi Arabian Cultural Mission Fellowship. The authors thank Natalie Norton for assistance with horse handling and organization.

Table A-1. Percent aggregation measured by optical aggregometry for all experimental groups (n=4 horses each) after *in vitro* addition of ketanserin or DMSO to equine platelet rich plasma (PRP). Low concentration ketanserin groups were exposed to 200 ng/mL ketanserin, while high concentration ketanserin were exposed to 1000 ng/mL ketanserin. Because the ketanserin stock solution was made in DMSO prior to dilution in saline for testing, DMSO control groups of equivalent dilution were studied as well. Groups were exposed to ketanserin or DMSO for either 10 min or 60 min. Data are listed as mean \pm SD * significantly different from baseline ($p < 0.005$).

	Baseline	10 min Dosing with Ketanserin			60 min Dosing with Ketanserin		
		Low conc.	High conc.	Control (DMSO)	Low conc.	High conc.	Control (DMSO)
ADP (15 μM)	66.0 \pm 9.8	64.5 \pm 13.4	60.0 \pm 11.7	64 \pm 13.1	46.3 \pm 5.6*	46.8 \pm 9.0*	58 \pm 20.2
Collagen (15 μg/mL)	92.3 \pm 6.0	95.8 \pm 10.4	87.5 \pm 3.3	88.7 \pm 3.8	87.2 \pm 4.5	92.2 \pm 7.3	97 \pm 11.0

Table A-2. Percent aggregation measured by optical aggregometry in platelet rich plasma obtained from horses treated with a single dose of 0.1 mg/kg IV ketanserin at time 0. Data are listed as mean \pm SD. * Significantly different from baseline ($p < 0.0001$), † significantly different from aggregation at t=1 h ($p < 0.002$), ‡ significantly different from aggregation at t = 4 h ($p = 0.001$), § significantly different from aggregation at t = 24h ($p < 0.003$).

	Time (hr)					
	0 (Baseline)	1	4	8	12	24
ADP (15 μM)	71.2 \pm 5.3	61.3 \pm 9.1	41.8 \pm 7.9*†	45.7 \pm 9.1*†	50.0 \pm 14.1*	60.0 \pm 8.5‡
Collagen (15 μg/mL)	72.3 \pm 5.7	58.0 \pm 21.9	43.7 (5.8)*§	43.4 \pm 17.2*§	49.5 \pm 8.6*§	70.3 \pm 11.1

Table A-3. Percent aggregation measured by optical aggregometry in platelet rich plasma obtained from three horses treated with 3 doses of 0.1 mg/kg IV ketanserin at time 0, 8, and 16 h. Data are listed as mean (SD).

	Time (hr)					
	0 (Baseline)	4	8	12	16	24
ADP (15 μM)	52.3 \pm 13.0	54.7 \pm 16.7	49.3 \pm 17	49.1 \pm 15.5	47.7 \pm 16.8	45.0 \pm 14.5
Collagen (15 μg/mL)	72.3 \pm 10.7	76.7 \pm 21.0	54.3 \pm 26.5	69.9 \pm 15	72.1 \pm 16.0	62.4 \pm 19.7

Table A-4. Plasma and serum 5HT concentrations (ng/mL) in three horses treated with ketanserin 0.3 mg/kg IV q. 8h, starting at t=0. There were no significant differences in either plasma or serum 5HT (P=0.360 and 0.195, respectively). Data are listed as mean (SD).

	Time (hr)					
	0 (Baseline)	4	8	12	16	24
Plasma 5HT	5.9 ± 2.0	11.0 ± 3.8	6.0 ± 1.8	7.3 ± 2.8	6.0 ± 1.4	9.6 ± 4.3
Serum 5HT	1,130 ± 849	1,230 ± 268	1,470 ± 589	579 ± 421	815 ± 355	580 ± 386

REFERENCES

1. Ren, Q., S. Ye, and S.W. Whiteheart, *The platelet release reaction: just when you thought platelet secretion was simple*. *Curr Opin Hematol*, 2008. **15**(5): p. 537-41.
2. Li, N., et al., *Effects of serotonin on platelet activation in whole blood*. *Blood Coagul Fibrinolysis*, 1997. **8**(8): p. 517-23.
3. De Clerck, F. and B. Xhonneux, *Effects of ketanserin, a selective 5-HT₂ serotonergic antagonist, on the secondary recruitment of human platelets in vitro*. *Agents Actions*, 1986. **17**(5-6): p. 515-26.
4. Meyers, K.M., C. Lindner, and B. Grant, *Characterization of the equine platelet aggregation response*. *Am J Vet Res*, 1979. **40**(2): p. 260-4.
5. De Meyer, S.F., et al., *Antiplatelet drugs*. *Br J Haematol*, 2008. **142**(4): p. 515-28.
6. Nishihira, K., et al., *Serotonin induces vasoconstriction of smooth muscle cell-rich neointima through 5-hydroxytryptamine_{2A} receptor in rabbit femoral arteries*. *J Thromb Haemost*, 2008. **6**(7): p. 1207-14.
7. Schaub, R.G., K.M. Meyers, and R.D. Sande, *Serotonin as a factor in depression of collateral blood flow following experimental arterial thrombosis*. *J Lab Clin Med*, 1977. **90**(4): p. 645-53.
8. Verheyen, A., et al., *Serotonin-induced blood flow changes in the rat hindlegs after unilateral ligation of the femoral artery. Inhibition by the S₂ receptor antagonist ketanserin*. *Arch Int Pharmacodyn Ther*, 1984. **270**(2): p. 280-98.
9. Loots, W. and F. De Clerck, *5-Hydroxytryptamine dominates over thromboxane A₂ in reducing collateral blood flow by activated platelets*. *Am J Physiol*, 1993. **265**(1 Pt 2): p. H158-64.

10. Arndt, J.W., et al., *Serum serotonin concentrations in dogs with degenerative mitral valve disease*. J Vet Intern Med, 2009. **23**(6): p. 1208-13.
11. Hammond, A., et al., *Platelets in equine recurrent airway obstruction*. Res Vet Sci, 2007. **82**(3): p. 332-4.
12. Bailey, S.R., et al., *Plasma concentrations of endotoxin and platelet activation in the developmental stage of oligofructose-induced laminitis*. Vet Immunol Immunopathol, 2009. **129**(3-4): p. 167-73.
13. Baxter, G.M., et al., *In vitro reactivity of digital arteries and veins to vasoconstrictive mediators in healthy horses and in horses with early laminitis*. Am J Vet Res, 1989. **50**(4): p. 508-17.
14. Allen, D., Jr., et al., *Evaluation of equine digital Starling forces and hemodynamics during early laminitis*. Am J Vet Res, 1990. **51**(12): p. 1930-4.
15. Peroni, J.F., et al., *Black walnut extract-induced laminitis in horses is associated with heterogeneous dysfunction of the laminar microvasculature*. Equine Vet J, 2005. **37**(6): p. 546-51.
16. Menzies-Gow, N.J., et al., *Roles of thromboxane A2 and 5-hydroxytryptamine in endotoxin-induced digital vasoconstriction in horses*. Am J Vet Res, 2008. **69**(2): p. 199-207.
17. Bailey, S.R., et al., *The effects of vasoactive amines found in the equine hindgut on digital blood flow in the normal horse*. Equine Vet J, 2004. **36**(3): p. 267-72.
18. Elliott, J. and S.R. Bailey, *Gastrointestinal derived factors are potential triggers for the development of acute equine laminitis*. J Nutr, 2006. **136**(7 Suppl): p. 2103S-2107S.

19. Bailey, S.R., F.M. Cunningham, and J. Elliott, *Endotoxin and dietary amines may increase plasma 5-hydroxytryptamine in the horse*. Equine Vet J, 2000. **32**(6): p. 497-504.
20. Weiss, D.J., A.M. Trent, and G. Johnston, *Prothrombotic events in the prodromal stages of acute laminitis in horses*. Am J Vet Res, 1995. **56**(8): p. 986-91.
21. Weiss, D.J., et al., *Microvascular thrombosis associated with onset of acute laminitis in ponies*. Am J Vet Res, 1994. **55**(5): p. 606-12.
22. Persson, B., J. Heykants, and T. Hedner, *Clinical pharmacokinetics of ketanserin*. Clin Pharmacokinet, 1991. **20**(4): p. 263-79.
23. De Clerck, F., et al., *The involvement of 5-HT₂-receptor sites in the activation of cat platelets*. Thromb Res, 1984. **33**(3): p. 305-21.
24. Bush, L.R., *Effects of the serotonin antagonists, cyproheptadine, ketanserin and mianserin, on cyclic flow reductions in stenosed canine coronary arteries*. J Pharmacol Exp Ther, 1987. **240**(2): p. 674-82.
25. Takano, S., *Role of 5-hydroxytryptamine in platelet thrombus formation and mechanisms of inhibition of thrombus formation by 5-hydroxytryptamine_{2A} antagonists in rabbits*. Arch Int Pharmacodyn Ther, 1995. **330**(3): p. 297-308.
26. Ogawa, T., et al., *Involvement of platelet-derived 5-hydroxytryptamine in thromboxane A₂-induced aggregation in cat platelets*. Blood Coagul Fibrinolysis, 1998. **9**(3): p. 233-40.
27. Aljuffali, I.A., et al., *Pharmacokinetic and pharmacodynamic assessment of ketanserin in horses, part I: Pharmacokinetic and Pharmacodynamic Modeling*. J Vet Pharm Ther, 2010.

28. Haritou, S.J., et al., *Seasonal changes in circadian peripheral plasma concentrations of melatonin, serotonin, dopamine and cortisol in aged horses with Cushing's disease under natural photoperiod*. J Neuroendocrinol, 2008. **20**(8): p. 988-96.
29. Hranilovic, D., et al., *Hyperserotonemia in autism: the potential role of 5HT-related gene variants*. Coll Antropol, 2008. **32 Suppl 1**: p. 75-80.
30. Yamada, S., et al., *T102C polymorphism of the serotonin (5-HT) 2A receptor gene in patients with non-fatal acute myocardial infarction*. Atherosclerosis, 2000. **150**(1): p. 143-8.
31. Arranz, M., et al., *Association between clozapine response and allelic variation in 5-HT_{2A} receptor gene*. Lancet, 1995. **346**(8970): p. 281-2.
32. Jarvis, G.E., R.J. Evans, and M.F. Heath, *The role of ADP in endotoxin-induced equine platelet activation*. Eur J Pharmacol, 1996. **315**(2): p. 203-12.

APPENDIX B

IN VIVO TECHNIQUES AND METHODS

A. *In Vivo* Tumor Implantation

This method describes the implantation of human tumor cells, maintained in cell culture, into mice

Matrigel Matrix Handling

Matrigel basement membrane matrix is a soluble form of basement membrane extracted from Engelbreth-Holm-Swarm (EHS) mouse sarcoma [1]. This matrix rich in pro-growth protein including laminin, collagen IV, heparan sulfate proteoglycans, entactin, TGF-beta, epidermal growth factor, insulin-like growth factor and fibroblast growth factor [2, 3]. High protein concentration in Matrigel matrix promotes tumor growth. BD Matrigel Matrix is used routinely for *in vivo* tumor implantation including prostate cancer [4-6].

BD Matrigel Matrix (phenol red free) was used for *in vivo* tumor xenograft in 4-6 week old nude (NCR, nu/nu) male mice. Matrigel was thawed in a refrigerator for 24 hr prior to injection. After thawing, the vial was swirled to assure that material was evenly dispersed. The thawed vial of Matrigel matrix was placed inside a cell culture hood, sprayed vial top with 70 % ETOH, and handled using aseptic techniques. Matrigel matrix can be gently pipetted using an ice-cooled 1000 μ L pipette tip or small syringe attached to a low gauge needle. The required volume was transferred into a sterile microcentrifuge

tube and the remaining Matrigel was divided (500 μ L) into ice-cooled microcentrifuge tubes and frozen immediately.

Note: BD Matrigel Matrix gels rapidly and is viscous at room temperature. It should be thawed overnight in a refrigerator and keep it on ice before use. Pre-cooled pipettes, tips and tubes should be used when handling Matrigel matrix. Gelled Matrigel can be re-liquified if placed at 4 °C for 24 hr.

Tumor Implantation

1. PC-3 cells were seeded in T-175 flasks few days prior to implantation.
2. Subconfluent PC-3 cells maintained in tissue culture media were harvested using 0.25% trypsin.
3. Trypsin containing cells were mixed with cell culture media containing 10 % fetal bovine serum.
4. Cells were centrifuged ($600 \times g$ for 3 min) and re-suspended in serum-free media.
5. Cells were counted using a hemocytometer and resuspended (if needed) in serum free media to achieve a final concentration of 1×10^7 cells/ml.
6. Cell viability was evaluated as follows:
 - a. A 100 μ l of PC-3 cell suspension (dilute cells if the original suspension is highly concentrated, i.e., more than 150 cells in the field, in serum free medium) is transferred into a test tube.
 - b. 20 μ l of 0.4 % Trypan Blue dye was added and mixed thoroughly.
 - c. The cell suspension was allowed to stand for 5 min at room temperature.
 - d. The hemocytometer was filled with 20 μ L.

- e. A light microscope was used to count viable cells only (non-viable cells are stained blue and viable cells should exclude the dye).
7. The cell suspension was mixed with BD Matrigel Matrix (1:1, v/v) to a final cell concentration of 5×10^6 cells/ml.
 8. Matrigel cell suspensions should be loaded into a low dead volume syringe and kept on ice prior to implantation.
Note: An appropriate needle size (21-25G) should be selected to prevent cell lyses.
 9. 200 μ L of the mixture (1×10^6 cells) was implanted subcutaneously (sc) into the mouse flank.
 10. Individual animal's weight were measured and recorded.
 11. Injection site should be cleaned and wiped with 70 % isopropyl alcohol.
 12. After subcutaneous needle insertion, a wide subcutaneous pocket was formed by swaying the needlepoint right and left then the mixture was injected into the pocket.
 13. Ear punch was soaked in 70 % isopropyl alcohol to disinfect it before use. Each mouse's ear was marked with the appropriate number.

B. Harvesting Animal Tissues for Histopathological Examination

1. Individual animal's weight were measured and recorded.
2. Anesthetized animals were euthanized by cervical dislocation followed by cardiac removal. Cervical dislocation performed by holding the neck of the animal on one hand and the tail base on the other hand and pulling in an opposite direction (you should hear the cervical joint snap).

3. Animals were positioned on their back and a small incision on the abdominal cavity was made with a small scissor to expose the interior organs. The stomach and the gut were moved to the side using cotton tipped applicator.
4. The inferior vena cava was visualized then incised and a 21G needle filled with heparinized normal heparinized (5U/mL) saline was inserted into the left ventricle of the heart. Perfusion was started slowly, until the eyes appear clear and internal organs, e.g., liver and liver appear discolored (~100 mL).
5. Tissues (tumor, heart, lung, kidney, liver spleen and brain) were removed by microdissection holding surrounding tissues or mesenteries in order not to damage the tissue of interest.

Note: crude tissue handling can introduce artifacts to the sample.
6. Half of each tissue was flash frozen immediately in liquid nitrogen and stored at -80 °C. The other half of each tissue was cut into several slices using sharp razor blade. Sliced tissues were stored in container containing 10 % buffered formalin and kept at 4 °C for histological processing.
7. After 24 hr, fixed tissues were transferred into 70 % ethanol and stored at 4 °C until transferred for paraffin-embedding and sectioning.

C. ALZET[®] Osmotic Pump Study

ALZET[®] osmotic pumps are designed to deliver a fixed volume of solution at a constant rate. The required concentration to achieve the required mass flow rate of topotecan was calculated. Concentration of topotecan in the infusion solution can be calculated by the following equation:

$$k_0 = Q \cdot C$$

where, k_0 ($\mu\text{g/hr}$) is the mass delivery rate, C ($\mu\text{g}/\mu\text{l}$) is the concentration of drug solution, and Q ($\mu\text{l/hr}$) is the infusion rate of the pump (0.11 $\mu\text{l/hr}$ for ALZET[®] (model-1004)). Model 1004 pump has a nominal reservoir volume of 100 μl and amount of topotecan should be calculated to be in this volume.

Note: Check the instructions sheets (supplied in each box of pumps) for actual pumping rate.

Solution Preparation

1. Topotecan was dissolved in 25mM KH_2PO_4 buffer (pH adjusted to 3.0 with phosphoric acid).
2. Buffer solution was mixed with equal volume of polyethylene glycol-200 to make up the final concentration and volume.
3. The final solution was filtered using 0.45 μm sterile filter and kept in sterile microcentrifuge tube(s) at room temperature.

Filling Procedure

The following steps were performed in a laminar flow hood using sterile techniques:

1. Each empty pump weight was individually measured with the flow moderator.
2. The instructions sheet for the mean fill volume for each specific lot of pumps should be checked prior to use.
3. The filling tube (supplied with each package) was attached to a small volume syringe and draw up the solution.

4. The syringe and the attached tube were checked to be free of air bubbles; allow extra syringe volume for spillage.
 5. With the flow moderator removed the pump was held in an upright position and the filling tube completely insert through the opening at the top of the pump.
 6. The solution was injected slowly while the pump was in an upright position.
 7. When the solution appeared at the pump opening filling was stopped and the filling tube was removed carefully.
- Note:** Rapid filling of ALZET[®] pumps should be avoided because it can introduce air bubbles into the pump reservoir.
8. Excess solution was wiped off and the flow moderator was insert until the cap is attached to top of the pump; the flow moderator must be inserted fully into the body of the pump and any solution overflow were wiped off.
 9. The weight of the filled pump and flow moderator were determined.
 10. The difference in the weights obtained in Steps 1 and 9 is the net weight of the loaded solution.
 11. The calculated fill volume should be more than 90 % of the reservoir volume that was specified on the instruction sheet.

Priming ALZET[®] Pumps

Filled pumps need to be primed in a sterile saline solution at 37° C prior to implantation using the following steps:

1. Pumps were filled as described in the previous section.

2. Prefilled pumps were placed in sterile 0.9 % saline at 37° C for 48 hr prior to implantation.
3. After 48 hr, pumps were removed from the saline solution and implanted immediately.

ALZET® Pump Implantation

We implanted the ALZET® pumps into mice subcutaneously with the middle of the back slightly posterior to the scapulae.

1. Individual animal's weight were measured and recorded.
2. Each animal was anaesthetized in the induction box (with 2-3 % isoflurane) followed by placing the animal on sterile drape with a nose cone delivering isoflurane at 1.5-2%.
3. Once the animal is anesthetized, iodine-iodide was applied over the implantation site.
4. A mid-scapular incision (0.5 cm) was made adjacent to the pump placement site.
5. A probe with an eye was inserted into the incision site to create a pocket.
6. A filled pump was inserted into the pocket, delivery portal first.

Note: This will minimize interaction between the compound delivered and the healing of the incision.

7. The wound was closed with non-absorbable sutures.
8. Surgical pain was managed with subcutaneous injection of buprenorphine at 0.05 mg/kg.
9. Triple antibiotic (bacitracin, neomycin, and polymyxin B) was applied liberally to the incision site.
10. Each mouse's ear was marked using an ear punch that was soaked in 70 % isopropyl

alcohol.

11. Animals were then transferred into clean cages and placed under a heating lamp.

12. All animals were monitored for 24 hr for any sign of postsurgical complications.

REFERENCES

1. Kleinman, H., et al., *Basement membrane complexes with biological activity*. Biochemistry, 1986. **25**(2): p. 312-318.
2. Kleinman, H., et al., *Isolation and characterization of type IV procollagen, laminin, and heparan sulfate proteoglycan from the EHS sarcoma*. Biochemistry, 1982. **21**(24): p. 6188-6193.
3. Vukicevic, S., et al., *Identification of multiple active growth factors in basement membrane Matrigel suggests caution in interpretation of cellular activity related to extracellular matrix components*. Experimental Cell Research, 1992. **202**(1): p. 1-8.
4. Pretlow, T., et al., *Transplantation of human prostatic carcinoma into nude mice in Matrigel*. Cancer research, 1991. **51**(14): p. 3814.
5. Wilson, M. and A. Sinha, *Human prostate tumor angiogenesis in nude mice: metalloprotease and plasminogen activator activities during tumor growth and neovascularization of subcutaneously injected matrigel impregnated with human prostate tumor cells*. The Anatomical Record, 1997. **249**(1): p. 63-73.
6. Stephenson, R., et al., *Metastatic model for human prostate cancer using orthotopic implantation in nude mice*. JNCI Cancer Spectrum, 1992. **84**(12): p. 951.